Chapter 13

DAMAGE TO AIRCRAFT

INTRODUCTION

This chapter treats the damage to aircraft that results from the environment produced by the air blast wave and the thermal radiation from a nuclear explosion. The effects of nuclear radiation on electronic components and circuits are discussed in Section VII, Chapter 9, and some general vulnerability estimates for electronic systems in aircraft are given in Section IV, Chapter 14.

Section I of this chapter describes the blast and thermal effects on aircraft in general terms. Section II describes the response of the aircraft to the various categories of effects, largely in the form of illustrative problems, most of which contain numerical examples. Both in-flight and parked aircraft are considered.

A wide range of test data and a variety of analytical methods have been accumulated over the years to predict both the safe delivery of nuclear weapons and aircraft kill. Criteria for safety and for kill also have been developed; however, all of the aspects of the problems have not been treated in equal depth. The range of available methods that have been developed vary from relatively simple techniques to complex analyses requiring large, high-speed digital computers to obtain the solution. Unfortunately, there is very little information available concerning the relative accuracy and reliability of the various methods.

The discussion provided herein attempts to provide a clear description of the overall problem of aircraft exposed to blast and thermal effects of nuclear explosions. This description provides a means for those who are concerned with, but who do not have an extensive technical background in this area, to obtain an appreciation of the effects and to obtain first order approximations for the problems of aircraft safety and kill. A comprehensive review of a large body of data pertinent to vulnerability and safety analyses of aircraft subjected to the effects of nuclear explosions is contained in "Handbook for Analysis of Nuclear Effects on Aircraft (U)," DASA 2048 (see bibliography). As shown in DASA 2048, assessment of damage to aircraft is a strong function of the detailed characteristics of the specific aircraft of interest. Thus, it is impossible to provide a simple, short method to determine vulnerability in a general manner. DASA 2048 provides several methods for analyzing various classes of aircraft, arranged in order of increasing complexity. The simplest method described in DASA 2048 for each class of aircraft was selected to illustrate the analysis of that class of aircraft in Section II of this chapter. A brief abstract of DASA 2048, including a methodology matrix, is contained in Appendix D of this manual.

The term aircraft, as used in this chapter, applies to both airplanes and helicopters. Where differentiation between the two types of aircraft is intentional, the terms airplane and helicopter are used.

SECTION I

BLAST AND THERMAL EFFECTS ON AIRCRAFT

The problem of determining the effects of nuclear weapon explosions on aircraft has been recognized since the development of the

[redacted]

first nuclear weapons during the mid 1940s. For many years, aircraft represented the only means of delivering nuclear weapons to their targets; hence, it was natural to investigate the capabilities of aircraft with respect to delivering nuclear weapons. Nuclear weapons posed new and vital questions to military planners. Previously, when considering the delivery of conventional bombs by aircraft, the limitations on the capabilities of the aircraft were imposed by factors such as the range and payload of the aircraft and enemy defensive actions. With the emergence of nuclear weapons, a new factor was imposed. The energy output of these new weapons was so great that the delivery aircraft was in danger of being damaged by the explosion of the weapon it had delivered.

[redacted] Subsequently, military planners became interested in the effects of a nuclear explosion on parked aircraft. Early efforts to understand this problem were largely experimental.

[redacted] Finally, the possibility of nuclear antiaircraft weapons prompted analysis of the conditions under which an aircraft could be killed by the effects of nuclear weapons. Thus, the complete gamut of nuclear weapon effects on aircraft is of interest, from sure-safe conditions to sure-kill conditions, for both in-flight and parked aircraft.

[redacted] This section provides background concerning nuclear weapon blast and thermal effects on aircraft, discusses the type, scope and format of the methods of weapon effects analysis presented in Section II, and explains how the results of the analyses may be used together with prescribed criteria to obtain either sure-safe or sure-kill regions for aircraft exposed to blast and thermal effects.

13-1 Sure-Safe and Sure-Kill Envelopes [redacted]

[redacted] The terms "sure-safe" and "sure-kill" are self explanatory with respect to their general meaning; however, the terms must be examined more explicitly to provide a basis for understanding the analyses that are described in succeeding paragraphs. If the response of an aircraft to one of the effects of nuclear weapons is known, this response must be compared to some criterion to determine whether the aircraft is "safe" or "killed." For example, the aircraft may be termed safe with respect to that weapon effect as long as the particular weapon effect does not degrade the performance of the aircraft or crew in any way. The specification of a sure-kill, or lethal, criterion is more complex, because it is difficult to define the amount of response that will result in a sure-kill. The response must be sufficient to produce some kind of damage to the aircraft or crew. It could be stated that a sure-kill manifests itself by virtually "immediate loss" of the aircraft, but the relation of immediate loss to an amount of damage is difficult. Although some effort has been devoted to this problem, it still remains a major source of error in determining sure-kill conditions. The best available lethal criteria, with the sample response prediction methods, are presented in Section II.

[redacted] If both response prediction methods and criteria that relate response to sure-safe and sure-kill conditions are available, the particular geometry that defines the relative positions of the nuclear explosion and the aircraft must be defined. The direction and flight path of the aircraft is an important part of the geometry. Two terms, "orientation" and "range," must be defined. For example, if the aircraft were directly above the burst and in straight and level flight, the orientation would be completely defined; however, the distance between the burst and the aircraft, which is range, would not be defined. The complete geometry of the problem, at the time of burst, is described by giving the range and the orientation.

[redacted] For a specified orientation and range, the aircraft response to some nuclear effect can be determined. This response can be compared

[redacted]

to the maximum response to that effect that can be tolerated without degradation of the performance of the aircraft or crew, i.e., the criterion for sure-safe response. If the calculated response is less than the sure-safe criterion, the aircraft is safe for that range and orientation. Since weapon effects, and hence aircraft response to weapon effects, decrease with increasing range, a shorter range at the same orientation must be considered to find the range at which the calculated response matches the sure-safe criterion. When this range, which is called the sure-safe range, is determined, this range and the orientation assumed define a point on a sure-safe envelope.

If the sure-safe range is determined for *all* orientations, a surface in space is defined. If the aircraft is placed at the origin of that surface, any nuclear burst, of the specified yield, which takes place on that surface will produce an aircraft response that matches the sure-safe criterion. Any burst outside of that surface will produce a lesser response; the aircraft will be safe for any burst outside of the surface. Conversely, the aircraft may be unsafe for any burst inside the surface.

The surface described above is sometimes referred to as the "sure-safe volume," since it describes the volume in space outside of which a nuclear burst will produce a level of response that is safe for the aircraft and crew. If a plane is passed through this surface, the intersection of the plane and the surface defines a closed line called an "envelope." A sure-safe envelope is simply a plane section of a sure-safe volume.

The sure-kill surface or volume may be defined in a similar manner. The sure-kill volume, often called the lethal volume, defines the volume in space inside of which a nuclear burst will produce a level of response that will result in an aircraft kill. A sure-kill envelope is a plane section of a sure-kill volume.

For in-flight aircraft, the range and orientation with respect to a given burst point are functions of time as a result of the motion of the aircraft. The time must be specified to specify the geometry completely. In defining the time, it is important to distinguish between types of weapon effects: those effects that take place or at least begin to take place immediately after the burst; and those that do not take place until some time after the burst. Nuclear and thermal radiation, whose effects begin to be felt virtually immediately fall into the first category. Gust and overpressure effects, which are not felt by the aircraft until the arrival of the blast wave are in the second category. Two times of significance are associated with the problem. The first is the burst time and the second is the intercept time, or the time at which the blast wave reaches, or intercepts, the aircraft. For effects in the first category, only the burst time is significant; hence, the orientations and ranges are those corresponding to the burst-time position of the aircraft. For effects in the second category, both the burst time and the intercept time are significant.

In calculating response, it is convenient to use the intercept time, because it is at intercept time that the response begins. Hence, application of the response methods results directly in intercept-time volumes and envelopes. The military planner, however, is generally interested in burst-time envelopes, since he wants to know what the effects of a nuclear burst occurring at some point relative to the aircraft will be on an aircraft. He generally is not interested in where the aircraft will be when it is intercepted by the blast wave, but only that some given response will be achieved when it is intercepted. Thus, it becomes necessary to transform intercept-time envelopes into burst-time envelopes. This transformation can be accomplished rather easily. Each range on an intercept-time envelope represents the distance which the blast wave must

travel in order to reach the aircraft. For a given yield and altitude, a time of arrival of the blast wave may be associated with any distance traveled. Hence, the time, measured from burst time, corresponding to any point on the intercept-time envelope may be calculated from weapon characteristics. Using this time, and knowing the aircraft velocity and maneuver condition, a position occupied by the aircraft at burst time may be calculated for each point on an intercept-time envelope. These positions define the burst-time envelopes.

In determining the burst-time envelopes, the assumption is made implicitly that the aircraft maintains a constant speed and maneuver between the time of burst and the time of interception by the blast wave. Within the scope of this manual, the assumption has been made that the airplane velocity does not exceed Mach 2. For an airplane velocity exceeding Mach 2, certain effects that have been ignored in transforming intercept-time envelopes into burst-time envelopes become important. This assumption is valid for low yield weapons, because of the small distances and times involved. For large yield weapons, however, when the blast wave arrival time may be on the order of several seconds, there is time for a pilot to change his course. It would be impossible to guess the course changes; hence, assumption of an unaltered flight path cannot be avoided reasonably. At the same time, this assumption must be considered as a source of error in the case of large yield weapons.

NUCLEAR WEAPON EFFECTS ANALYSIS

A basic description of nuclear weapon blast and thermal phenomena is contained in Chapters 2 and 3 of this manual. The effects of these weapon phenomena on an aircraft are described in the following paragraphs. These effects include material velocity (gust) effects, overpressure effects, thermal radiation effects, and combinations of these effects.

13-2 Gust Effects

The blast wave and the associated material velocity and overdensity are described in Section I of Chapter 2. As the blast wave engulfs an aircraft, the angle of attack of the aircraft is changed by the material velocity. The effect is similar to that produced by atmospheric gusts, and the term gust has become associated with this effect.

Another parameter that is important in determining aerodynamic loads is the dynamic pressure. The dynamic pressure is the product of the air density and the square of the velocity of the aircraft relative to the surrounding air. Since both the density and the relative velocity are changed by the blast wave, the dynamic pressure is changed.

The changes in angle of attack and dynamic pressure produce changes in the aerodynamic loads on the aircraft. Several methods may be used to predict the resulting aerodynamic loads. The simplest is the so-called quasi-steady state method. In this method, the angle of attack and dynamic pressure existing at each instant of time are considered to have existed for a time that is sufficiently long that a steady-state condition has been attained. The aerodynamic forces are then the steady-state forces corresponding to the instantaneously-existing conditions. Since the instantaneously-existing conditions actually are changing rapidly as the blast wave engulfs the aircraft and subsequently decays, the method is called quasi-steady. More sophisticated methods account for the truly transient nature of the response to the aerodynamic loads under the rapidly changing conditions. Such methods are called unsteady aerodynamic methods.

One more complication arises in predicting aerodynamic loads. Aerodynamic loads gen-

erally are assumed to be proportional to the angle of attack, i.e., the loads are assumed to be linear with angle of attack. In the sure-kill case, however, severe loadings are required to produce damage corresponding to a sure-kill condition. These severe loadings generally can occur only if the gust induced angle of attack is large, often well beyond the angle of attack range for which linearity can be assumed reasonably, and nonlinear aerodynamics are of interest. The coupling of unsteady and nonlinear aerodynamics is an extremely complex problem that has been solved only semi-empirically.

The aerodynamic loads described above produce rigid-body accelerations of the aircraft, both in translation and rotation. These accelerations result in translational and rotational velocities and displacements. The translational velocity and the rotational displacement are particularly important in the production of additional aerodynamic loads. If an aircraft is intercepted by a blast wave from directly below, the material velocity is upward. This increases the angle of attack of the aircraft and causes an upward translational velocity, so the aircraft tends to "ride" with the gust. The tendency to ride with the gust causes a reduction in the angle of attack of the aircraft and alleviates the aerodynamic loads. The alleviation that results from riding with the gust is a function of the wing loading for an airplane. The wing loading is the ratio of the airplane weight to the airplane wing area. An airplane with a high wing loading is heavy with respect to its aerodynamic loading; it rides very little with the gust and produces very little load alleviation. Conversely, an airplane with a low wing loading will produce considerable load alleviation by riding with the gust.

The rotational displacement that results from rotational acceleration also alleviates the loading, although the effect is more complex. Roughly, a stable aircraft will rotate into the gust, which reduces the angle of attack and alleviates the loads. Generally, the translational load alleviation is more important than the rotational load alleviation during the time period of interest.

The aerodynamic loads also produce accelerations and displacements in the elastic modes of the aircraft, e.g., the fuselage bends. The elastic displacements and velocities also change the angle of attack and hence the aerodynamic loads. There is thus an interaction between the elastic motion and the aerodynamic loads; this interaction is called the aeroelastic effect. The aeroelastic effect is generally of secondary importance, but there are cases in which it can be of considerable importance.

One more type of motion interacts with the aerodynamic loading. If the sure-kill problem for an in-flight aircraft is considered, the inelastic response often must be considered. A major component, such as the fuselage, ordinarily will fail in an instability, or buckling, type of mode; however, a buckling failure does not necessarily produce a catastrophic failure of the aircraft, i.e., a sure-kill condition. A structure that has undergone a major buckling failure will be weaker than it was prior to the failure; however, it may maintain the capability of carrying a substantial load. The load carrying capability may be sufficient to permit the aircraft to complete its mission. This situation has been demonstrated analytically, in simulation experiments, and in a full-scale test during Operation TEAPOT, a nuclear test in Nevada in 1955.

As the inelastic deformation of the structure increases, its load carrying capability decreases. At some point, the load carrying capability becomes sufficiently low that a sure-kill condition exists. Inelastic deformations required to produce a sure-kill condition may be very large when compared to elastic deformations; the aerodynamic loads induced by inelastic motions may be much larger than the aeroelastic effect described previously.

[redacted]

The final influence on the aerodynamic loadings for in-flight aircraft is pilot or autopilot action upon interception of the aircraft by the blast wave. Pilot action would be too slow to influence the situation substantially during the time period of interest. Autopilot response has been ignored in all known approaches to the problem, presumably because of the low probability that the aircraft would be on autopilot for realistic engagement conditions. It might be noted, however, that an autopilot that is maintaining constant barometric altitude could react violently to the change in pressure accompanying the blast wave.

The concepts of rigid-body, elastic, and inelastic motion have been introduced in outlining the various influences on the aerodynamic loads. Each of these types of motion is important for some type of sure-safe or sure-kill envelope. For example, parked aircraft may be lifted from the ground. This is a rigid-body mode, which must be considered for both sure-safe and sure-kill conditions for parked aircraft.

Parked aircraft also may be damaged by bending of the fuselage or vertical tail as a result of aerodynamic loading of the vertical tail. For sure-safe conditions, this bending will be elastic; for sure-kill conditions, inelastic response also may be important.

Rigid-body motions generally are not important for in-flight aircraft. These motions enter the problem in two ways: (1) their influence on the aerodynamic loads is significant; (2) rigid-body translational accelerations are rough indices of the amount of elastic or inelastic deformation of the major aircraft components, and they may be used in crude methods instead of such deformations, which are the quantities of real interest. More realistic analyses should consider elastic response for sure-safe conditions and inelastic response for sure-kill conditions.

Most of the preceding remarks apply both to airplanes and to helicopters. The only new facets added by helicopters are the rotors. There are three types of helicopter main rotor blades: hinged, rigid (hingeless), and teetering. Each type must be considered separately, because each has its own characteristics.

The important characteristic of a hinged rotor is the hinge, which is offset somewhat from the center of rotation. This permits free rotation of the blade outboard of the hinge in an up-and-down, or flapping, direction. Analysis of this type of blade has shown that bending of the blade is not an important mechanism for either sure-safe or sure-kill conditions. Flapping of the blade about the hinge seems to be more important. Extreme flapping could result in a collision between the blade and the fuselage and/or the flapping stops. Even blade flapping appears to be less important than overpressure damage to the overall system, so gust effects are not considered for hinged blade helicopters in this chapter.

Rigid, or hingeless blades, do not use a flapping hinge. Bending may be important for these blades, and it is considered in this chapter.

Finally, a teetering blade roughly combines the characteristics of the hinged and hingeless blades. A teetering blade is essentially a seesaw about a hinge at the center of rotation. The two blades on the two sides of the hinge are connected rigidly. If there is a loading on the two blades, this loading can always be divided into a symmetrical and an anti-symmetrical component. The loadings on the two blades are identical for the symmetrical component; the loadings on the two blades are exactly opposite for the anti-symmetrical component. The response to the anti-symmetrical component is exactly the same as if each blade were separately hinged at the center of rotation, rather than being connected rigidly. The anti-symmetrical gust loading component on teetering blades can therefore be ignored for the same reasons that gust loading on hinged blades was ignored.

The teetering blade responds to sym-

[redacted]

[redacted]

metric loading as if there were no hinge at the center of rotation, i.e., the teetering blade responds to a symmetric loading as if it were a hingeless blade, and the symmetric component of the gust loading must be considered.

[redacted] In general, gust effects are only of minor importance for parked aircraft, but they are of primary importance for in-flight aircraft.

13-3 Overpressure Effects [redacted]

[redacted] The gust effects influence the major components of the aircraft, such as the wings and/or the blades, the fuselage, the horizontal tail, and the vertical tail. The overpressure, on the other hand, influences smaller elements of the structure, i.e., the skin, the stringers, and the frames, particularly on the fuselage.

[redacted] When an aircraft is struck by a blast wave, the pressure on the side of the fuselage facing the burst point is increased above the incident value by reflection, and a local loading of short duration is generated (see Figure 9-3). As the blast wave continues to engulf the aircraft, the pressure on the side of the fuselage facing the burst point decays to the pressure behind the blast wave. The characteristic loading is a high reflected pressure (from two to eight times the overpressure associated with the blast wave), which decays very rapidly, in a few milliseconds, to the value of pressure behind the blast wave. This high pressure, short duration pulse is followed by the much longer duration, but lower pressure, pulse that is characteristic of the blast wave.

[redacted] It is primarily the high reflected pressure, short duration pulse that is responsible for damage to skin panels, stringers, and frames. These structural elements are vulnerable to such short duration loadings because of their high frequencies. For the converse reason, the much lower frequency major components are not influenced to a great extent by the short duration loading.

[redacted] The short duration pulse produces dishing-in of skin panels and buckling of stringers and frames or portions of stringers and frames. As in the case of analysis of response to gust effects, analysis of overpressure response only requires consideration of the elastic response for the sure-safe case, but inelastic response should be included for sure-kill conditions.

[redacted] Early efforts to determine overpressure damage relied virtually entirely on experimental results. Simple approaches were advanced later, which analyze the response of skin panels, stringers, and frames to static loadings, and then modify the results by some dynamic factor to account for the true dynamic character of the loading.

[redacted] With regard to overpressure damage, airplanes and helicopters may be analyzed in the same way. The distinguishing feature of the helicopter, the rotor blade, is virtually invulnerable to overpressure effects, so the helicopter is no different from an airplane in this regard.

[redacted] Overpressure damage is generally the predominant effect for parked aircraft; however, overpressure damage is usually of minor importance in comparison with gust effects for in-flight aircraft. Overpressure only becomes important for in-flight aircraft in those regions where gust effects are small, i.e., for bursts almost directly in front of or directly behind the aircraft.

13-4 Thermal Radiation Effects [redacted]

[redacted] In considering the effects of the thermal radiation from a nuclear explosion, two distinct problems must be addressed: (1) the portion of the thermal radiation emitted by the explosion that reaches the aircraft; and (2) the effect on the aircraft that is produced by the incident radiation.

[redacted] The radiant exposure of an aircraft in flight varies widely with atmospheric conditions,

[redacted]

orientation of the aircraft with respect to the burst, aircraft velocity, the ground reflecting surfaces, and the location of clouds (see Chapter 3). Scatter and reflection add to the direct radiation, and, under some circumstances, the thermal energy incident on an aircraft in space may be two to three times as great as would be computed at a given slant range for direct radiation only. Conversely, when a heavy cloud layer is between the burst and the aircraft, the radiant exposure may be only a fraction of the predicted value of direct radiation for a given range. In other situations, reflected radiation from clouds may contribute significant thermal energy to areas of the aircraft shaded from direct radiation. During weapon effects tests of an aircraft flying in a cloud above the burst, the radiant exposure at the top of the aircraft and its cockpit area was observed to be as much as one-fourth of the direct radiation on the lower surfaces. This experiment demonstrated the need for protection of weapon delivery aircraft from radiant exposure from any direction.

The motion of the aircraft during the time in which significant thermal radiation is being emitted by the fireball can exert an important influence on the thermal radiation incident upon the aircraft. Obviously, this is particularly true for high-speed aircraft. "Fly-away factors" have been devised which are first order corrections for aircraft motion.

The absorptivity of the aircraft skin and the angle of incidence of the thermal radiation affect the amount of energy that will be absorbed by the structure; the boundary layer in the air flow adjacent to the structure leads to convective cooling. Very thin skins are heated to damaging temperatures rapidly, because the energy is absorbed by the skin much more rapidly that it can be dissipated by conduction and convective cooling. In recent years, designers of military aircraft have reduced aircraft vulnerability to thermal effects by coating materials with low absorptivity paints, by eliminating ignitable materials from exposed surfaces, and by substitution of thicker skins for very thin skins.

An aircraft thin skin panel, supported by internal structure, which is usually much cooler, can be heated sufficiently that it may be buckled by thermal stresses in the sure-safe case, or it may melt in the case of sure-kill. In either case, there will be essentially no change in temperature through the thickness of a thin skin. The thick skin case is a step higher in complexity. The temperature distribution across the thickness of the skin must be considered in determining thermal stresses. A still more complex temperature distribution occurs in built-up structures, with air gaps acting as insulators between spars, stringers, and skin. For all but the simplest configurations, computer programs are necessary to define these temperature distributions accurately.

Analyses of thermal radiation effects on aircraft generally only concern themselves with temperature rather than with stresses, since buckling of thin skin is generally of little or no consequence. Sure-safe envelopes usually are based upon a rather arbitrary temperature, or temperature rise, in the thinnest skin. The temperature chosen is based roughly upon some percentage reduction in strength or stiffness that results from the increased temperature. Sure-kill envelopes are based upon melting of the skin.

Biological injury to the crew from intense thermal radiation, and damage to nonstructural elements that would affect mission performance adversely also must be considered when dealing with thermal criteria. In many cases, these problems can be minimized by adequate protective measures such as cockpit curtains.

A military weapon delivery aircraft properly prepared for its delivery mission with reflective paint and with the crew and all vulner-

[redacted]

able materials shielded from direct thermal radiation will not be damaged by thermal radiation at distances where damage from air blast would be severe. Other aircraft not so prepared may sustain serious damage at very low thermal levels as a result of ignition of items such as rubber and/or fabric seals, fixed landing gear tires, cushions, and headrest covers. Aircraft painted with dark paint are especially vulnerable to thermal radiation damage, because the dark painted surfaces absorb three to four times the thermal energy that is absorbed by polished aluminum surfaces or surfaces protected with reflective paint.

[redacted] As in the case of overpressure effects, there is no difference between helicopters and airplanes with regard to the analysis of thermal radiation effects. The importance of thermal radiation effects relative to the other effects depends upon the yield of the weapon being considered. Relative to other effects, the importance of thermal radiation increase with increasing yield. For small yields, thermal radiation is generally of secondary importance for both parked and in-flight aircraft; thermal radiation from high yield weapons may be dominant for both.

13-5 Combined Effects [redacted]

[redacted] The effects of combinations of various weapon phenomena have been examined, but relatively little has been accomplished in the generation of methods for analyzing combined effects. One reason for this is the difficulty in analyzing each effect individually with adequate accuracy. In general, only qualitative comments may be made concerning combined effects.

[redacted] The first possibility is the interaction between gust and overpressure effects. For in-flight aircraft, the levels of overpressure required to produce a given response are well above the levels associated with significant response to gust effects, and little coupling is expected. For parked aircraft, the gust effects of most importance are lift-off and crushing of the landing gear; overpressure damage will not influence these phenomena significantly. Thus, gust-overpressure coupling appears to be of secondary importance.

[redacted] In considering the thermal interactions with either overpressure or gust, it should be recalled that the usual thermal analyses are concerned with temperatures and not with stresses. To examine the interaction between thermal stresses and gust or overpressure effects would require a combined analysis of a higher level of sophistication than is usually employed for the individual effect. Moreover, the few exploratory investigations indicate that transient thermal stresses seem to be less important as a coupling factor than degradation in material properties that result from elevated temperature. Degradation of material properties generally will be of minor importance at ranges associated with significant gust effects for in-flight aircraft, except in the case of high yield weapons. For high yield weapons, the time period between heating of the structure and interception of the aircraft by the blast wave may permit considerable cooling to take place, and thus minimize interaction effects even in this case.

[redacted] For parked aircraft, the interaction between thermal and overpressure effects could be significant. The state of the art in overpressure effects analysis, however, is such that inclusion of anything more than the effect of degraded material properties (see Section IV, Chapter 9) would be unreasonable.

[redacted] In summary, the only interactions between effects that seem to be of much importance are those between thermal effects and gust or overpressure effects. In those cases, any consideration of interactions should be restricted to use of material properties in the gust or overpressure analyses corresponding to the elevated temperatures produced by the thermal radiation.

[redacted]

Furthermore, consideration of even this interaction should be restricted to the most sophisticated methods of gust and overpressure analysis, and is not recommended for users of this manual.

SECTION II

AIRCRAFT RESPONSE TO BLAST AND THERMAL EFFECTS

AIRCRAFT RESPONSE TO GUST EFFECTS

13-6 Aerodynamic Coefficients for Aircraft

When the blast wave arrives and commences to envelop the aircraft, a complicated pattern of shocks passes over the surfaces of the aircraft very quickly. During this period, frequently called the "diffraction period" (see Section II, Chapter 9), the transient airloads are difficult to predict, and sophisticated methods are required even for the simplest combination of aircraft configuration and blast orientation. However, for many cases of blast loading, such as a supersonic airplane enveloped by a blast from below, the lift and normal force during the diffraction period are nearly the same as during the early post-diffraction period. In other cases, the duration of the diffraction loading is so short that the influence on the response of major aircraft components is very small. Hence, it is reasonable to make first estimates of the transient airloads on a quasi-steady basis by using instantaneous quantities (angle of attack, density, etc.) and steady-state coefficients to compute steady state forces. This simplification is adopted in the aerodynamics methods presented in this chapter.

Methods for calculating gust loadings are presented for two orientations: symmetric loading, with the gust velocity from directly above or below the aircraft; and lateral loading, with the gust velocity directly from the side.

When a wing (tail) is added to a fuselage, certain mutual interference effects may arise between the components. For example, a body induces high upwash velocities near the wing-body (tail-body) juncture, which is commonly termed body-induced wing (tail) interference. The local body flow properties such as Mach number and dynamic pressure also affect the wing (tail) loading. The wing (tail) in turn affects the loads on the body.

Another interference effect, normally considered in stability and control, is that on the tail that results from a wing set at an angle of attack. The downwash that is caused by the trailing vortices from the wing generally reduces the lift on the horizontal tail surfaces during straight and level flight. The magnitude of the reduction depends on the span of the wing relative to the span of the tail, the lift distribution on the wing, and a number of other factors. A blast wave changes the loading in the wing, which alters the strength of the vortex sheet behind the wing, but the change in the strength of the vortex sheet that results from the blast wave does not affect the lift on the tail at early times after blast arrival to any great extent. The blast wave also deflects the vortex sheet away from the plane of the wing. The effect of the vortex sheet on the lift on the tail depends strongly upon the position of the sheet relative to the tail surface. Methods to predict the transient location of the vortex sheet have not been demonstrated for strong blasts; therefore, the interference of the wing on the tail is not included in transient load estimates.

The airloads on the vertical tail produced by lateral blasts are more difficult to predict than the airloads on the wing, because, in addition to the body and the wing, the horizontal tail influences the flow field at the vertical tail. At an angle of attack, the downwash from the wing could influence the vertical tail. The lateral flow over the body has a maximum

velocity at the top where the vertical tail is located. Also, at large angles of attack or sideslip, there are vortices shed from the body that could affect the loads on the vertical tail; presumably the effect of the vortices would be most severe at combined angles of attack and sideslip, a combination which is outside the cases considered here. The horizontal tail interacts with the flow field about the vertical tail, serving to some extent as a reflection plane, so that aerodynamically the vertical tail appears to have an aspect ratio that is larger than the geometric aspect ratio (this is the so-called "end-plating" effect). At supersonic speeds, shocks emanate from the wing and horizontal tail and provide further influence on the vertical tail loads.

Problem 13-1. Calculation of the Aerodynamic Coefficient for Wing and Horizontal Tail

[redacted] The transient airloads may be obtained on a quasi-steady basis using the instantaneous quantities (angle of attack, density, etc.) and steady-state coefficients. Typically, the theoretical methods predict a lift for a swept wing-body combination which is about 10 percent greater than for an isolated wing without a body, provided that the wing and body are at the same incidence. In wind tunnel tests, however, the lift on a swept wing-body combination was found to be the same as on an isolated wing. In these cases, the area of the isolated wing includes the area submerged within the body. Other methods indicate that the lift on a delta wing-body combination with a typical ratio of body diameter to wing span and traveling at supersonic speeds is within 2 percent of the lift for the same delta wing alone. In view of these results, the lift on the wing (tail)-body combinations is computed for an isolated wing (tail) having the same wing area, including the wing (tail) area submerged within the fuselage.

[redacted] The calculation of the aerodynamic coefficient for wings and/or horizontal tails, C_{L_α}, is presented in the following series of steps.

1. Using the silhouette profile of the aircraft (for example, see Figures 13-1 and 13-2), from which lengths and surfaces may be found, determine the following:

S = wing/horizontal tail area (sq ft), defined as the extension of the leading and trailing edges of both wings/horizontal tail to the aircraft centerline.

c_r = wing/horizontal tail root chord, i.e., the length along the fuselage centerline (ft) subtended by extensions of the leading and trailing edges.

c_t = wing/horizontal tail tip chord (ft), defined as the length along the fuselage centerline subtended by the wing tip.

b = wing/horizontal tail span, tip to tip (ft).

Λ_{LE} = sweepback angle at wing/horizontal tail leading edge, measured from a line perpendicular to the fuselage centerline (deg).

M = Mach Number = V/c, where V is the aircraft velocity and c is the ambient speed of sound.

2. Calculate the taper ratio λ:

$$\lambda = \frac{c_t}{c_r}$$

and the aspect ratio AR:

$$AR = \frac{b^2}{S}.$$

3. Calculation of the slope of the lift coefficient depends on the value of the Mach number, M. Three regions are defined as follows:

Region 1: $M \leq 0.85$,

Region 2: $M \geq 1.2$,

Region 3: $0.85 < M < 1.2$.

Region 1. Steps a through d present the calculation of the slope C_{L_α} for $M \leq 0.85$.

a. Calculate the value of β^2:

$$\beta^2 = 1 - M^2.$$

[redacted]

b. Determine the tangent of the sweep angle of the mid-chord line, tan $\Lambda_{c/2}$:

$$\tan \Lambda_{c/2} = \tan \Lambda_{LE} - \frac{2}{AR}\left[\frac{1 - \lambda}{1 + \lambda}\right].$$

c. Compute the parameter,

$$AR\left[\beta^2 + \tan^2 \Lambda_{c/2}\right]^{1/2},$$

and enter Figure 13-3, with the value of the parameter to obtain the corresponding value of C_{L_α}/AR.

d. Calculate the slope of the lift coefficient curve as follows:

$$C_{L_\alpha} = \left[\frac{C_{L_\alpha}}{AR}\right] AR.$$

Region 2. Calculation of C_{L_α} for $M \geq 1.2$ is performed by the following steps.

a. Calculate the value of β:

$$\beta = (M^2 - 1)^{1/2}.$$

b. Calculate the values of the parameters:

$$\frac{\beta}{\tan \Lambda_{LE}},$$

and

$$(AR) \tan \Lambda_{LE}.$$

c. Enter Figure 13-4 and select the figure corresponding to the taper ratio λ. Select the curve corresponding to the value of the parameter $(AR) \tan \Lambda_{LE}$. If

$$\frac{\beta}{\tan \Lambda_{LE}} < 1,$$

use the left side of the figure to obtain the value of $\tan \Lambda_{LE} C_{N_\alpha}$. Calculate C_{L_α} as follows:

$$C_{L_\alpha} = \frac{\tan \Lambda_{LE} C_{N_\alpha}}{\tan \Lambda_{LE}},$$

where the normal force coefficient C_{N_α} and C_{L_α} are taken to be equal within the scope of this method.

If

$$\frac{\beta}{\tan \Lambda_{LE}} > 1,$$

determine its reciprocal,

$$\frac{\tan \Lambda_{LE}}{\beta},$$

and use the right side of the figure to obtain the value of βC_{N_α}.

The slope is calculated by:

$$C_{L_\alpha} = \frac{\beta C_{N_\alpha}}{\beta},$$

where C_N is represented as C_L within the scope of this method.

Region 3. The following steps a through c, are used to calculate C_{L_α} for $0.85 < M < 1.2$.

a. Calculate C_{L_α} at $M = 0.85$ following the method in Region 1.

b. Calculate C_{L_α} at $M = 1.2$ following the method in Region 2.

c. Interpolate linearly for the slope at the actual Mach number:

$$C_{L_\alpha} = C_{L_\alpha}(\text{at } M = 0.85) + \frac{M - 0.85}{0.35}\left[C_{L_\alpha}(\text{at } M = 1.2) - C_{L_\alpha}(\text{at } M = 0.85)\right].$$

[redacted]

[redacted]

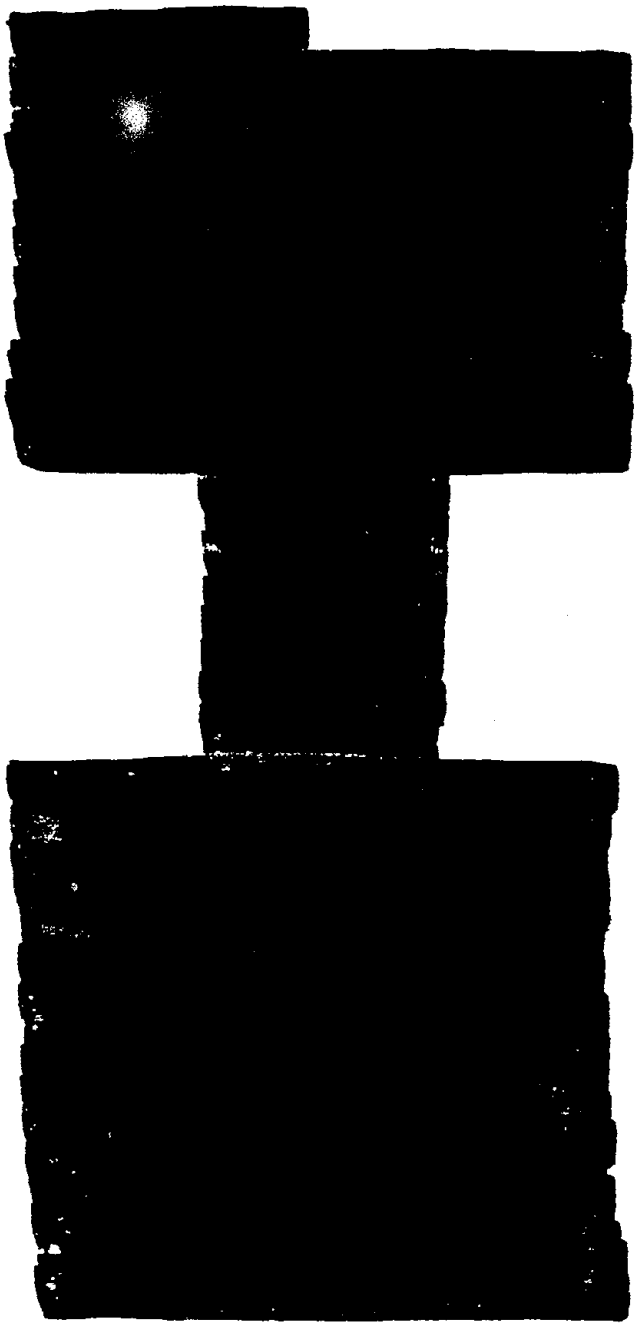

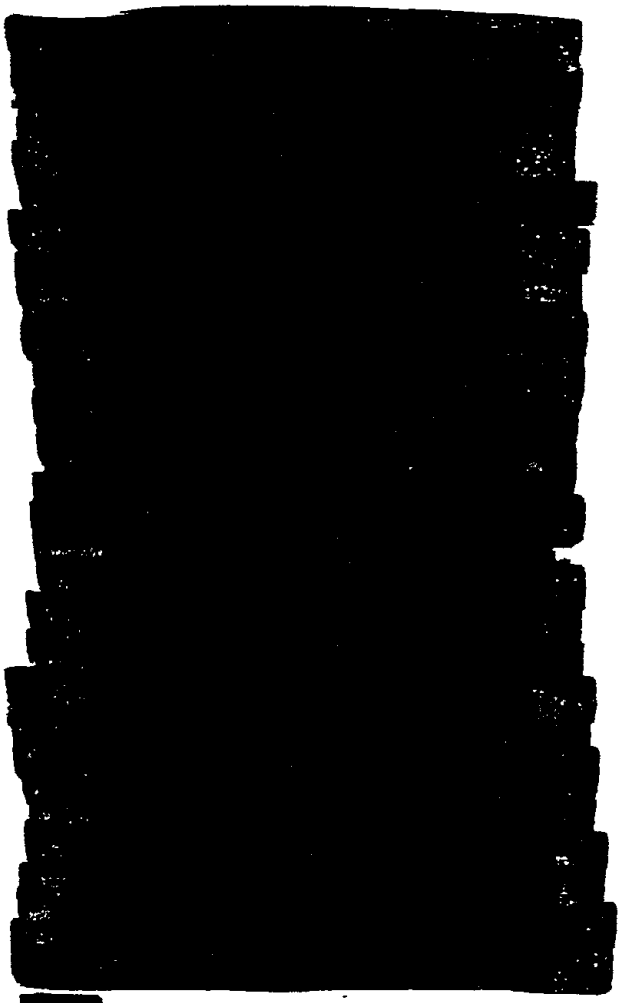

DNA
(b)(1)

[redacted] *Reliability:* The aircraft is assumed to be in a symmetric maneuver prior to blast interception. Blast origin is in the aircraft plane of symmetry. Interference effects of wing on tail, body on wing, and body on tail are neglected. A quasi-steady approach is assumed to be adequate to define blast-induced loads.

[redacted] *Related Material:* See paragraphs 13-1 and 13-2. See also Table 13-1.

[redacted]

[redacted]

Table 13-1. [redacted] Selected Data Based on U.S. Standard Atmosphere, 1962 English Units [redacted]

Altitude feet	Temperature °F	Pressure psi	Density Ratio* ρ/ρ_o	Temperature Ratio T/T_o	Sound Speed ft/sec
0	59.0	14.696	1.0000	1.000	1116
1 000	55.4	14.17	.9711	.993	1113
2 000	51.9	13.66	.9428	.986	1109
3 000	48.3	13.17	.9151	.979	1105
4 000	44.7	12.69	.8881	.973	1101
5 000	41.2	12.23	.8617	.966	1097
10 000	23.4	10.11	.7386	.931	1077
15 000	5.5	8.297	.6295	.897	1057
20 000	-12.3	6.759	.5332	.863	1037
25 000	-30.0	5.461	.4486	.828	1016
30 000	-47.8	4.373	.3747	.794	995
35 000	-65.6	3.468	.3106	.760	973
40 000	-69.7	2.730	.2471	.752	968
45 000	-69.7	2.149	.1945	.752	968
50 000	-69.7	1.692	.1531	.752	968
55 000	-69.7	1.332	.1206	.752	968
60 000	-69.7	1.049	.09492	.752	968
65 000	-69.7	.826	.07475	.752	968
70 000	-67.4	.651	.05857	.756	971
75 000	-64.7	.514	.04591	.762	974
80 000	-62.0	.406	.03606	.767	978
85 000	-59.3	.322	.02837	.772	981
90 000	-56.5	.255	.02236	.777	984
95 000	-53.8	.203	.01765	.782	988
100 000	-51.1	.162	.01396	.788	991
110 000	-41.3	.103	8.692-3	.807	1003
120 000	-26.1	.0667	5.428	.836	1021
130 000	-10.9	.0438	3.446	.865	1038
140 000	4.3	.0292	2.222	.894	1056
150 000	19.4	.0197	1.454	.924	1073
160 000	27.5	.0135	9.770-4	.939	1082
170 000	27.5	9.23-3	6.690	.939	1082
180 000	18.9	6.31	4.652	.923	1072
190 000	8.1	4.27	3.225	.902	1060
200 000	-2.7	2.87	2.217	.881	1048

NOTE: 7.011-3 means 7.011×10^{-3}

*$\rho_o = 2.38 \times 10^{-3}$ slugs/ft^3
$= 7.65 \times 10^{-2}$ lbs/ft^3

[redacted]

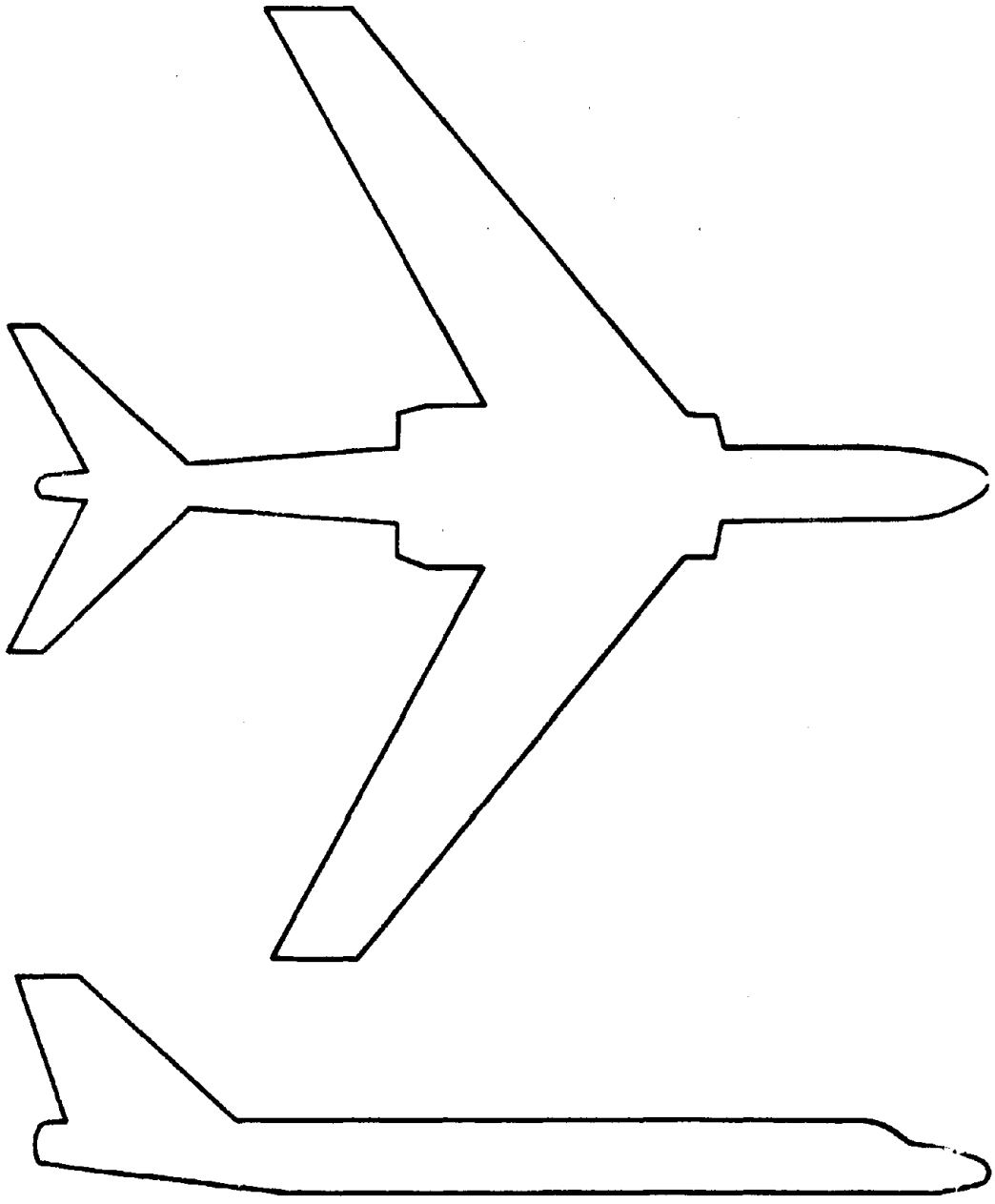

SCALE: 1" = 30'

Figure 13-1. [redacted] Example Airplane (American) [redacted]

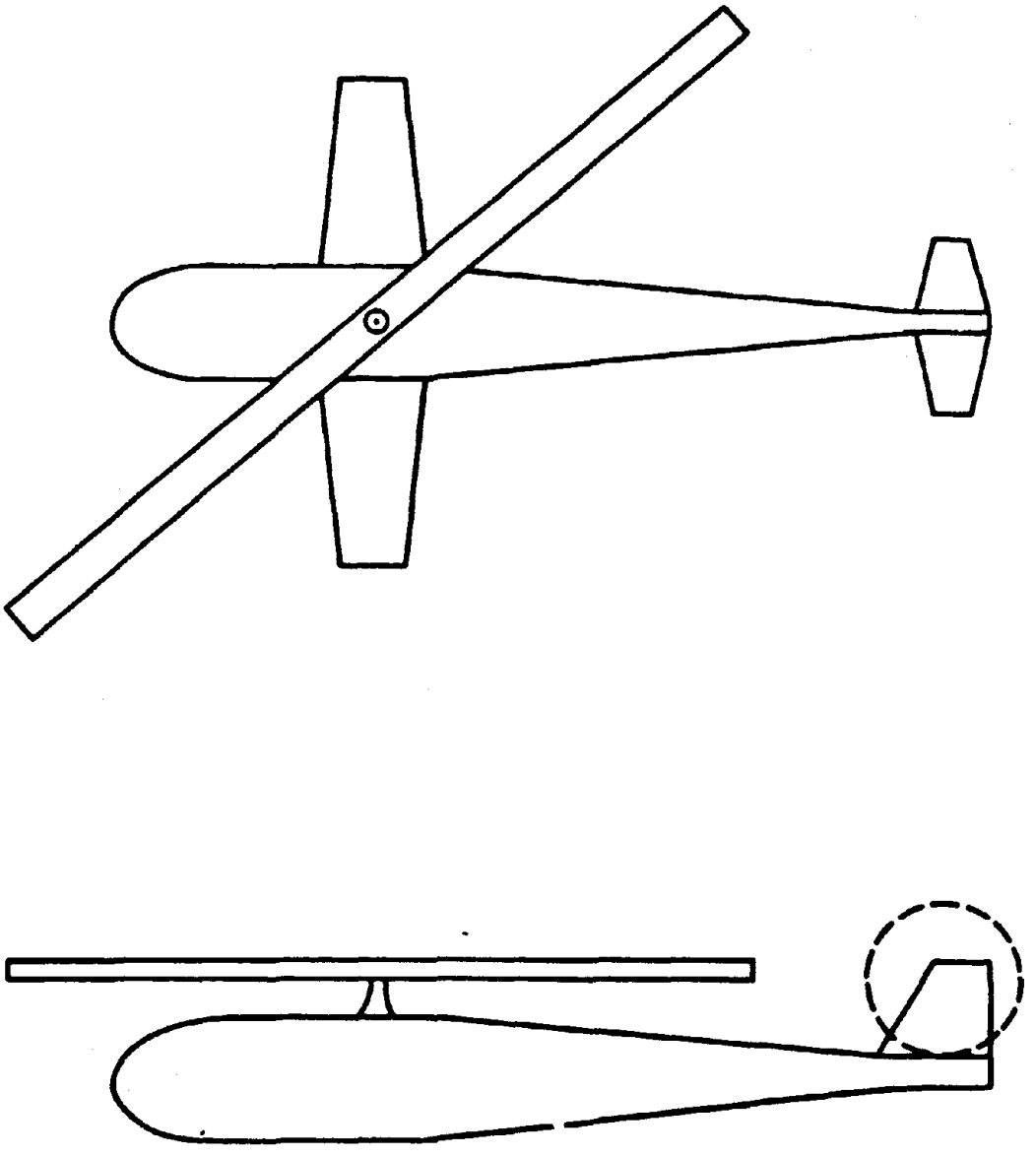

SCALE: 1" =10'

Figure 13-2. [redacted] Example Helicopter [redacted]

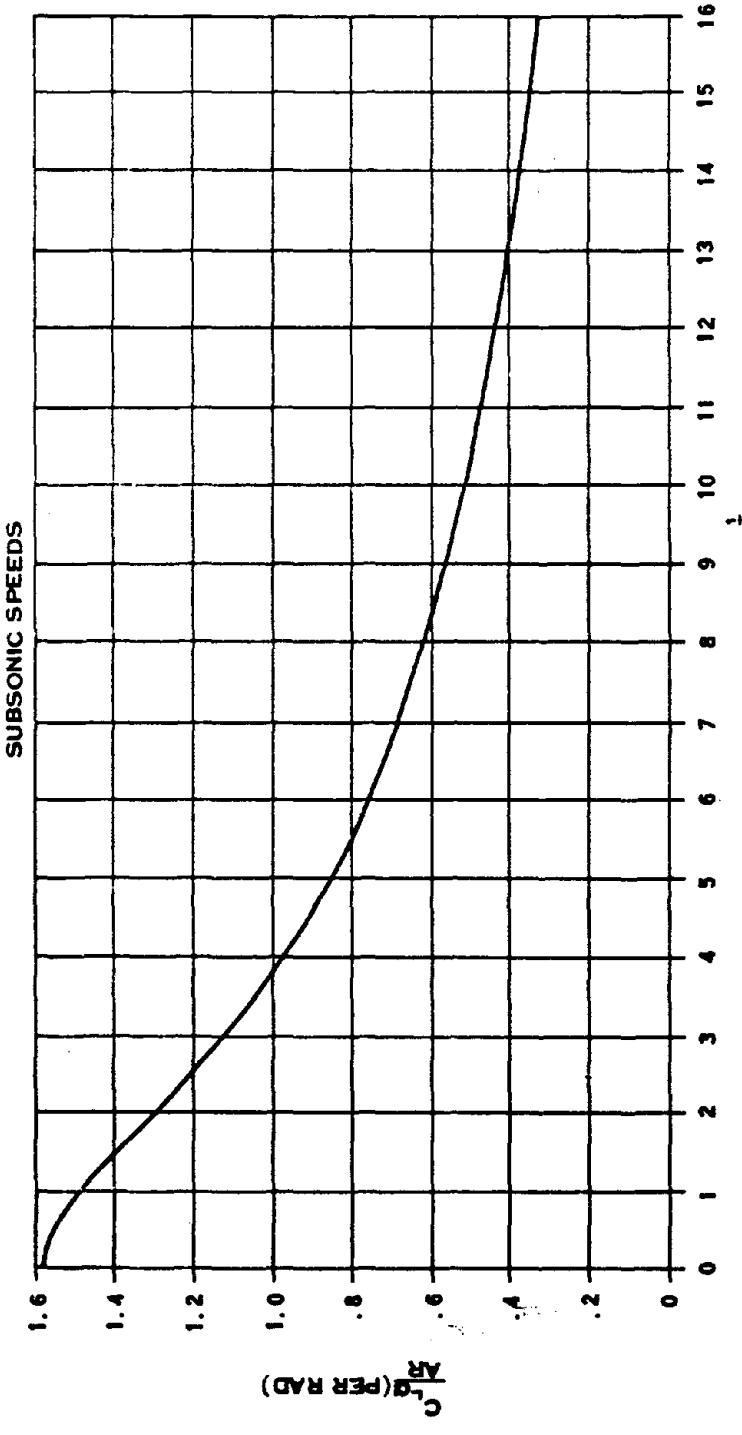

Figure 13-3. [redacted] Subsonic Wing Lift Curve Slope

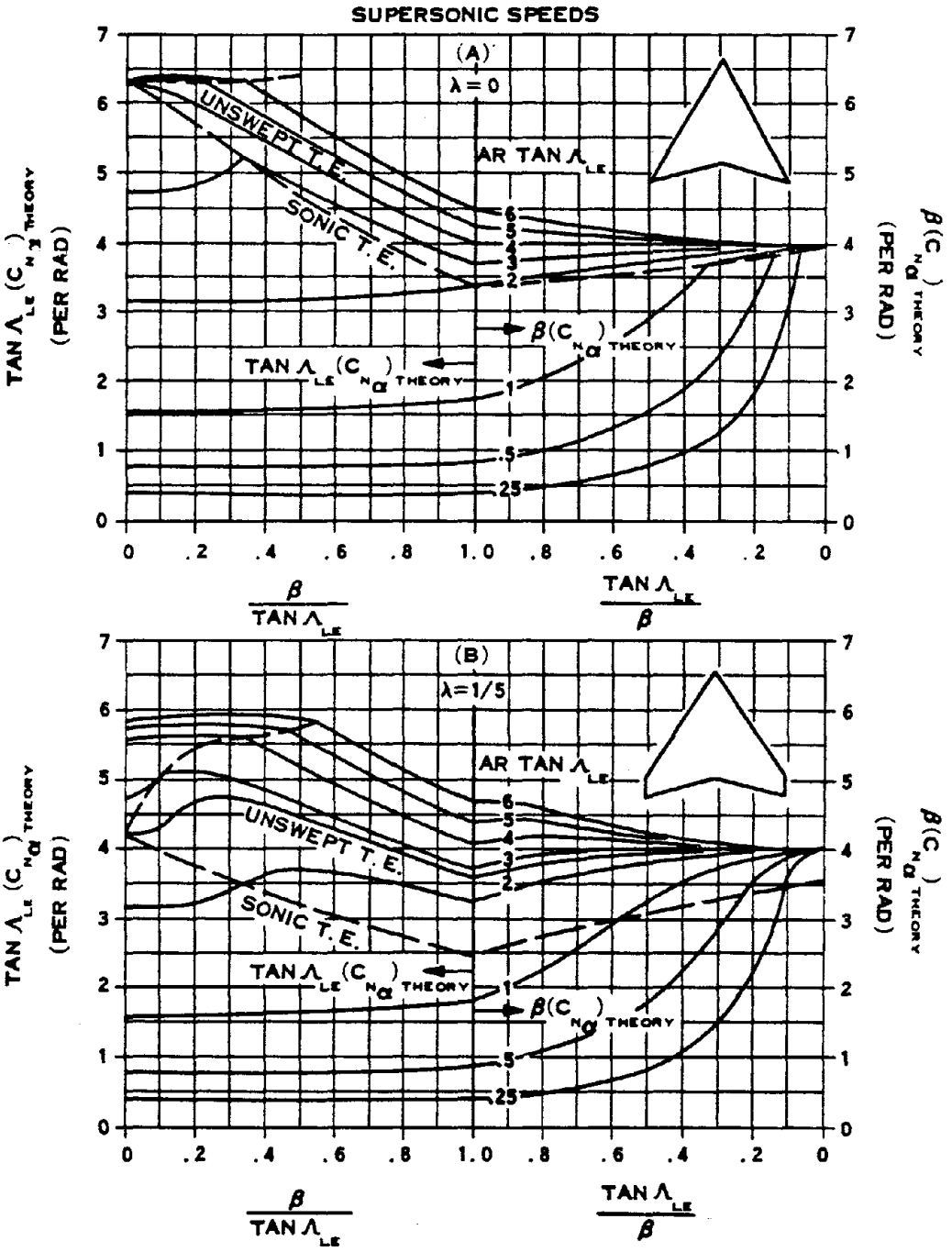

Figure 13-4a. [redacted] Wing Supersonic Normal Force Curve Slope [redacted]

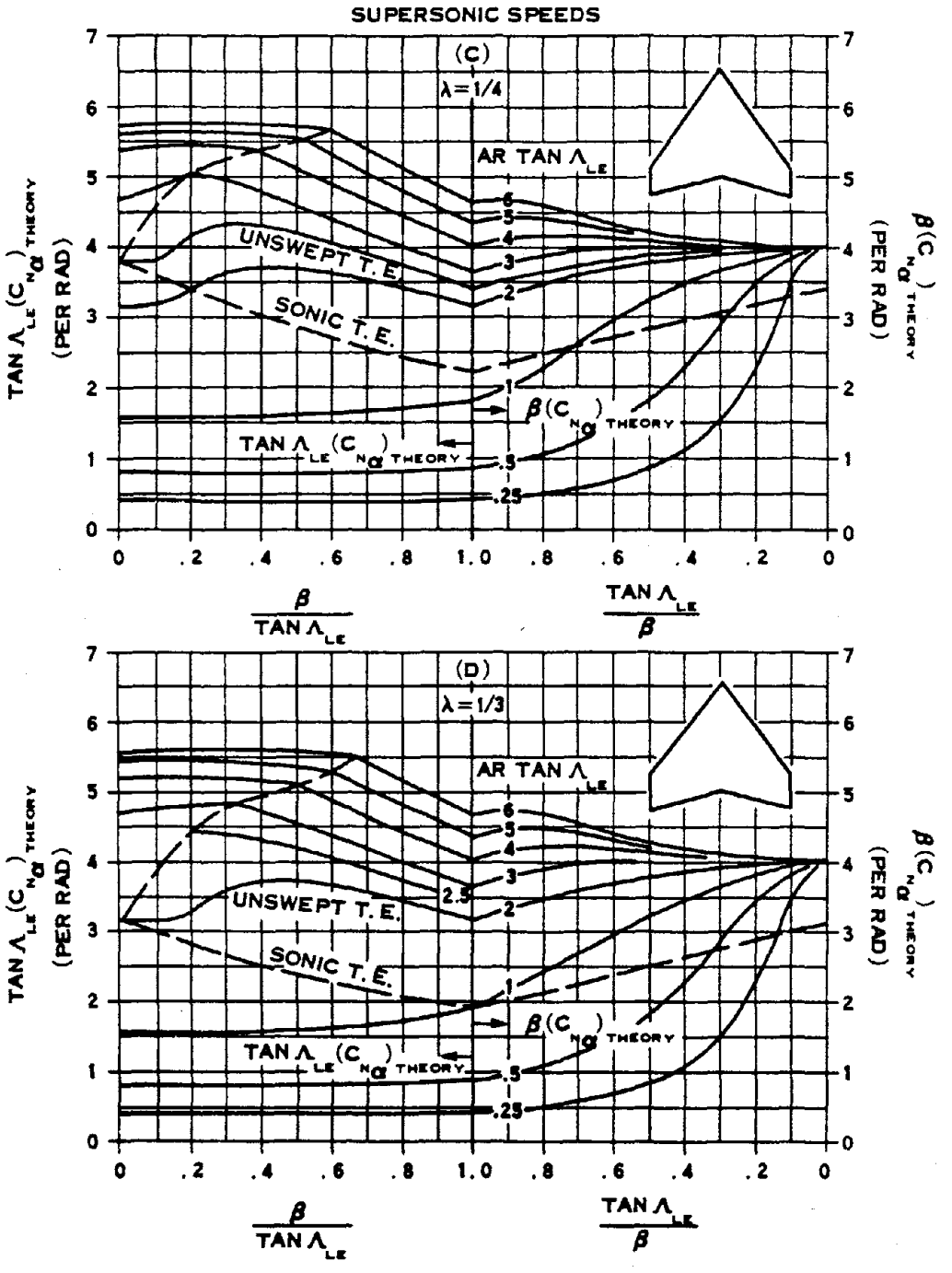

Figure 13-4b. [redacted] Wing Supersonic Normal Force Curve Slope [redacted]

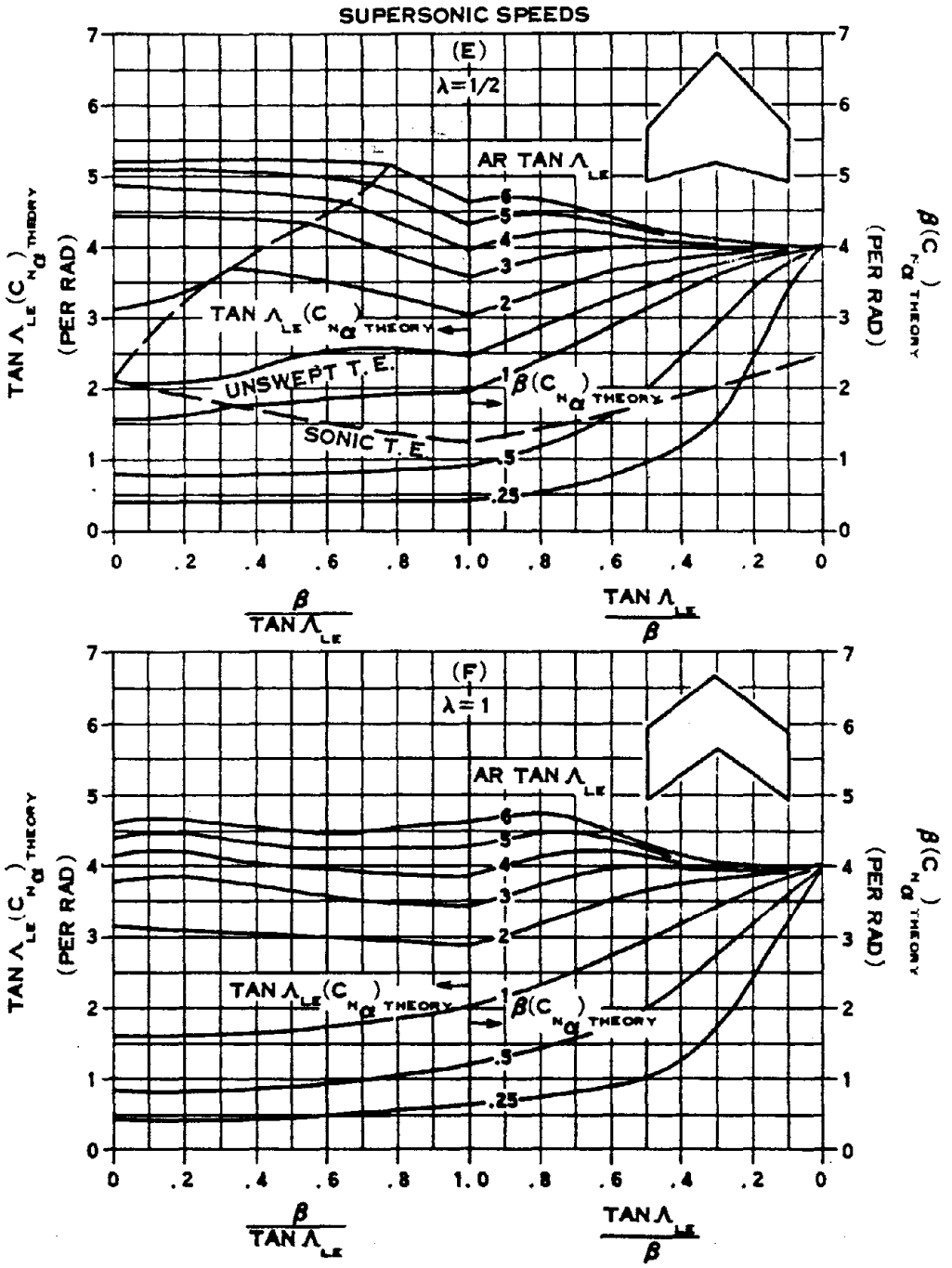

Figure 13-4c. [redacted] Wing Supersonic Normal Force Curve Slope [redacted]

Problem 13-2. Calculation of the Aerodynamic Coefficient for the Vertical Tail

An effective aspect ratio is derived to account for interference effects from the body and the horizontal tail to predict the lateral force on the vertical tail at subsonic speed:

$$AR_{\text{eff}} = \left\{\frac{(AR)_B}{AR}\right\}\left\{1 + K_H\left[\frac{(AR)_{HB}}{(AR)_B} - 1\right]\right\}(AR),$$

where AR is the aspect ratio of the isolated vertical tail, with the span and area of the vertical tail measured to the fuselage centerline; the factor $(AR)_B/AR$ is the ratio of the aspect ratio of the vertical tail in the presence of the fuselage to the aspect ratio of the isolated tail (this ratio is shown in Figure 13-5); the factor K_H accounts for the relative size of the horizontal and vertical tails, and it varies from 0 to about 1.1; and the factor $(AR)_{HB}/(AR)_B$ is the ratio of the vertical tail aspect ratio in the presence of *both* the horizontal tail and body to that of the vertical tail in the presence of the body alone, which varies from 0.9 to 1.2 for typical configurations. Within the accuracy goals of the present calculations, it is reasonable to take this ratio as unity, which gives

$$(AR)_{\text{eff}} = \left(\frac{(AR)_B}{AR}\right) AR.$$

A first approximation for the lift coefficient for the vertical tail, $\bar{C}_{L_\alpha}$, is determined from the wing lift curve slopes shown in Figures 13-3 and 13-4, using the effective aspect ratio $(AR)_{\text{eff}}$. The value of C_{L_α} should be corrected by an empirical factor k, which is a function of the vertical tail span and the body diameter:

$$C_{L_\alpha} = k\,\bar{C}_{L_\alpha}.$$

The diameter k may be obtained from Figure 13-6. All coefficients are based on the dynamic pressure and the elevation area of the isolated vertical tail.

For *direct* side-on blast orientation cases for parked aircraft, the normal force coefficient is obtained from drag data for flat plates in streams normal to the plates. Data indicate that a drag coefficient of 1.2 would apply to plates having an aspect ratio from unity to about 10, which essentially encompasses the range of aspect ratios for vertical tails of current aircraft. Therefore, for analysis of effects on side-on gusts on parked aircraft, a coefficient of 1.2 has been used.

The drag force on the fuselage also becomes important for parked aircraft subjected to side-on gusts. Values of the steady-state drag coefficient vary from about 0.35 to 1.2, depending upon the Reynolds number, which dictates whether the flow is laminar or turbulent. In the case of unsteady drag, a drag coefficient slightly below the laminar value of 1.2 appears to be applicable at early times. Therefore, a drag coefficient of 1.2 has been used for the fuselage for the analysis of the effects of side-on gusts on parked aircrafts.

For supersonic speeds, the slope of the lift coefficient curve C_{L_α} is estimated by the normal force slope for similar wings. In this calculation, C_{L_α} is computed for a wing having a planform of the isolated vertical tail plus its image about the fuselage centerline, using the method given in Problem 13-1, e.g., C_{L_α} is computed for the isolated vertical tail with its image as if it were a wing. The isolated vertical tail which extends from the tip to the fuselage centerline is considered; its area includes, in addition to the exposed part, that area within

the fuselage bounded by the extensions of the leading and trailing edges and the fuselage centerline.

The calculation of the aerodynamic coefficient for vertical tails is presented in the following steps. Several of the lengths and areas that are required already will have been determined in the particular response method being followed, which requires the calculation of C_{L_α} (see Problem 13-1).

1. Using the silhouette profile of the aircraft (for example, see Figures 13-1 and 13-2), from which lengths and surfaces may be found, determine the following:

S = vertical tail area (sq ft), defined by the extensions of the leading and trailing edges to the fuselage centerline.

c_r = vertical tail root chord (ft), i.e., the length along the fuselage centerline subtended by the leading and trailing edges.

c_t = vertical tail tip chord (ft), defined as the length along the fuselage centerline subtended by the vertical tail tip.

b = vertical tail span, fuselage centerline to tip (ft).

Λ_{LE} = sweepback angle of vertical tail leading edge, measured from the vertical (deg).

d = fuselage depth at the intersection of the vertical tail leading edge and the fuselage (ft).

M = Mach Number = V/c, where V is the velocity of the aircraft, and c is the ambient speed of sound.

2. Calculate the taper ratio λ:

$$\lambda = \frac{c_t}{c_r}$$

and the aspect ratio AR:

$$AR = \frac{b^2}{S}.$$

3. Calculation of the aerodynamic coefficient for the vertical tail depends on the value of the Mach number, M. Three regions are defined as follows:

Region 1: $M \leqslant 0.85$,

Region 2: $M \geqslant 1.2$,

Region 3: $0.85 < M < 1.2$.

Region 1. Steps a through g present the calculation of the aerodynamic coefficient for the vertical tail C_{L_α} for $M \leqslant 0.85$.

a. Calculate the value of β^2:

$$\beta^2 = 1 - M^2.$$

b. Determine the tangent of the sweep angle of the mid-chord line, $\tan \Lambda_{c/2}$:

$$\tan \Lambda_{c/2} = \tan \Lambda_{LE} - \frac{2}{AR}\left[\frac{1 - \lambda}{1 + \lambda}\right].$$

c. Calculate the parameter b/d. With the value of this parameter and the value of λ from step 2, enter Figure 13-5 to obtain the value of AR_B/AR.

d. Calculate the effective aspect ratio

$$(AR)_{eff} = \left(\frac{(AR)_B}{AR}\right) AR.$$

e. Compute the parameter

$$(AR)_{eff}\left[\beta^2 + \tan^2 \Lambda_{c/2}\right]^{1/2},$$

and enter Figure 13-3 with this parameter to obtain the value of C_{L_α}/AR.

f. With the value of b/d from step c, enter Figure 13-6 to obtain the value of k, an empirical factor, which is a function of the vertical tail span and the body diameter.

g. Calculate the aerodynamic coefficient for the vertical tail C_{L_α}:

$$C_{L_\alpha} = k \left(\frac{C_{L_\alpha}}{AR}\right) (AR)_{\text{eff}}.$$

Region 2. The calculation of C_{L_α} is the same as that given for Region 2, in Problem 13-1, except that AR is twice that calculated in step two of Problem 13-1, i.e.,

$$AR = 2\left(\frac{b^2}{S}\right).$$

The remaining steps are described once again below.

a. Calculate the value of β:

$$\beta = (M^2 - 1)^{1/2}.$$

b. Calculate the values of the parameters:

$$\frac{\beta}{\tan \Lambda_{LE}}$$

$$(AR) \tan \Lambda_{LE}.$$

c. Enter Figure 13-4 and select the figure corresponding to the taper ratio λ. Select the curve corresponding to the value of the parameter $(AR) \tan \Lambda_{LE}$. If

$$\frac{\beta}{\tan \Lambda_{LE}} < 1,$$

use the left side of the figure to obtain the value of $\tan \Lambda_{LE} C_{N_\alpha}$. Calculate C_{L_α} as follows:

$$C_{L_\alpha} = \frac{\tan \Lambda_{LE} C_{N_\alpha}}{\tan \Lambda_{LE}},$$

where the normal force coefficient C_{N_α} and C_{L_α} are taken to be equal within the scope of this method.

If

$$\frac{\beta}{\tan \Lambda_{LE}} > 1,$$

determine its reciprocal,

$$\frac{\tan \Lambda_{LE}}{\beta},$$

and use the right side of the figure to obtain the value of βC_{N_α}. The slope is calculated by:

$$C_{L_\alpha} = \frac{\beta C_{N_\alpha}}{\beta},$$

where C_N is represented as C_L within the scope of this method.

Region 3. The following steps, a through c, are used to calculate C_{L_α} for $0.85 < M < 1.2$.

a. Calculate C_{L_α} at $M = 0.85$ following the method in Region 1.

b. Calculate C_{L_α} at $M = 1.2$ following the method in Region 2.

c. Interpolate linearly for the slope at the actual Mach number:

$$C_{L_\alpha} = C_{L_\alpha} (\text{at } M = 0.85) + \frac{M - 0.85}{0.35}\left[C_{L_\alpha} (\text{at } M = 1.2) - C_{L_\alpha} (\text{at } M = 0.85)\right].$$

[redacted] No numerical example is provided with this problem since the procedures are so similar to those of Problem 13-1, and since the calculation of the aerodynamic coefficient for the vertical tail is not required for the calculation of the simplified gust loading sure-safe and sure-kill envelopes described in succeeding problems.

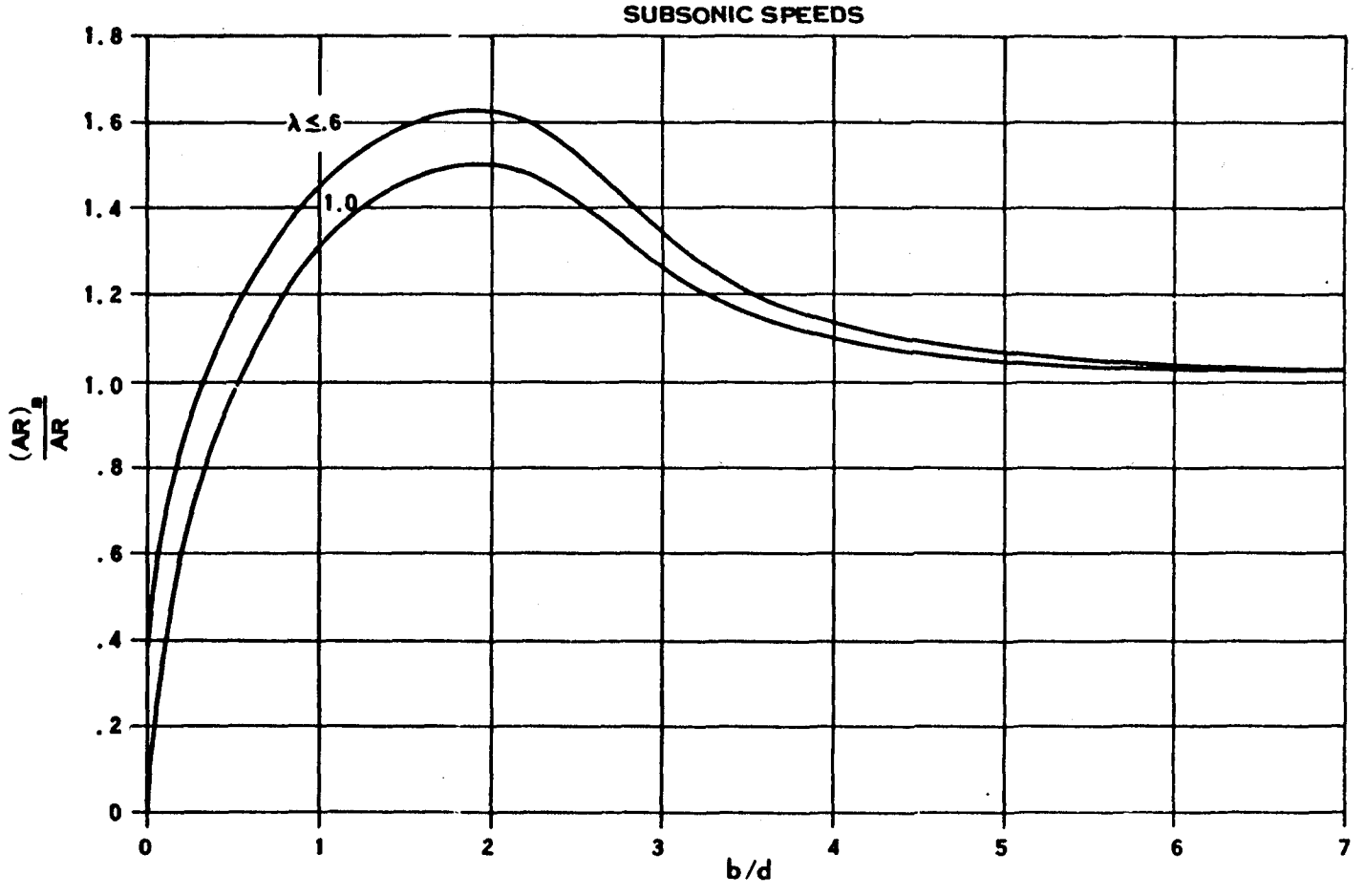

Figure 13-5. Ratio of the Aspect Ratio of the Vertical Tail in the Presence of the Body to That of the Isolated Vertical Tail at Subsonic Speeds

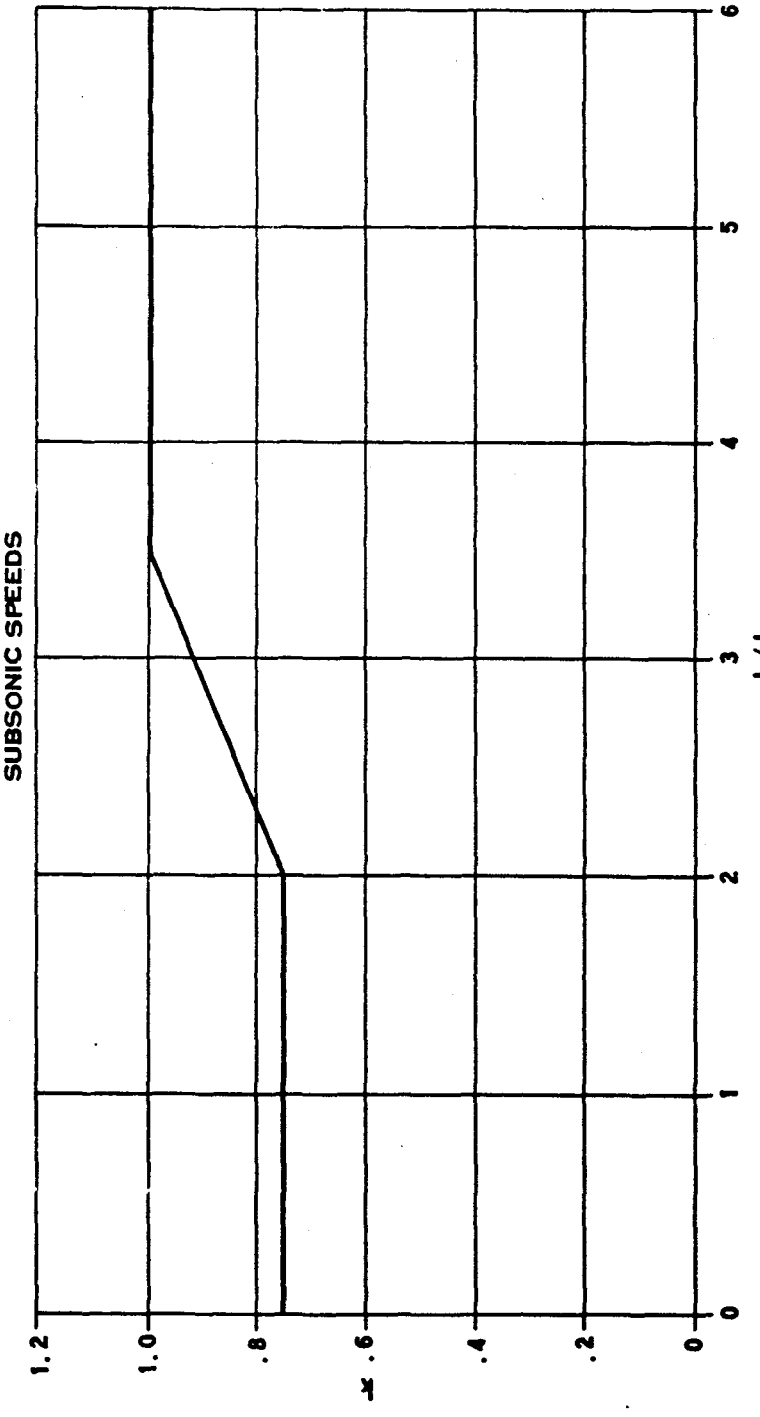

Figure 13-6. [redacted] Empirical Factor for Estimating C_{L_α} for Vertical Tails [redacted]

13-7 Gust Effects on In-Flight Aircraft

A nuclear explosion produces a blast wave that travels outward from the explosion, decaying in strength as it travels. The blast wave induces a flow velocity in the material (in this case, air), through which it passes. This material velocity, or gust, produces changes in the dynamic pressure and the angle of attack of an airplane that is intercepted by the blast wave. An increase in air density also is associated with the blast wave, and this increase in density also contributes to changing the dynamic pressure. The changes in angle of attack and dynamic pressure result in changes in the aerodynamic forces acting on the airplane. These changes in aerodynamic forces produce rigid-body and elastic motions of the airplane. In the sure-kill case, inelastic motions also are important. These motions produce additional aerodynamic forces. The aerodynamic forces and inertia forces may be summed to determine structural loads (such as bending moments) acting on the structure. Comparison of these structural loads with the allowable loads determines the safety of the airplane.

Gust effects on helicopters must be considered in two categories; first, the effects on the main rotor blades, and second, the effects on major components other than the main rotor blades. The second category of effects is very similar to the gust effects on airplanes. The only difference lies in the introduction of rotors as lift-producing devices. Helicopters have fuselages, horizontal tails, vertical tails, and, in some cases, even wings. These components may be analyzed in substantially the same way that the corresponding airplane components are analyzed.

The main rotor blades on the other hand, are unique to helicopters, and thus require special techniques. Three different types of blades must be considered: hinged, rigid (hingeless), and teetering. In the hinged version, a hinge somewhat offset from the center of rotation permits free rotation of the blade outboard of the hinge in an up-and-down, or flapping, direction. The rigid, or hingeless, blade does not use a flapping hinge. The teetering blade roughly combines the characteristics of the hinged and hingeless blades. A teetering blade is essentially a seesaw about a hinge at the center of rotation. The blades on each side of the hinge are rigidly connected.

Problems 13-3 and 13-4 describe the calculation of intercept-time envelopes for sure-safe and sure-kill regions for airplanes and helicopters, respectively.

13-8 Gust Effects on Parked Aircraft

The material velocity and the increased density behind the blast wave give rise to a dynamic pressure that may be sufficiently high to impose large aerodynamic forces on a parked vehicle. For purposes of damage analysis, dynamic pressure effects are classified in two categories:

1. Direct damage to structural components that result from aerodynamic loading.

2. Gross aircraft motions that might produce indirect damage to structural components as a result of lifting the aircraft from the ground and the subsequent impact, or as a result of overturning the aircraft or crushing the landing gear.

The possibility of lifting the aircraft exists whenever the vehicle is subjected to lift forces that are comparable to the vehicle weight, even if tie-downs are employed. An aircraft with a low wing loading (gross weight divided by the wing area, GW/S) is particularly susceptible to this type of damage since, in the parked position, the wing is set at a large angle of attack relative to the ground. Head-on encounter presents the most severe loading condition for this case.

[redacted]

[redacted] Skidding is possible whenever the drag, coupled with the lift, can overcome the frictional forces between the ground and the vehicle tires. With a large lift force, the normal force between ground and tire is reduced. The side force required to cause the vehicle to skid may thus be quite small compared with the weight of the vehicle. Vehicle orientations somewhere between head-on and side-on to the gust are expected to present the worst situation for this type of motion. No definitive criteria can be given for damage from skidding, because the damage criteria depend upon the distance of the aircraft from other objects.

[redacted] In some cases, the vehicle will overturn before skidding. Overturning will occur whenever the aerodynamic moments (about an axis joining appropriate wheel contact points) are of sufficient magnitude to overcome the stabilizing gravity moment and the frictional forces are sufficiently large to prevent skidding. A gust orientation somewhere between head-on and side-on is expected to provide the most severe condition. Other effects will almost always be predominant compared to overturning, and it is exceedingly difficult to devise a meaningful overturning solution that does not involve a substantial computer program.

[redacted] Negative lift results from tail-on encounters (blast approaching from the rear). The negative lift produces downward forces on the wheels, which, if sufficiently large, will damage the landing gear and perhaps the main supporting structure.

[redacted] Tie-downs would be expected to reduce the likelihood of lift-off, skidding, and overturning; however, tests have indicated that tie-downs are not very effective in reducing damage induced by motion when aircraft encounter high strength blast waves.

[redacted] Since helicopters do not have the large lifting surfaces that are present on airplanes, the problems of lift-off and crushing of the landing gear are much less severe for helicopters than for airplanes.

[redacted] Overpressure usually dictates the largest envelopes among all of the damage modes for parked aircraft. No calculation methodology is presented for gust effects on parked aircraft. The sure-safe and sure-kill overpressure envelopes may be accepted as the complete envelopes (see paragraph 13-9 and Problem 13-5).

[redacted]

Problem 13-3. Calculation of Intercept-Time Envelopes that Determine Sure-Safe and Sure-Kill Regions with Respect to Material Velocity on Airplanes in Flight

The analysis of gust effects on airplanes in flight is based upon determining the load factor produced on the airplane during the blast encounter, accounting roughly for the fact that this load factor is dynamically applied, and comparing the resultant effective load factor with the critical load factor. For sure-safe conditions, the critical load factor is based upon design limit conditions. For sure-kill conditions, the critical load factor is based upon design ultimate conditions and a lethal ratio factor. The lethal ratio factor is determined from a simple representation of post-failure response by a single degree of freedom system.

Standard shapes for the gust envelopes at intercept time are assumed applicable for all airplanes, weapon yields, and altitudes. Each point on the envelope shows the critical position of the airplane relative to the burst point at the time when the airplane is intercepted by the blast wave. The size of the envelopes is determined by evaluating the critical slant ranges, or distances from the burst point, associated with intercepts of the airplane from directly above, below and to the side.

The three slant ranges R_a, R_b, and R_s that represent critical distances from above, below and to the side of the airplane, respectively, from which intercept-time envelopes are determined, must be calculated. The data required for the calculations include:

h = airplane altitude (ft),

W = weapon yield (kt),

GW = airplane gross weight at time of interest (lbs),

V = preblast airplane velocity (ft/sec),

n = airplane preblast load factor (for a level flight, $n = 1$) (dimensionless),

N^+ = up-loading airplane limit load factor corresponding to gross weight condition being considered (dimensionless),

N^- = down-loading airplane limit load factor corresponding to gross weight condition being considered (N^- should be used as a negative number) (dimensionless),

Wing planform (see Figure 13-1).

Calculation of the three slant ranges for sure-safe conditions is performed by the following series of steps.

1. Enter Table 13-1 with the airplane altitude, h, to obtain P, the ambient pressure (psi), ρ, the ambient density (slugs/ft^3), and c, the ambient speed of sound (ft/sec).

2. Calculate the Mach number, M:

$$M = \frac{V}{c}.$$

With M, and data defining wing planform, calculate the slope of the lift coefficient curve for the wing, C_{L_α}, using the method described in Problem 13-1.

3. Enter Figure 13-7 and select the curve corresponding to GW, airplane gross weight. Obtain the value of DF, the dynamic factor corresponding to the weapon yield, W.

4. To determine the slant range, R_a, for a burst from above

$$N = N^-,$$

where N is the critical load factor.

5. If

$$n < 0 \text{ and } N < 0,$$

or

$$n < 0 \text{ and } N > 0,$$

reverse the signs of both n and N. Otherwise, leave the signs as they were calculated. If

$$n < 0.01,$$

set

$$n = 0.01.$$

Thus, n will become positive in this step, regardless of its original sign.

6. Calculate $\Delta L/L$, ratio of the incremental lift due to blast to the preblast value of lift as follows:

$$\frac{\Delta L}{L} = \left[\frac{N}{n} - 1\right]\left[\frac{1}{(DF)}\right].$$

7. Calculate w/c, the ratio of the component of the airplane velocity normal to the wing (w) to the speed of sound:

$$\frac{w}{c} = \frac{2n\ (GW)}{\rho\ VSC_{L_\alpha}c},$$

where S is the airplane wing area, and the other symbols have been defined.

8. Calculate the product of $\Delta L/L$ and w/c.

9. Select the curve in Figure 13-8 corresponding to the value of w/c obtained in step 7. Enter the graph with the value of $(w/c)\ (\Delta L/L)$ obtained in step 8, and read the corresponding value of the range parameter $\bar{R}$. If N is positive, use Figure 13-8a. If N is negative, use Figure 13-8b.

10. Compute R_a, the range (ft), which defines the distance at which a nuclear explosion would produce critical effects, as follows:

$$R_a = \bar{R}\left[\frac{14.7\ W}{P}\right]^{1/3}.$$

11. Repeat steps 4 through 10 to calculate R_b. In step 4, set

$$N = N^+$$

for bursts from below, and replace R_a with R_b in the equation of step 10.

12. Set

$$N = N^+,$$

and $n = 1$ (corresponding to straight on level flight). Repeat steps 6 through 10 to calculate R_s (R_s replaces R_a in the equation of step 10). A burst from the side is taken to be equivalent to a burst from below with the airplane in straight and level flight.

13. The ranges R_a, R_b, and R_s define the size of the standard sure-safe envelopes as illustrated in Figure 13-9. R_a represents the diameter of a sphere above the airplane; R_b is the diameter of a sphere below; and R_s is the diameter of a sphere to the side of the airplane. The X-Y plane is the plane of symmetry of the airplane, with the preblast velocity vector pointing in the direction of the positive X-axis; the Y-axis points in the direction of the right wing; the Z-axis is directed upward, thus determining an orthogonal, left-handed system. The envelopes are symmetric with respect to the X-Z plane.

Calculation of the slant ranges R_a, R_b, and R_s, that define the size of the standard envelopes at intercept time for sure-kill conditions is performed by the following series of steps.

1. Follow steps 1 through 3 in the calculation of the ranges for sure-safe conditions.

[redacted]

2. Enter Figure 13-10 and select the curve corresponding to GW, airplane gross weight. With weapon yield, W, obtain the value of LR, the lethal ratio.

3. To determine R_a, the slant range for burst from above, calculate N, the critical load factor:

$$N = (1.5)(N^-)(LR),$$

where the factor 1.5 is the usual factor between limit load and ultimate load. Follow steps 5 through 10 in the calculation for sure-safe conditions.

4. To determine R_b for burst from below, calculate N:

$$N = (1.5)(N^+)(LR),$$

and follow steps 5 through 10 in the calculation for sure-safe conditions.

5. To determine R_s, the slant range for burst from the side, calculate N:

$$N = (1.5)(N^+)(LR)$$

and let $n = 1$ since burst from the side is taken as burst from below corresponding to a straight and level flight. Repeat steps 6 through 10 in the calculation for sure-safe conditions.

6. Construct the sure-kill envelopes as described in step 13 in the calculation for sure-safe conditions.

[redacted]

DNA (4)(1)

[redacted]

PAGE 13-32 DELETED

[redacted]

[redacted]

[redacted]

[redacted]

DNA (E-X(1))

The resulting intercept time envelopes are illustrated in Figure 13-9.

[redacted] *Reliability:* A typical airplane is used to represent each airplane class for purposes of defining a dynamic factor and a lethal ratio factor. The airplane is in a symmetric flight prior to blast intercept. This definition includes a straight and level flight. All degrees of freedom are ignored except for the two previously mentioned. The atmosphere is assumed homogeneous, having characteristics associated with the altitude at which the airplane is flying. The standard shapes for the gust envelopes at intercept time are assumed to be applicable for all airplanes, weapon yields, and altitudes. The maximum error in the calculation is estimated to be a factor of 2.

[redacted] *Related Material:* See paragraphs 13-1, 13-2, 13-6, and 13-7. See also Table 13-1.

[redacted]

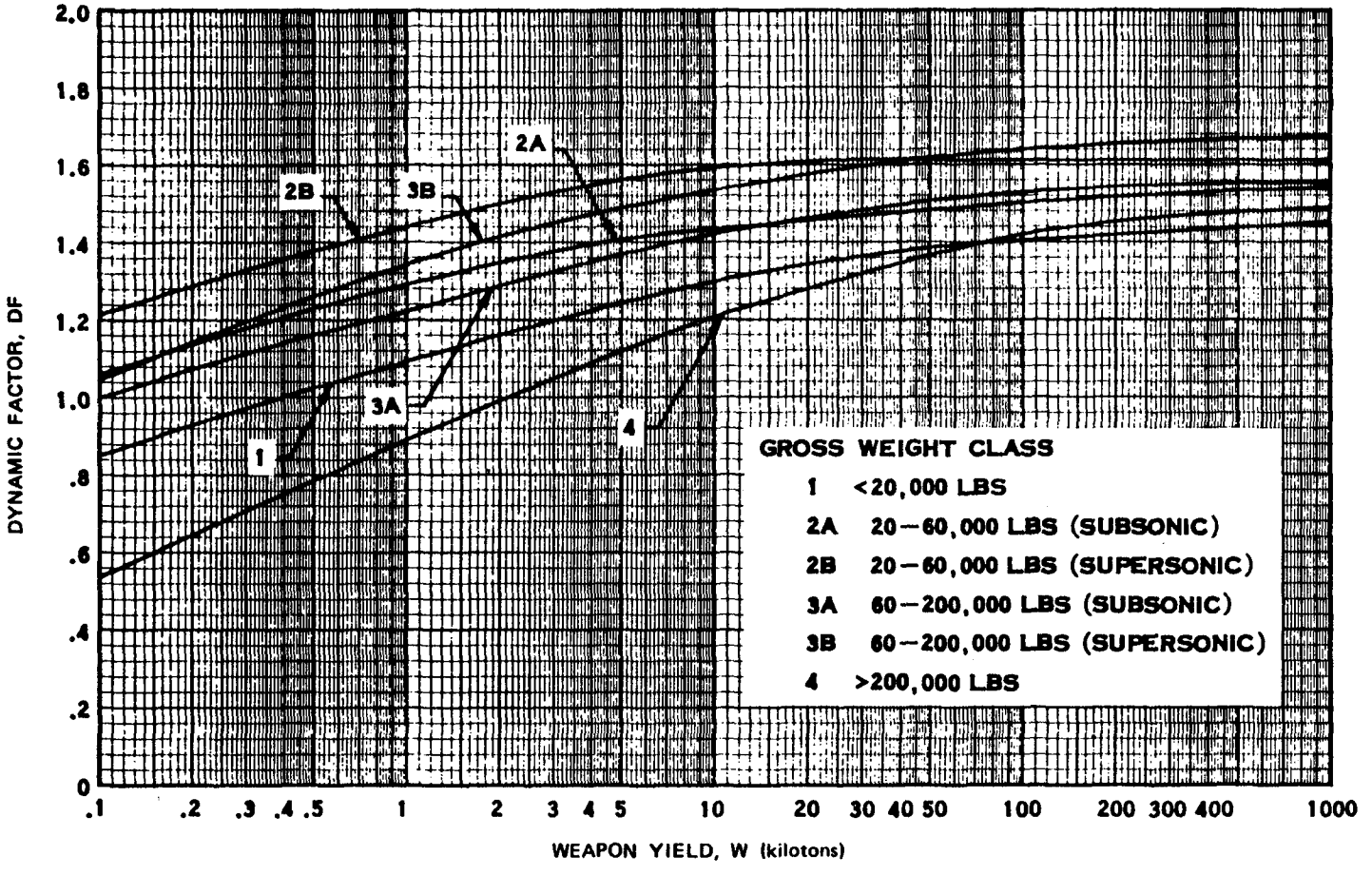

Figure 13-7. [redacted] Dynamic Factor vs Weapon Yield [redacted]

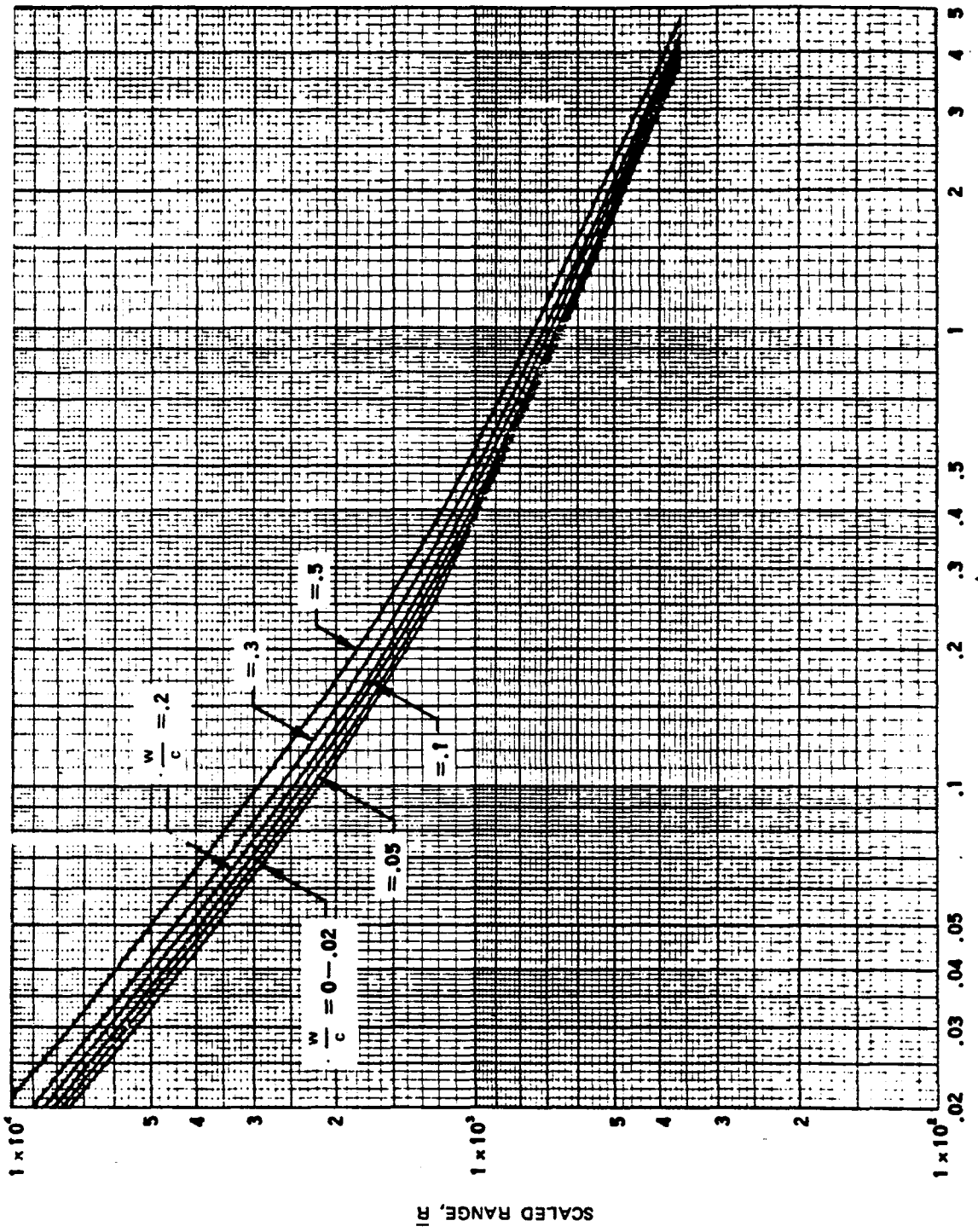

Figure 13-8a. [redacted] $\frac{w}{c} \times \frac{\Delta L}{L}$ as a Function of Scaled Range (N > 0) [redacted]

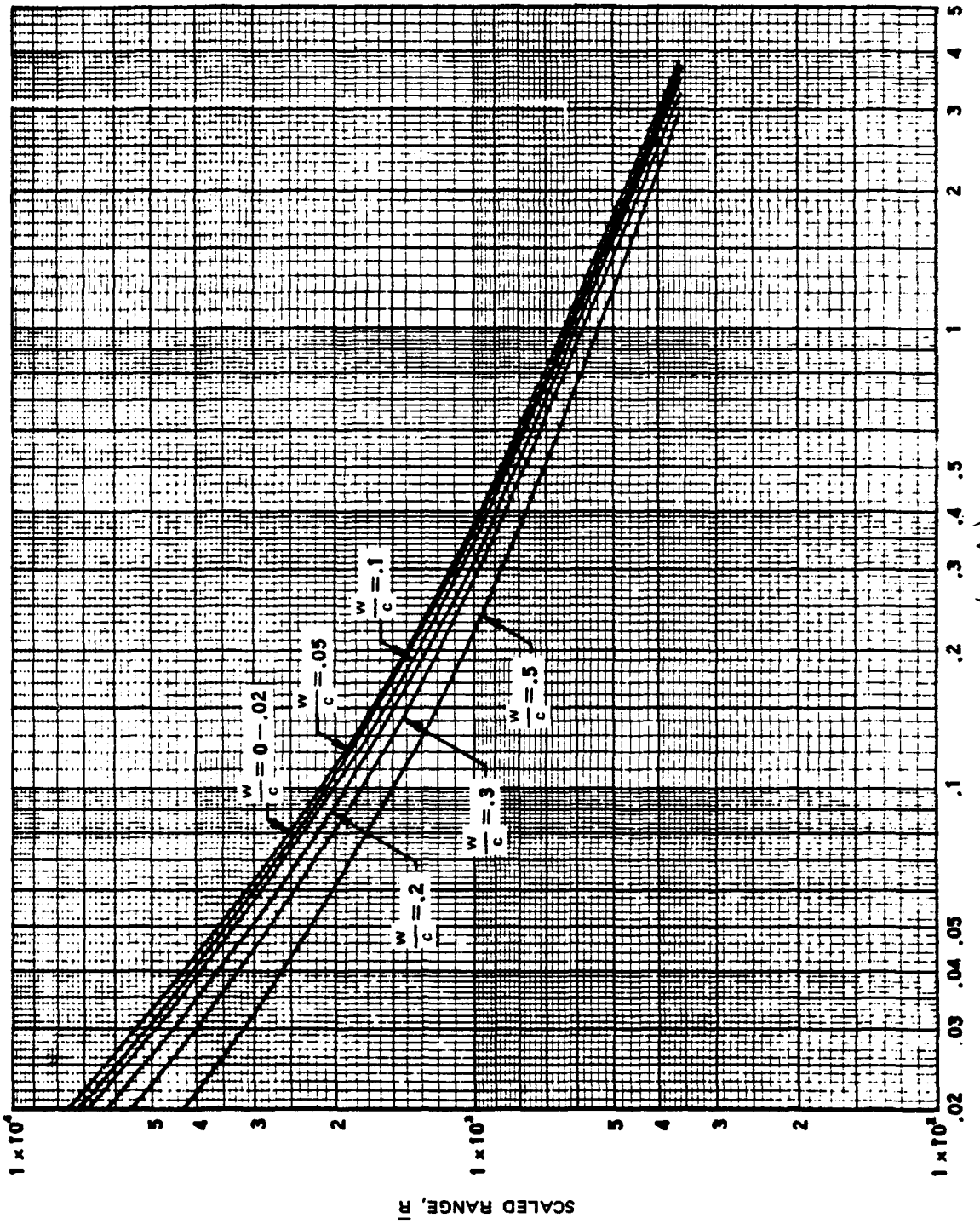

Figure 13-8b. [redacted] $\frac{w}{c} \times \frac{\Delta L}{L}$ as a Function of Scale I Range ($N < 0$) [redacted]

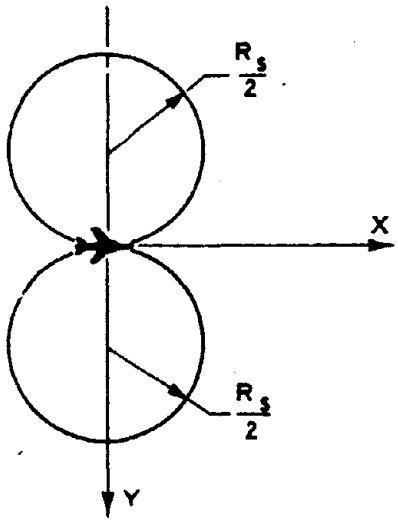

TOP VIEW (SECTION IN X–Y PLANE)

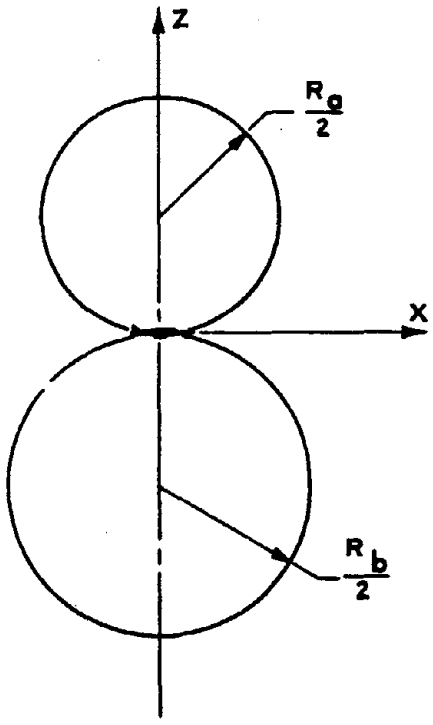

SIDE VIEW (SECTION IN X–Z PLANE)

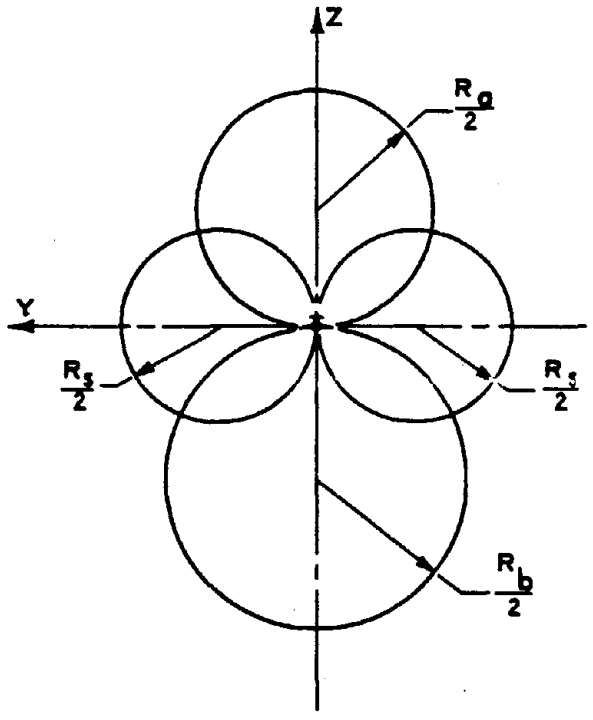

FRONT VIEW (SECTION IN Y–Z PLANE)

Figure 13-9. [redacted] Standard Shapes for Gust Envelopes at Intercept Time [redacted]

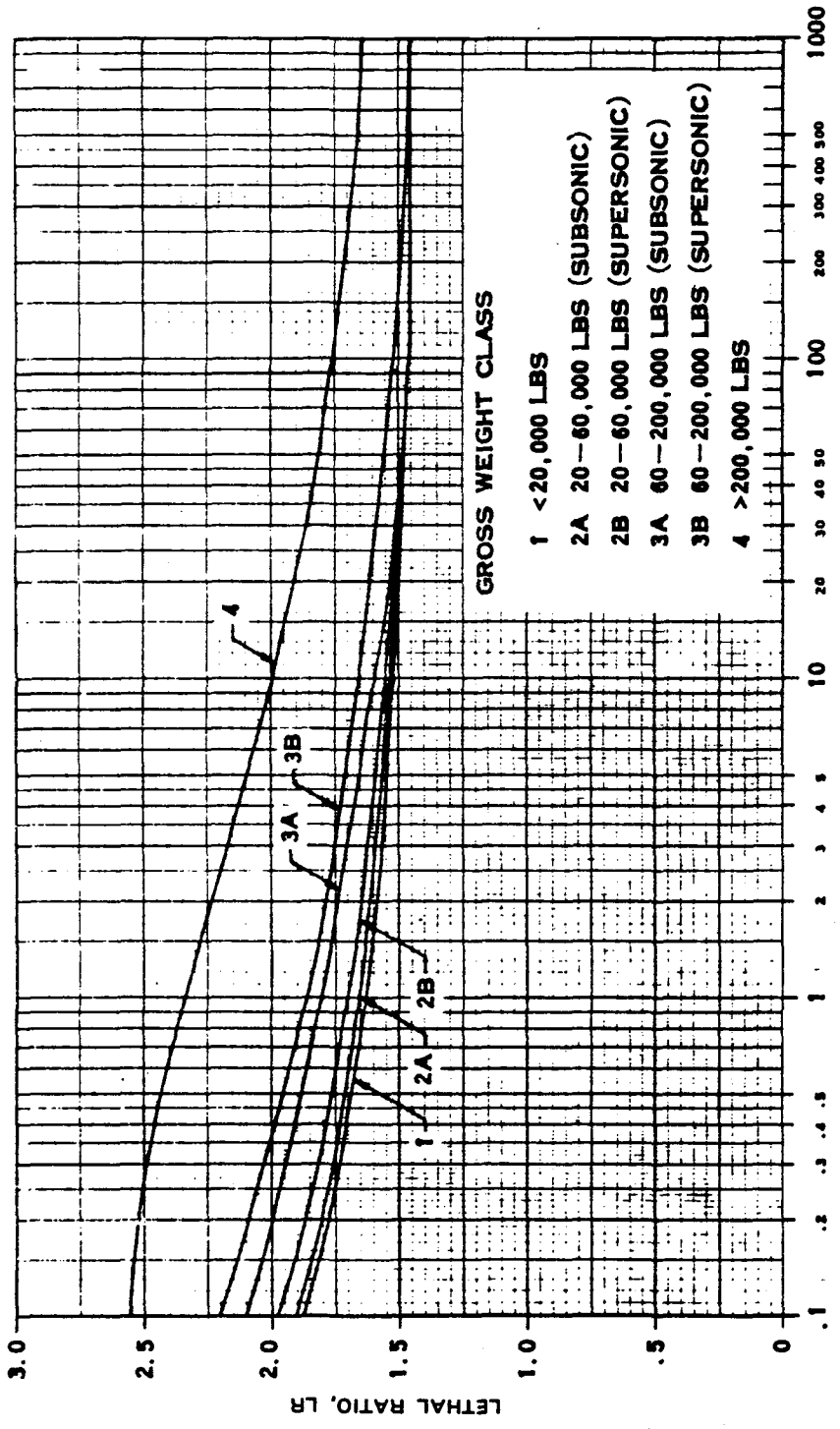

Figure 13-10. [redacted] Lethal Ratio vs Weapon Yield [redacted]

Problem 13-4. Calculation of Intercept-Time Envelopes Determining Sure-Safe and Sure-Kill Regions with Respect to Gust Effects of the Material Velocity Behind the Blast Wave on Helicopters in Flight

The analysis of gust effects on helicopters is based upon determining the load factor produced during the blast encounter, accounting roughly the fact that this incremental load factor is dynamically applied, and comparing the resultant effective load factor with the critical load factor. For sure-safe conditions, the critical load factor is based upon design limit conditions. For sure-kill conditions, the critical load factor is based upon design ultimate conditions and a lethal ratio factor.

Gust effects on helicopters must be considered in two categories: first, the effects on the main rotor blades (hinged, rigid and teetering); and second, the effects on major components other than the main rotor blades, which are very similar to the gust effects on airplanes.

The constraints in the calculation are as follows:

- Representative values of helicopter parameters can be used in defining a dynamic factor and a lethal ratio factor. All other calculations involve the actual helicopter characteristics.
- The helicopter is in a symmetric maneuver prior to blast intercept. This definition includes straight and level forward or hovering flight.
- For a hinged blade, blade response to gust is not considered in this problem; the flapping of a teetering rotor is not considered in the calculation.
- The lift distribution along the blade is linear, starting at zero at the hub and fitted to the actual running lift at the 3/4 blade span position.
- Rigid-body motions of the helicopter are neglected, and the rotor tilt angle is ignored.
- Inflow resulting from the gust is considered to occur too late to influence the response. The effect of the preblast inflow on dynamic pressure is ignored.
- The preblast atmosphere is homogeneous, having characteristics associated with the altitude at which the helicopter is flying.
- Standard shapes for the gust envelopes at intercept time are applicable for all helicopters, weapon yields, and altitudes.

The envelopes calculated in this problem are intercept-time envelopes. The size of the envelopes is determined by evaluating the critical slant ranges, or distances from the burst point, associated with intercepts of the helicopter from directly above, below and to the side.

The three slant ranges R_a, R_b, and R_s representing the critical distances from above, below and to the side, respectively, are calculated first for sure-safe conditions in the following series of steps. The data that are required for the calculations include:

h = helicopter altitude (ft)

W = weapon yield (kt)

GW = helicopter gross weight at time of interest (lbs)

V = preblast helicopter velocity (ft/sec)

Ω_{MR} = main rotor angular velocity (rad/sec)

R_{MR} = main rotor blade radius (ft)

c_{MR} = main rotor blade chord (ft)

b_{MR} = number of blades in main rotor (dimensionless)

n = helicopter preblast load factor; for straight and level flight, $n = 1$ (dimensionless)

N^+ = up-loading helicopter limit load factor corresponding to gross weight condition being considered (dimensionless)

N^- = down-loading helicopter limit load factor corresponding to gross weight condition being considered. Note: N^- should be used as a negative number (dimensionless)

Wing planform (if helicopter has wings).

1. Determine the ambient atmospheric conditions at helicopter altitude h from Table 13-1; P, the ambient pressure (psi); ρ, the ambient density (slugs/ft^3); and c, ambient speed of sound (ft/sec).

2. If the helicopter has no wings, or if a helicopter having wings is hovering, i.e., $V = 0$, go to step 4. Otherwise, calculate the total wing area, S_W, which is defined as the extension of the leading and trailing edges of both wings to the helicopter centerline (ft^2).

3. Using the wing planform (Figure 13-2), with the Mach Number, M, equal to zero, calculate the slope of the lift coefficient curve for the wing, $C_{L\alpha}^W$, using the method described in Problem 13-1. Let $C_{L\alpha}^{MR} = 5.7$, where $C_{L\alpha}^{MR}$ is the lift curve slope for the main rotor.

4. Enter Figure 13-11 with the weapon yield, W, and obtain the corresponding value of DF, the dynamic coefficient.

5. To determine the slant range, R_a, for a burst from above

$$N = N^-,$$

where N is the critical load factor.

6. If

$$n < 0 \text{ and } N < 0,$$

or

$$n < 0 \text{ and } N > 0,$$

reverse the signs of both n and N. Otherwise, leave the signs as they were calculated. If

$$n < 0.01,$$

set

$$n = 0.01.$$

Thus, n will become positive in this step, regardless of its original sign.

7. Calculate $\Delta L/L$, the ratio of the incremental lift due to blast to the preblast value of lift as follows:

$$\frac{\Delta L}{L} = \left[\frac{N}{n} - 1\right]\left[\frac{1}{(DF)}\right].$$

8. Calculate the parameter η:

a. If the helicopter has wings,

$$\eta = \frac{2n\,(GW)}{\rho c\left[\frac{1}{2}C_{L\alpha}^{MR}\left(b_{MR}R_{MR}c_{MR}\right)\Omega_{MR}R_{MR} + C_{L\alpha}^{W}VS_W\right]}.$$

b. If the helicopter has no wings,

$$\eta = \frac{2nGW}{\rho c\left[\frac{1}{2}C_{L\alpha}^{MR}\left(b_{MR}R_{MR}c_{MR}\right)\Omega_{MR}R_{MR}\right]}$$

9. Obtain the product

$$\left[\frac{\Delta L}{L}\right]\eta.$$

10. Enter Figure 13-12a if $N > 0$ or 13-12b if $N < 0$, and select the curve corresponding to the value of η from step 8. With the value of

$$\left[\frac{\Delta L}{L}\right]\eta$$

from step 9, obtain the range parameter $\bar{R}$.

[redacted]

[redacted]

11. Compute R_a, the range (ft), which defines the distance at which a nuclear explosion would produce critical effects, as follows:

$$R_a = \bar{R}\left[\frac{14.7\ W}{P}\right]^{1/3}.$$

12. Repeat steps 5 through 11 to calculate R_b. In step 5, set

$$N = N^+$$

for bursts from below, and replace R_a with R_b in the equation of step 10.

13. Set

$$N = N^+,$$

and $n = 1$ (corresponding to straight on level flight). Repeat steps 7 through 11 to calculate R_s (R_s replaces R_a in the equation of step 10). A burst from the side is taken to be equivalent to a burst from below with the helicopter in straight and level flight.

14. The ranges R_a, R_b, and R_s define the size of the standard sure-safe envelopes as illustrated in Figure 13-13. R_a represents the diameter of a sphere above the helicopter; R_b is the diameter of a sphere below; and R_s is the diameter of a sphere to the side of the helicopter. The X-Y plane is the plane of symmetry of the helicopter with the preblast velocity vector pointing in the direction of the positive X-axis; the Y-axis points to the right side of the helicopter; the Z-axis is directed upward, thus determining an orthogonal, left-handed system. The envelopes are symmetric with respect to the X-Z plane.

(U) Calculation of the slant ranges R_a, R_b, and R_s, that define the size of the standard envelopes at intercept time for sure-kill conditions is performed by the following series of steps.

1. Follow steps 1 through 4 in the calculation of the ranges for sure-safe conditions.

2. Enter Figure 13-14 with weapon yield, W, and obtain the value of LR, the lethal ratio.

3. To determine R_a, the slant range for burst from above, calculate N, the critical load factor:

$$N = (1.5)(N^-)(LR),$$

where the factor 1.5 is the usual factor between limit load and ultimate load. Follow steps 6 through 11 in the calculation for sure-safe conditions.

4. To determine R_b for burst from below, calculate N:

$$N = (1.5)(N^+)(LR),$$

and follow steps 6 through 11 in the calculation for sure-safe conditions.

5. To determine R_s, the slant range for burst from the side, calculate N:

$$N = (1.5)(N^+)(LR)$$

and let $n = 1$ since burst from the side is taken as burst from below corresponding to a straight and level flight. Repeat steps 7 through 11 in the calculation for sure-safe conditions.

6. Construct the sure-kill envelopes as described in step 14 in the calculation for sure-safe conditions.

[redacted]

PAGES 13-42 THRU 13-43 DELETED

[redacted]

[redacted]

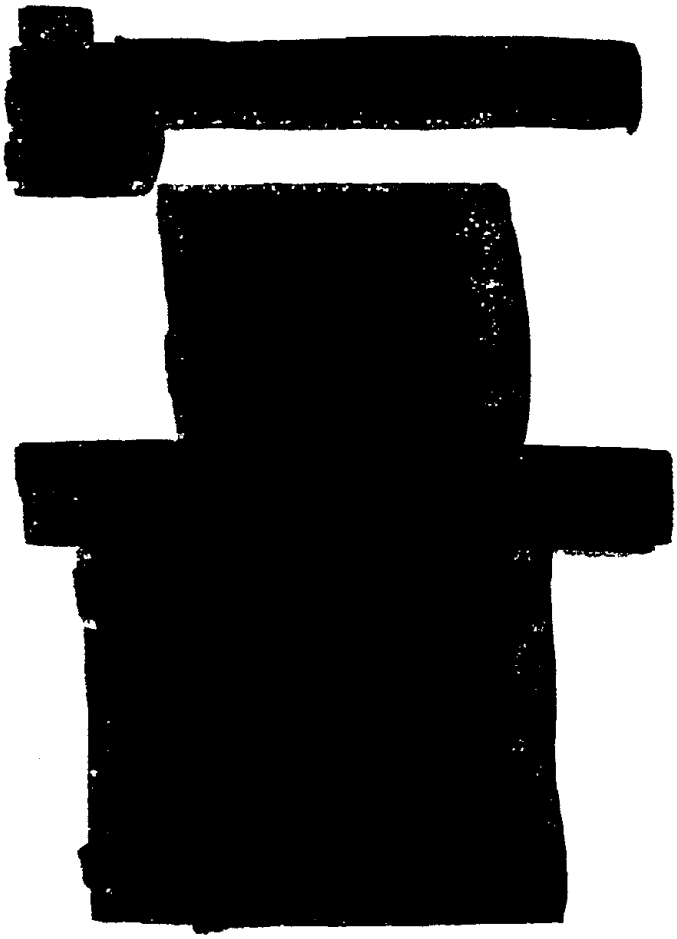

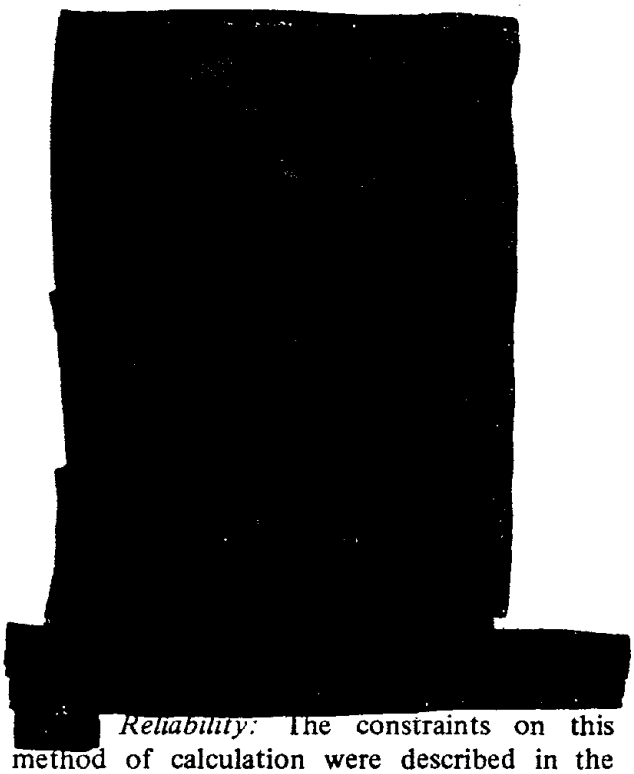

DNA
(C-X1)

[redacted] *Reliability:* The constraints on this method of calculation were described in the introductory paragraphs of this problem. The maximum error is a factor of 2.5.

[redacted] *Related Material:* See paragraphs 13-6 and 13-7, and Problem 13-1. See also Table 13-1.

[redacted]

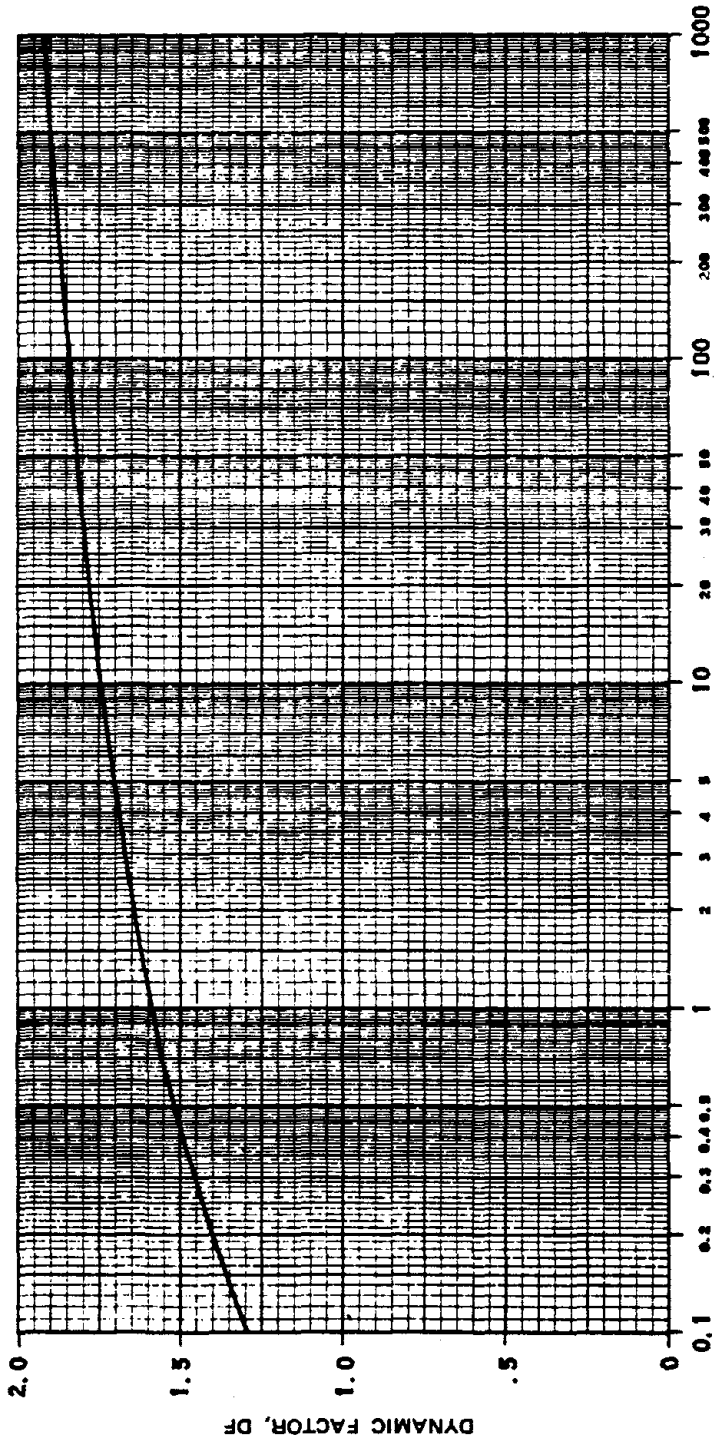

Figure 13-11. [redacted] Dynamic Factor vs Weapon Yield [redacted]

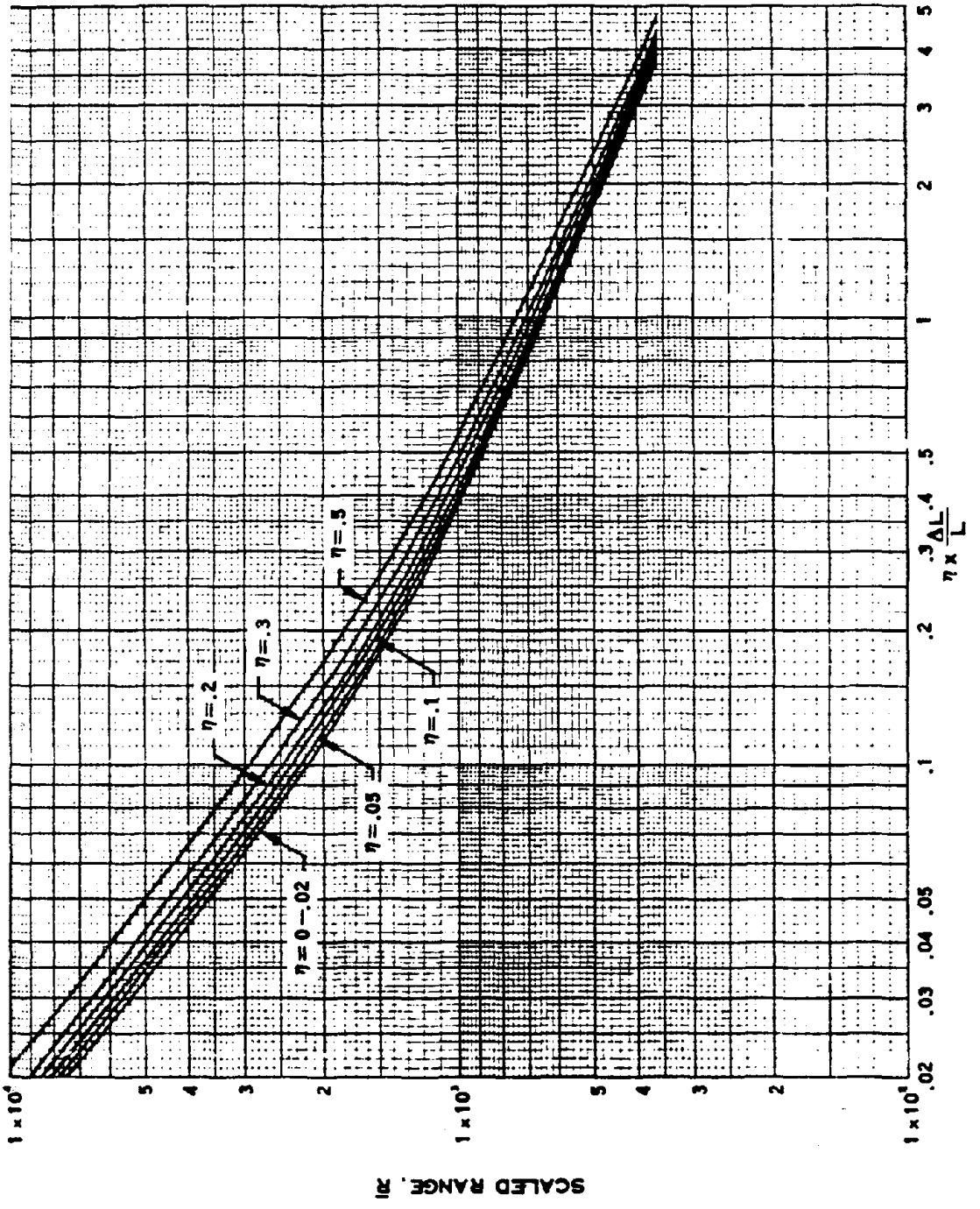

Figure 13-12a. η x $\frac{\Delta L}{L}$ as a Function of Scaled Range (N > 0)

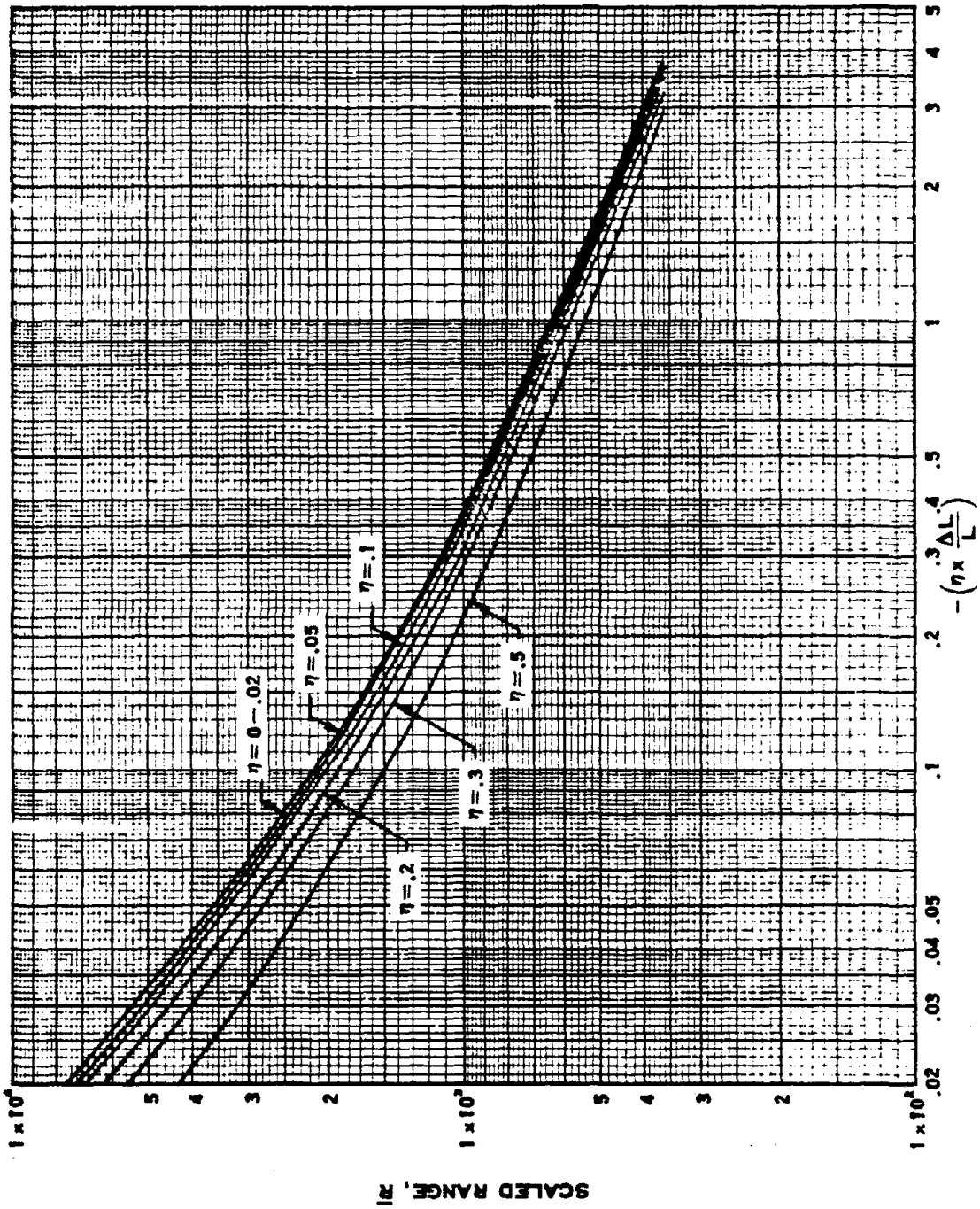

Figure 13-12b. [redacted] $\eta \times \frac{\Delta L}{L}$ as a Function of Scaled Range (N < 0) [redacted]

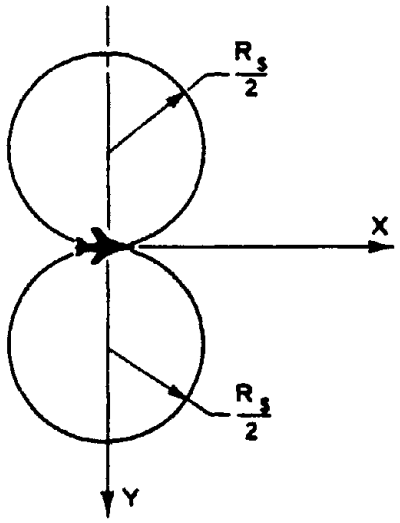

TOP VIEW (SECTION IN X–Y PLANE)

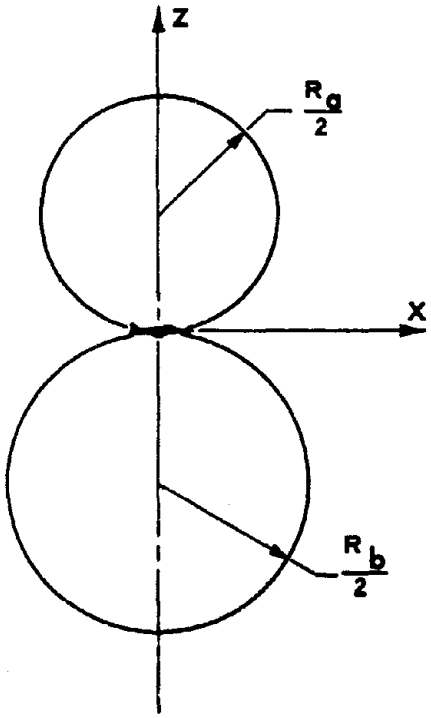

SIDE VIEW (SECTION IN X–Z PLANE)

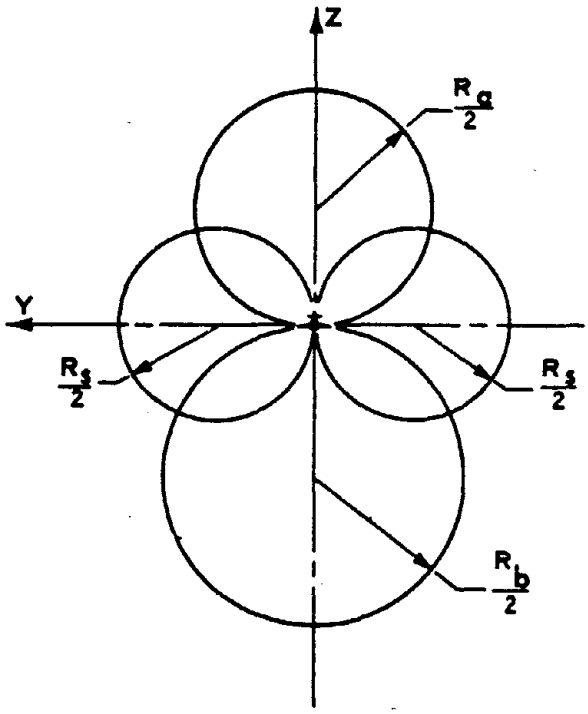

FRONT VIEW (SECTION IN Y–Z PLANE)

Figure 13-13. [redacted] Standard Shapes for Gust Envelopes at Intercept Time [redacted]

[redacted]

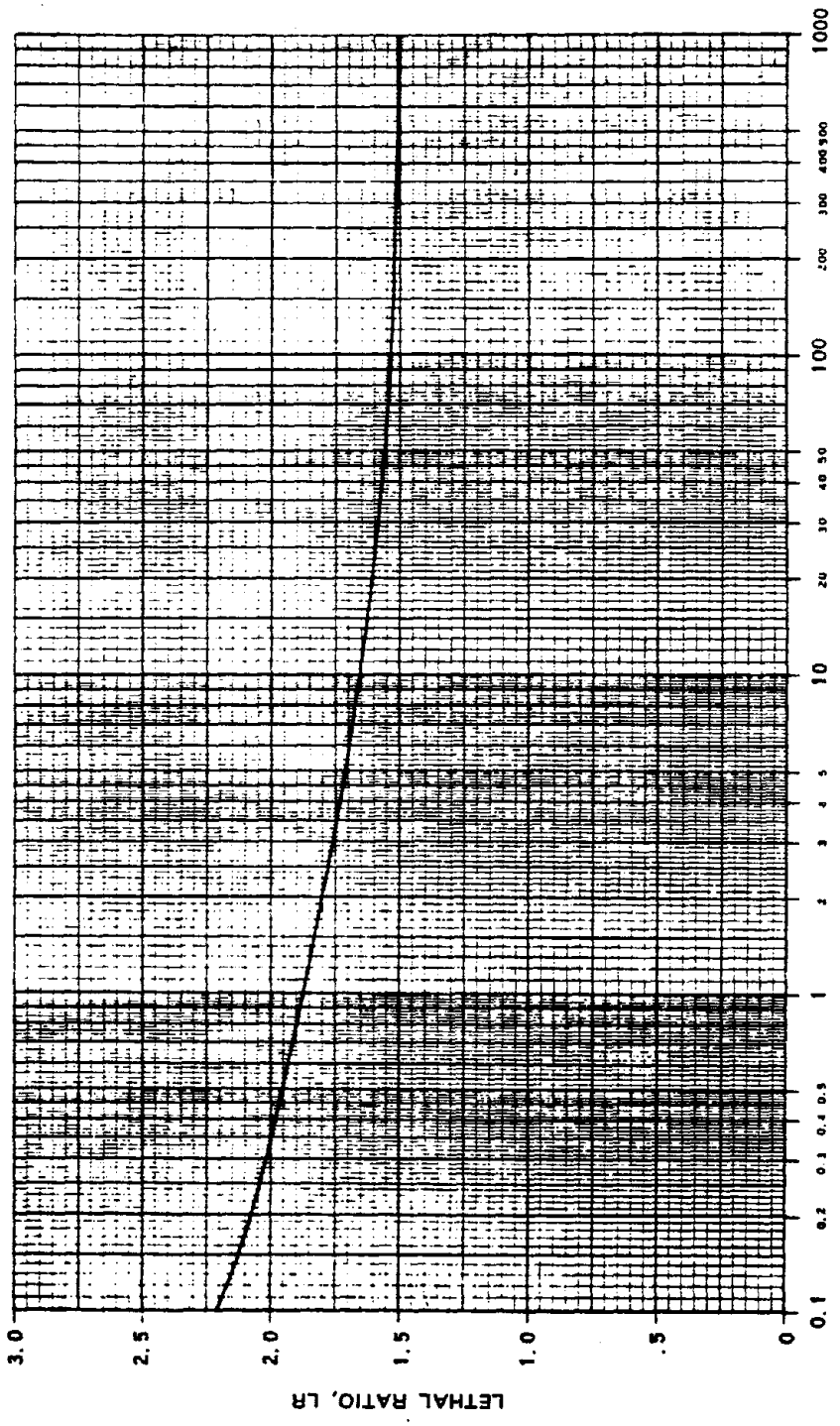

Figure 13-14. [redacted] Lethal Ratio vs Weapon Yield

[redacted]

AIRCRAFT RESPONSE TO OVERPRESSURE EFFECTS

13-9 Overpressure Effects on In-Flight and Parked Aircraft

If an aircraft is located in the vicinity of the nuclear explosion, the expanding blast wave eventually engulfs the aircraft. Depending on the distance of the aircraft from the burst, the pressure rise, or overpressure, experienced by an aircraft can be of a sufficient magnitude to damage the structural components.

An aircraft subjected to an overpressure loading can experience structural damage in several ways. Skin panels may yield or rupture; longerons, stringers, and frames may fail by compressive yielding or local buckling. The fuselage generally is the most susceptible to these types of damage; hence, *only the fuselage is examined for overpressure effects.* The method presented in this section for analyzing overpressure damage is applicable to all types of aircraft and helicopters both in-flight and parked. Methods for performing the analysis are given in Problem 13-5.

[redacted]

Problem 13-5. Calculation of the Boundaries in Space that Define the Sure-Safe and Sure-Kill Regions with Respect to the Effects of Overpressure Behind the Blast Wave on Aircraft In-Flight or Parked

[redacted] As discussed in paragraph 13-9, overpressure loading can produce structural damage in several ways; however, since the fuselage generally is the most susceptible item, only fuselage damage is considered in the following analysis.

[redacted] The major constraints in the analysis are:

- Overpressure damage to an aircraft is the same for all aircraft in a given class.
- The preblast atmosphere is homogeneous, having characteristics associated with the aircraft altitude.

[redacted] The data required for the analysis are aircraft altitude (ft), weapon yield, and aircraft class. Table 13-2 lists various aircraft classes and corresponding overpressure limits for sure-safe and sure-kill conditions.

[redacted]

[redacted]

[redacted] The overpressure analysis is performed in a series of steps as described below.

1. Determine the ambient pressure P at the aircraft altitude, h, from Table 13-1.

2. Knowing the class of aircraft being considered, obtain the critical overpressure level, Δp, for either sure-safe or sure-kill conditions from Table 13-2.

3. Using the value of the critical overpressure, determine the corresponding value of sea level overpressure by the scaling law given in paragraph 2-14, i.e.,

$$\Delta p_o = \frac{P_o \Delta p}{P} = \frac{14.7\ \Delta p}{P},$$

where the subscript zero indicates sea level values of overpressure and ambient pressure, and the absence of a subscript indicates the corresponding values at altitude h.

4. Enter Figure 13-15* with Δp_o, and determine the corresponding slant range, R_1, from a 1 kt explosion in a sea level atmosphere.

5. Calculate the corresponding slant range, R, for a yield of W kt,

$$R = R_1 \left[\frac{14.7\ W}{P}\right]^{1/3}.$$

6. The critical volume is defined by a sphere of radius R centered on the aircraft. For in-flight aircraft, continue to step 7; for parked aircraft, go to step 8.

7. The volume defined in step 6 is an intercept-time volume; that is, each point on the surface shows the critical position of the aircraft relative to the burst point at the time when the aircraft is intercepted by the blast wave. Ordi-

* [redacted] Figure 13-15 is identical to Figure 2-2, Chapter 2. It is reproduced here for convenience of the user.

[redacted]

narily, burst-time volumes are desired for in-flight aircraft, rather than intercept-time volumes. A point on a burst-time volume defines the critical position of the aircraft relative to the burst point at the time of burst. Thus, a sure-kill burst-time volume shows the regions in space, relative to the airplane, in which the explosion of a given size nuclear weapon will result in the destruction of the aircraft. This is the information that ordinarily is desired. To obtain the burst-time volume, it is necessary to transform the intercept-time volume obtained in step 6 into a burst-time volume. This transformation is demonstrated in Problem 13-7. This concludes the analysis for in-flight aircraft.

8.* For parked aircraft only, the sphere found in step 6 (more properly, the hemisphere) must be modified for ground reflection effects. Enter Figure 13-16 with sea level overpressure determined in step 3, and read three horizontal range parameters, $\overline{HR}_i$ (i = 1, 2, 3).

9. Enter Figure 13-17 with $\overline{HR}_i$ and read three corresponding burst height parameters, $\overline{BH}_i$ (i = 1, 2, 3). (Note $\overline{BH}_1$ is always zero.)

10. Calculate the burst heights and horizontal ranges, in feet.

$$BH_i = \overline{BH}_i \left[\frac{14.7\ W}{P}\right]^{1/3}$$

$$HR_i = \overline{HR}_i \left[\frac{14.7\ W}{P}\right]^{1/3}.$$

11. Plot the burst height versus horizontal range, by connecting the three points determined in step 10. Draw a radial line from the origin to point 3. The volume defined by rotating this envelope about a vertical axis through the aircraft is the ground-effects volume, which is to be combined with the hemisphere already found. Ground reflection effects are seen to add a "collar" around the base of the hemisphere.

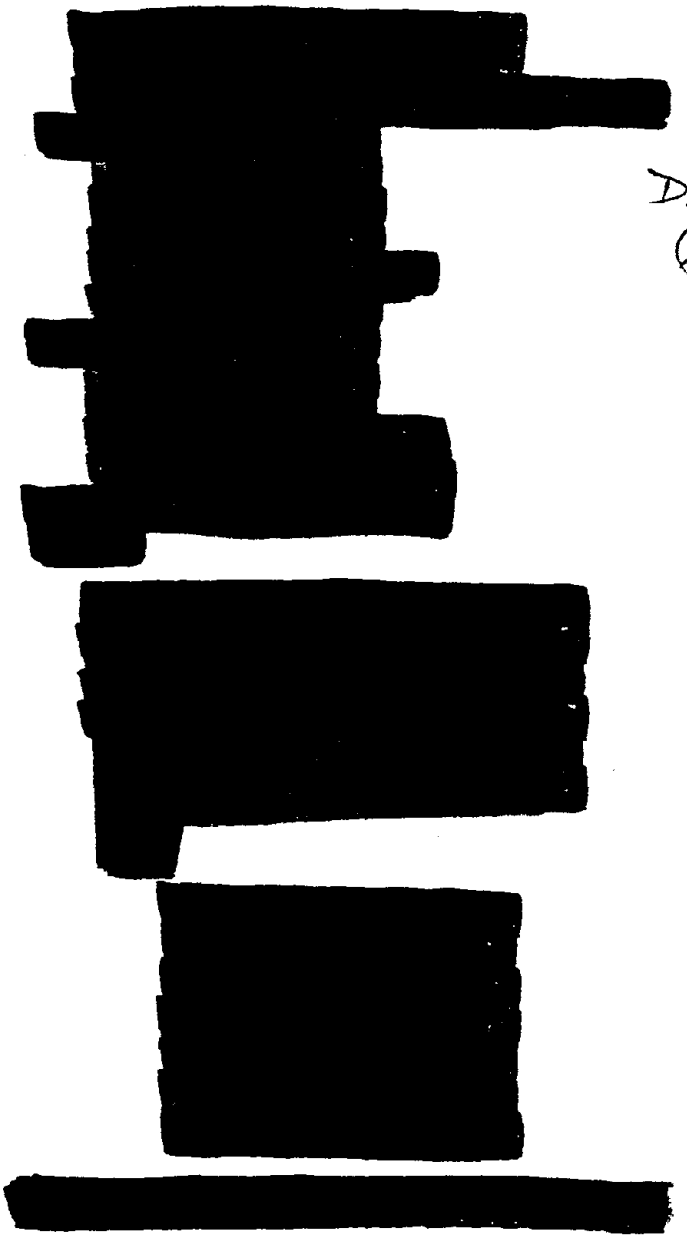

DWA (a)(1)

* The envelope generated by following steps 8 through 11 could be obtained by using the air blast height of burst curves in Chapter 2; however, these steps (and the accompanying figures) present the information in a more convenient form that is suitable to the accuracy of this analysis.

[redacted]

[redacted]

DNA (2)(1)

[redacted]

[redacted]

[redacted]

[redacted]

Answer: The resulting envelope is shown in Figure 13-18.

[redacted] *Reliability:* Overpressure damage to an aircraft is assumed to be the same for all aircraft in a given class. The preblast atmosphere is assumed to be homogeneous, having characteristics associated with the aircraft altitude. The maximum error in the calculation is estimated to be a factor of 1.8.

[redacted] *Related Material:* See paragraph 13-9. See also Table 13-1, and paragraph 2-14, Chapter 2.

[redacted]

[redacted]

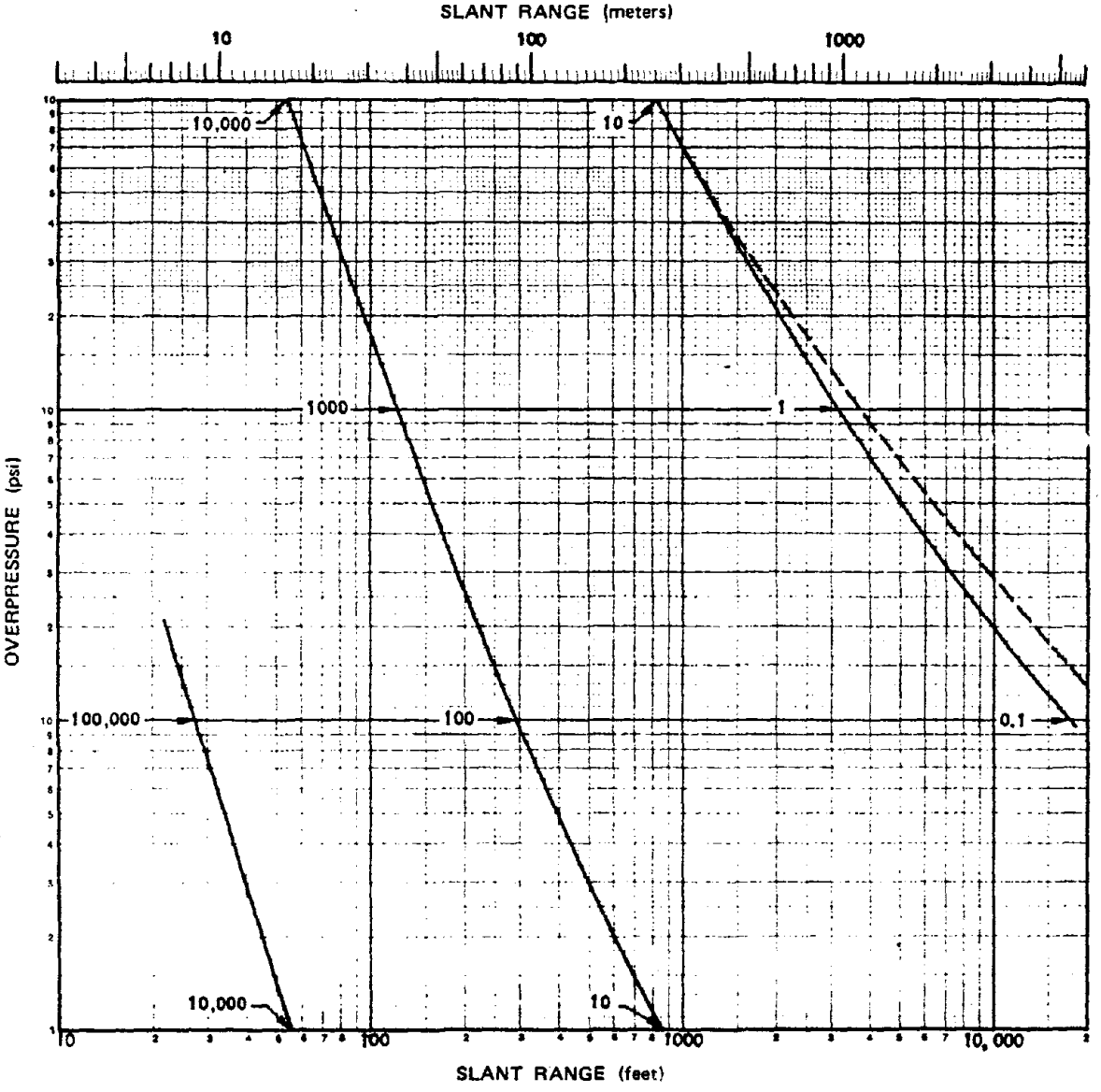

Figure 13-15. [redacted] Peak Overpressure from a 1 kt Free Air Burst in a Standard Sea Level Atmosphere [redacted]

[redacted]

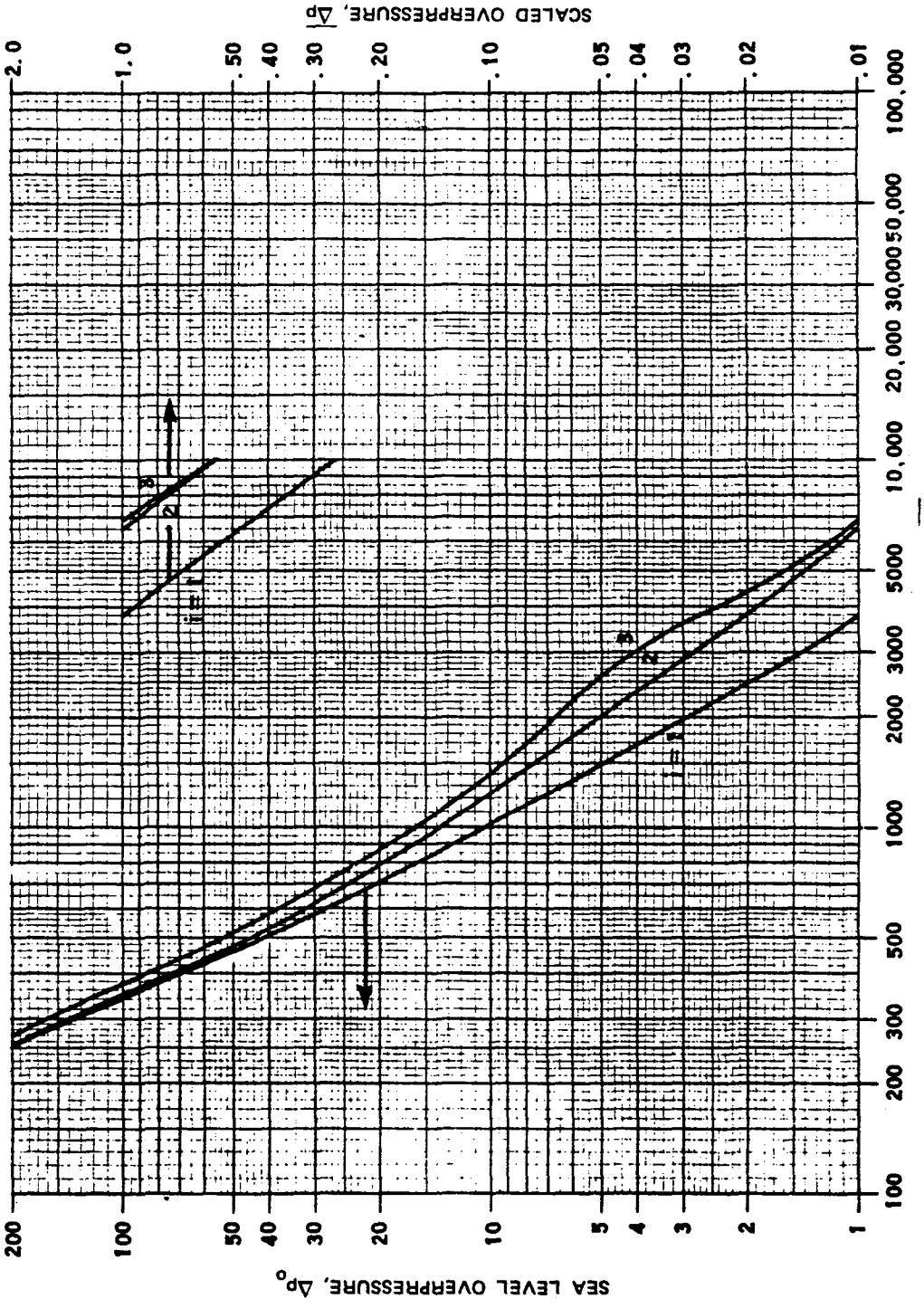

Figure 13-16. The Range Parameter $\overline{HR}_i$ as a Function of Sea Level Overpressure

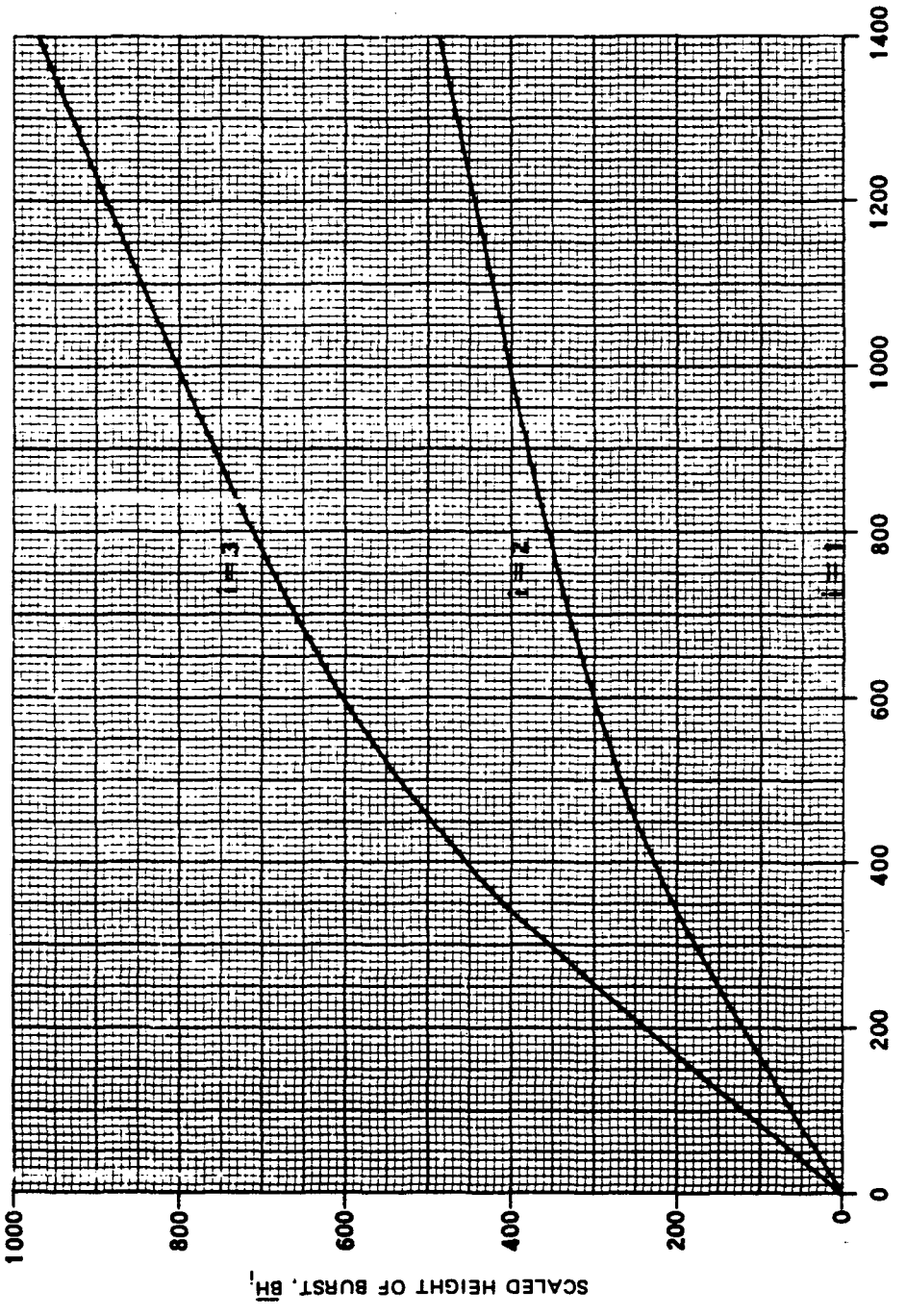

Figure 13-17a. [redacted] $\overline{BH}_i$ as a Function of $\overline{Hf}_i$, Short Ranges

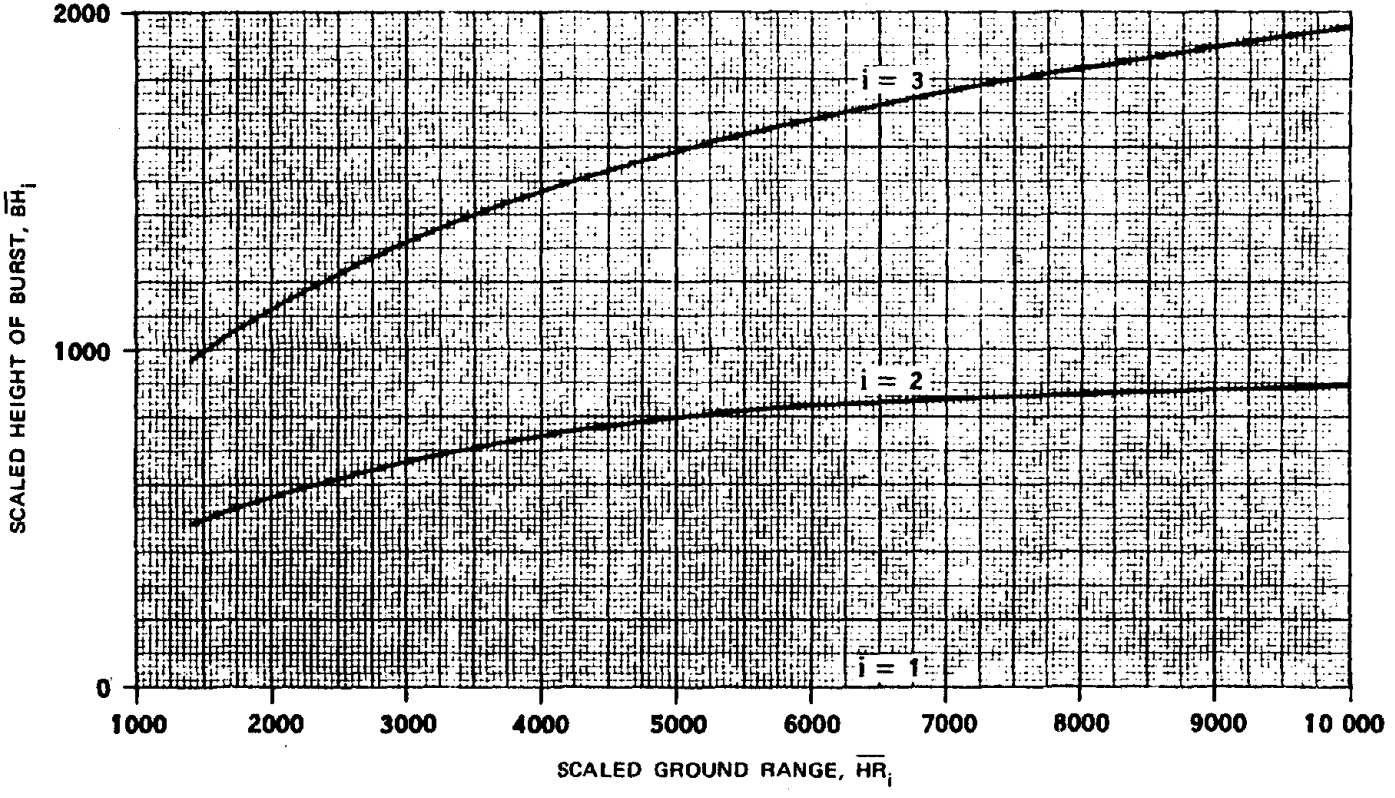

Figure 13-17b. [redacted] $\overline{BH}_i$ as a Function of $\overline{HR}_i$, Long Ranges [redacted]

[redacted]

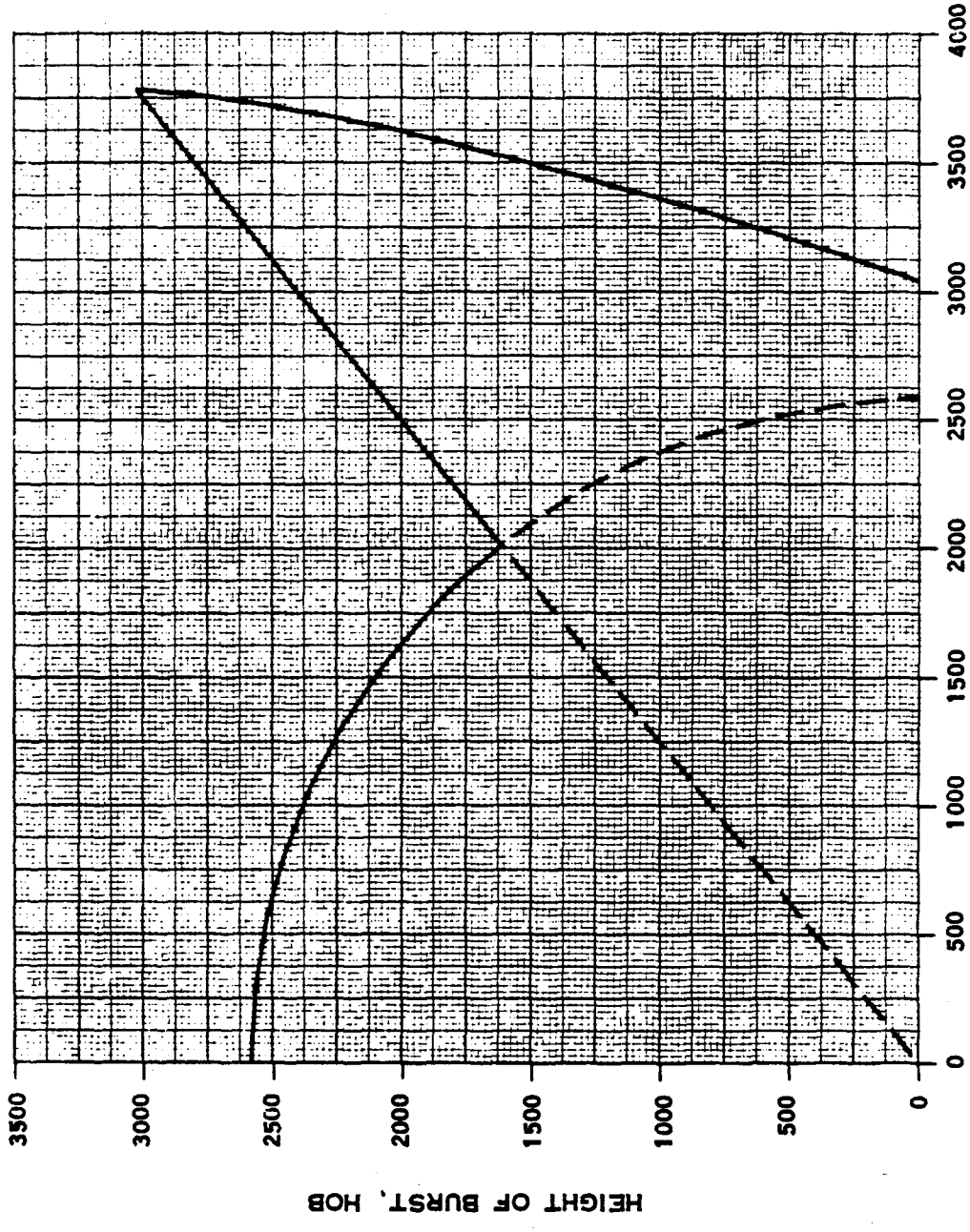

Figure 13-18. [redacted] Overpressure Envelope for [redacted] arked Aircraft [redacted]

[redacted]

AIRCRAFT RESPONSE TO THERMAL RADIATION EFFECTS

13-10 Thermal Effects on In-Flight and Parked Aircraft

The response of an aircraft to thermal energy is exhibited as a temperature rise in the aircraft skin. Several parameters influence the magnitude of the temperature rise. The most important parameters are skin thickness, skin material, surface condition, cooling effect of the air flowing over the outer surface of the aircraft, reradiation of thermal energy to the atmosphere, and conduction of the incident energy to the inner layers of the skin and substructure.

Sure-safe conditions are based on an allowable temperature rise of the aircraft skin; however, melting of the skin is required for sure-kill. To produce kill, the temperature must increase to the melt temperature, and further heat must be applied to cause melting. The method for analysis of thermal effects on aircraft that is described in Problem 13-6 applies to both airplanes and helicopters.

[redacted]

Problem 13-6. Calculation of Boundaries in Space (Envelopes) that Define the Sure-Safe and Sure-Kill Regions with Respect to Thermal Radiation on Aircraft In-Flight or Parked

[redacted] The analysis is based on calculating the amount of heat required to produce some specified effect. For sure-safe, this effect is raising the temperature of a skin panel to a value which produces a 20 percent reduction in the modulus of elasticity. This criterion is applied to the thinnest structural skin on the fuselage. For sure-kill, the specified effect is melting of the thickest skin on the fuselage. The critical amount of heat, Q_c, which is the heat required to produce the specified effect is assumed to be equal to the thermal energy absorbed by the skin, Q_a. The critical heat, Q_c, is

$$Q_c = \rho_m C_p t \Delta T,$$

where ρ_m is the weight density of the material, C_p is the specific heat of the material, t is the skin thickness, and ΔT is the effective critical temperature rise.

(U) The constraints in the calculation are:

- The aircraft skin is thermally thin, i.e., the incident thermal energy heats the skin uniformly throughout its depth.
- The equilibrium temperature is based on an average set of conditions for turbulent flow.
- At the equilibrium temperature, all degradations of material properties from room temperature values are negligible.
- Cooling effects resulting from airflow over the aircraft are negligible.
- Reradiation is negligible.
- Aircraft motion is neglected.
- Attenuation of the thermal energy by the atmosphere is negligible.
- Reflected radiation from the ground is negligible.
- The fireball is a point source.

(U) Under the constraints

$$Q_a = \alpha Q,$$

where Q is the radiant exposure, i.e., the energy received per unit area (normal to the direction of propagation under the assumed constraints), and α is the absorptivity coefficient for the aircraft surface being considered.

(U) From Chapter 3,

$$Q = \frac{10^{12} Wf}{4\pi R^2} \text{ cal/cm}^2,$$

where

W = weapon yield (kt),

f = thermal partition of energy (dimensionless),

R = distance (cm),

Since 39 cal/cm^2 = 1 Btu/in.^{2}, and 929 cm^2 = 1 ft^2,

$$Q = \frac{10^{12} Wf}{4\pi R^2 (39)(929)} \text{ Btu/in.}^2$$

or

$$Q = \frac{2.19 \times 10^6 Wf}{R^2} \text{ Btu/in.}^2$$

where R is now expressed in feet. Since

[redacted]

$$Q_a = \alpha Q,$$

$$Q_a = \frac{2.19 \times 10^6 Wf\alpha}{R^2},$$

and

$$R = \left[\frac{2.19 \times 10^6 Wf\alpha}{Q_a}\right]^{1/2},$$

or

$$R = 1{,}480\sqrt{\frac{Wf\alpha}{Q_a}},$$

which can be solved directly for the critical range R. If Q_c is taken to be equal to Q_a,

$$R = 1{,}480\sqrt{\frac{Wf\alpha}{Q_c}}$$

$$= 1{,}480\sqrt{\frac{Wf\alpha}{\rho_m C_p t \Delta T}}.$$

[redacted] The data required for solution include:

h = aircraft altitude (ft),

W = weapon yield (kt),

V = preblast aircraft velocity (ft/sec),

Detailed layout drawings of the fuselage, showing skin thickness,

Material of the skin, and

Surface condition of the skin.

[redacted] The analysis is performed in a series of steps.

1. Select the critical skin panels on the fuselage. Three panels should be selected, one each for bursts occurring directly below, directly above, and directly to the side of the aircraft. For each burst orientation, skin panels located in the following regions should be considered:

a. For a burst directly below the aircraft, the lower surface of the fuselage, within 45° of the normal to the bottom of the fuselage.

b. For a burst directly above the aircraft, the upper surface of the fuselage, within 45° of the normal to the top of the fuselage.

c. For a burst directly to the side of the aircraft, the side surface of the fuselage not covered by a and b above.

The selection of the critical skin panel from the locations defined above is based primarily on the thickness of the skin and depends upon whether sure-safe or sure-kill envelopes are sought.

- For sure-safe, select the *thinnest* structural skin. Nonstructural skin, such as access panels, should not be selected. If more than one material is used for the fuselage, investigate the thinnest skin for each material and base the envelopes on the *most* vulnerable.
- For sure-kill, select the *thickest* skin at a fuselage station near the forward end of the tail cone. If more than one material is used for the fuselage, investigate the thickest skin for each material and base the envelopes on the *least* vulnerable.

For a parked aircraft, skip steps 2 and 3 and proceed to step 4. For an in-flight aircraft, proceed to step 2.

2. Determine the ambient speed of sound c (ft/sec) at altitude h from Table 13-1.

3. Calculate the Mach Number,

$$M = \frac{V}{c}.$$

4. Determine the equilibrium temperature, T_e, of the skin.

a. For in-flight aircraft, enter Figure 13-19 with the Mach number, M, and the altitude, h, and read T_e.

b. For parked aircraft, use T_e = 60°F.

[redacted]

5. Determine the material properties for each of the skin panels selected from Table 13-3.

T_c = critical temperature (°F)

C_p = specific heat (Btu/lb°F)

ρ_m = weight density (lb/in.^{3})

For sure-kill only, determine

H = heat of fusion (Btu/lb)

6. Calculate the effective critical temperature rise, ΔT:

a. For sure-safe,

$$\Delta T = T_c - T_e.$$

b. For sure-kill,

$$\Delta T = T_c - T_e + \frac{H}{C_p}.$$

7. Determine the effective absorptivity coefficient, α, from Table 13-4.

8. Determine f from Figure 13-20*, and calculate the critical range in feet,

$$R = 1{,}480 \sqrt{\frac{Wf\alpha}{\rho_m C_p t \Delta T}}.$$

When steps 5 through 8 have been completed for a burst directly below the aircraft, they should be repeated for bursts directly above and directly to the side of the aircraft. Three ranges will have been determined, R_b, R_a, and R_s, where subscripts *"b," "a,"* and *"s"* designate below, above, and side, respectively. Note that, if the critical skin panels for R_a and R_s are of the same material and have the same surface conditions as the skin panel analyzed for R_b, only step 8 need be repeated, introducing the proper value of skin thickness, t.

9. Calculate the average of the three ranges, R_b, R_a, and R_s,

$$R_{av} = \frac{1}{3}\left(R_b + R_a + R_s\right).$$

10. The critical volume is defined by a sphere of radius R_{av} centered on the aircraft.

DNA (A)(1)

* Note that Figure 13-20 is identical to Figure 3-1. It is reproduced here for convenience.

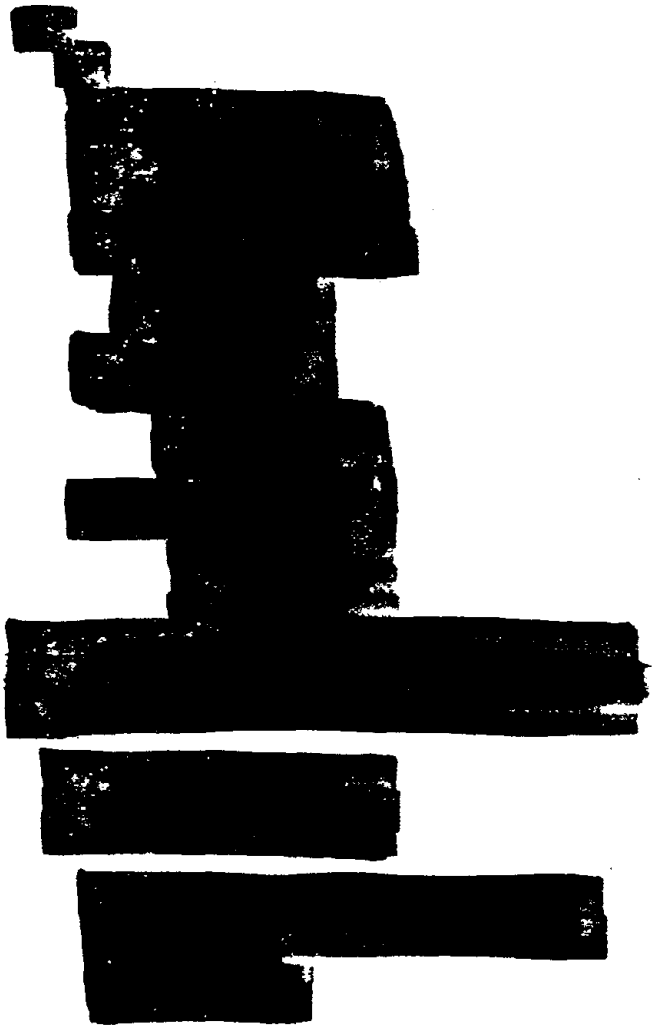

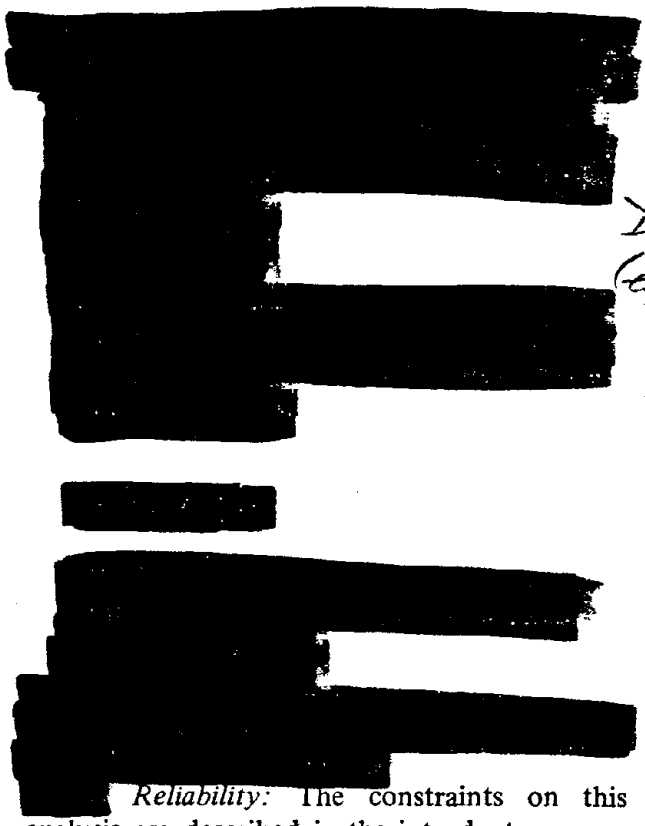

Reliability: The constraints on this analysis are described in the introductory paragraphs of this problem. The maximum error is between a factor of 1.5 and 3.

Related Material: See paragraphs 13-1, 13-4, and 13-10. See also Table 13-1.

Table 13-3. Average Properties of Selected Engineering Materials

Material	Critical Temperature, T_c (°F)		Specific Heat, C_p (Btu/lb°F)		Weight Density ρ_m (lb/in.^{3})	H (Btu/lb)
	Sure-Safe	Sure-Kill	Sure-Safe	Sure-Kill		
Steel	800	2,550	0.13	0.15	0.28	117
Inconel X	1,000	2,550	0.12	0.13	0.30	117
Aluminum	400	1,076	0.22	0.24	0.10	170
Magnesium	200	1,120	0.25	0.26	0.064	160
Titanium	500	2,850	0.13	0.24	0.17	187

[redacted]

Table 13-4. [redacted] Average Values of Absorptivities, α [redacted]

	Sure-Safe	Sure-Kill
Polished Metals	0.25	0.50
Unpolished metals	0.45	0.55
Painted metals		
Paint color		
White	0.30	0.50
Yellow	0.40	0.55
Olive	0.70	0.60
Black	0.90	0.65

[redacted]

[redacted]

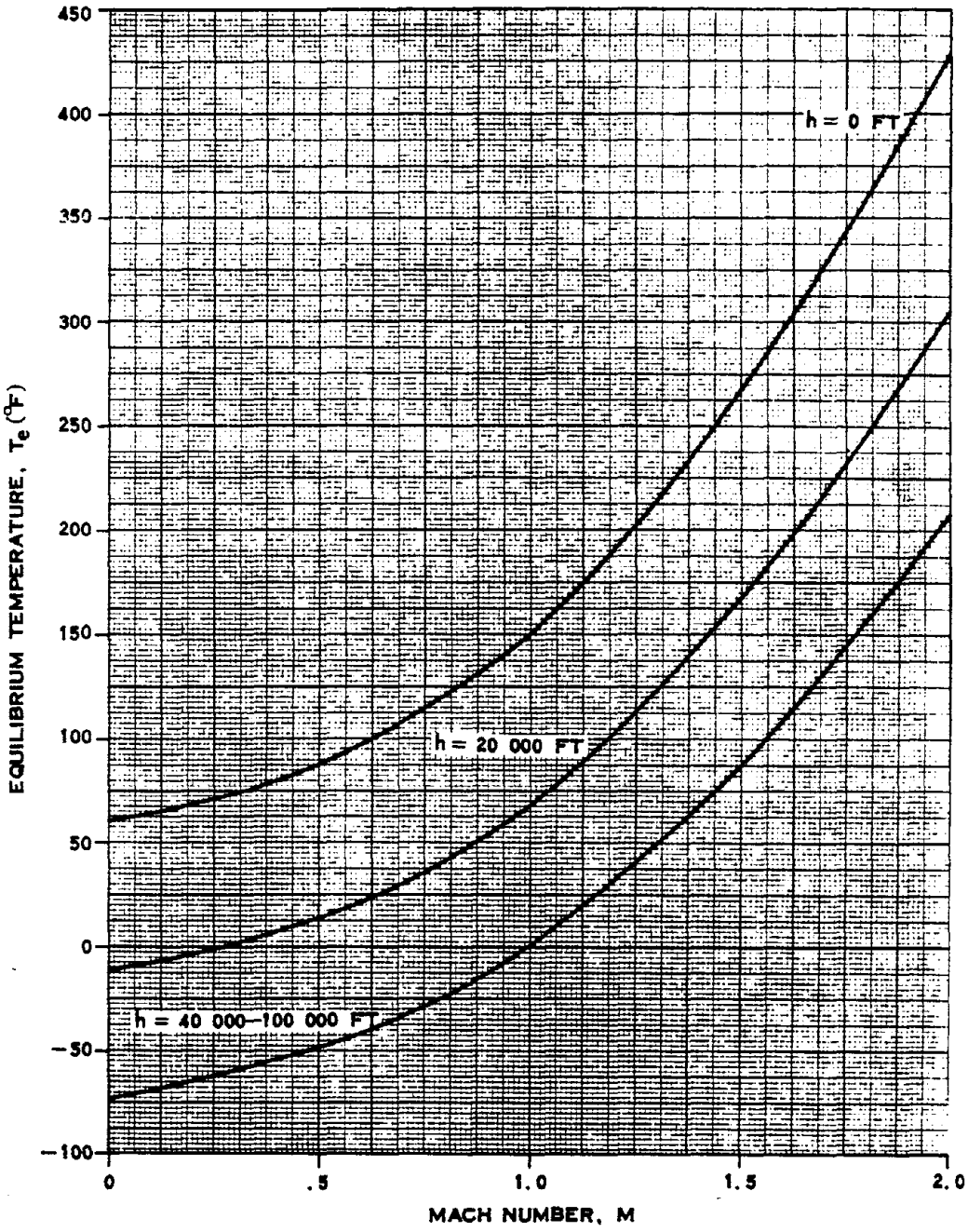

Figure 13-19. [redacted] Equilibrium Temperature as a Function of Mach Number [redacted]

PAGE 13-66 DELETED

[redacted]

BURST-TIME ENVELOPES

13-11 Requirement for Burst-Time Envelopes

The envelopes that are obtained by the methods described in Problems 13-3 through 13-6 define the locus of the center of burst relative to the *position of the aircraft at intercept,* for a specified criterion. It usually is preferable to define the corresponding envelope relative to the *position of the aircraft at burst time.* For parked aircraft and for those envelopes corresponding to thermal radiation, which reaches the aircraft almost instantaneously, the two envelopes are the same, i.e., the methodology presented in Problem 13-5 for overpressure effects on parked aircraft and that presented in Problem 13-6 for thermal effects on in-flight or parked aircraft apply equally well to intercept-time and to burst-time envelopes. When considering the response of in-flight aircraft to gust or overpressure, however, the relative positions of the aircraft and the burst center are different at the time of burst than at the time of intercept as a result of the distance traveled by the aircraft during the finite time required for the blast wave to propagate to the intercept point. Methods for transforming the intercept-time envelopes obtained by the methods described in Problems 13-3 through 13-5 for in-flight aircraft into burst-time envelopes for the same aircraft are described in Problem 13-7.

[redacted]

Problem 13-7. Calculation of Burst-Time Envelopes for Gust or Overpressure Effects from Intercept-Time Envelopes

[redacted] As discussed in paragraph 13-1, the assumption must be made that the aircraft is following an unaltered flight path when transforming intercept-time envelopes into burst-time envelopes. This assumption is necessary, since it would be impossible to guess the course changes. The assumption is valid for low yield weapons because of the small distances and times between burst and intercept. In the case of high yield weapons, the blast wave arrival time may be of the order of seconds, and the pilot may have time to change his course, so, for these weapons, the assumption must be considered as a source of error.

[redacted] Two major assumptions, arising from the limitations discussed above, are included in the simplified calculation method described below.

- The aircraft is represented by a point mass traveling at a constant velocity.
- The aircraft is performing a constant symmetric maneuver. As a result of this assumption, the flight path of the aircraft is circular (or straight, for the special case of no maneuver).

[redacted] Two left-handed, body-centered coordinate systems employed in the analysis are shown in Figure 13-21.

- The intercept reference frame (X_I, Y_I, Z_I), the origin of which is located at the aircraft's center of mass at intercept, with the X_I axis collinear with the velocity vector, positive forward, and the Z_I axis in the aircraft plane of symmetry, positive upward.
- The burst reference frame (X_B, Y_B, Z_B), the origin of which is located at the aircraft's center of mass at burst time, with the X_B axis collinear with the velocity vector, positive forward, and the Z_B axis in the aircraft plane of symmetry, positive upward.

[redacted] The X_I - Z_I and X_B - Z_B planes coincide, hence the Y_I and Y_B coordinates of any point are the same.

[redacted] If the center of burst has coordinates (X_I, Y_I, Z_I) in the intercept frame, its position in the burst frame is given by the coordinates (X_B, Y_B, Z_B), where

$$X_B = X_I \cos \Phi + (r - Z_I) \sin \Phi$$

$$Y_B = Y_I,$$

$$Z_B = X_I \sin \Phi - (r - Z_I) \cos \Phi + r,$$

and

r = radius of turn,

Φ = angular change in flight path between burst and intercept times.

The parameters r and Φ are obtained from the relations

$$r = \frac{V^2}{Ng},$$

$$\dot{\Phi} = \frac{V}{r},$$

where

V = preblast aircraft velocity,

N = maneuver normal load factor,

g = acceleration of gravity,

and a dot indicates differentiation with respect to time. It should be noted that N is the *maneuver* normal load, and not the load factor, n, used to calculate the intercept envelopes. N is related to the load factor n by

$$N = n - 1.$$

[redacted]

If the equation for $\dot{\Phi}$ is integrated from burst time to intercept time, the result is,

$$\Phi = \frac{Vt_a}{r}$$

where

t_a = time of arrival of the blast wave at the intercept point; i.e., the time required for the blast front to propagate to the intercept point.

For the special case when the aircraft is not performing a maneuver ($N = 0$), the equations for the position of the burst point in the burst frame simplify to

$$X_B = X_I + Vt_a$$

$$Y_B = Y_I$$

$$Z_B = Z_I.$$

By means of the above equations, the burst frame coordinates (X_B, Y_B, Z_B) may be found for any point on an intercept-time envelope (X_I, Y_I, Z_I). Unfortunately, a general planar burst-time envelope cannot be obtained by merely transforming an intercept envelope point by point. For maneuvering aircraft, only those envelopes in the X_I - Z_I plane (side view) or parallel to the X_I - Z_I plane, may be resolved directly into corresponding planar envelopes in the X_B - Z_B plane or parallel to it. All other intercept-time envelopes will transform into three-dimensional surfaces in the burst frame. In the case of no maneuver, any intercept-time envelope parallel to the X_I axis may be resolved directly into a burst-time envelope in the same plane. This includes envelopes in both the X_I - Z_I plane (side view), and the X_I - Y_I plane (top view). However, in neither case can the Y_B - Z_B plane (front view) envelope be obtained directly. In order to find the burst envelopes for side, front, and top views (or in any arbitrary plane), it is necessary to adopt an indirect procedure. Since the intercept-time envelopes define a volume in space, this entire volume may be transformed into an equivalent volume in the burst frame. The burst-time envelopes then may be determined as the intersection of this volume with the planes in which burst-time envelopes are desired.

The most convenient way of performing this volume transformation is to take "slices" through the intercept-time volume parallel to the X_I - Z_I plane, for selected values of Y_I. Each of these slices may be resolved directly into a slice of the burst-time volume in a plane corresponding to the same value of Y_B. Definition of the burst-time envelopes in several Y_B planes is equivalent to defining the burst-time volume.

The data required to perform the analysis include:

V = preblast aircraft velocity (ft/sec)

h = aircraft altitude (ft)

W = weapon yield (kt)

n = aircraft preblast load factor; for straight and level flight, n = 1 (dimensionless)

X_I, Y_I, Z_I = coordinates of points on intercept-time envelopes, as defined in Figure 13-21 (ft).

The analysis is performed in a series of steps, as follows.

1. Determine the ambient atmospheric conditions at altitude h from Table 13-1.

2. Calculate the maneuver normal load factor, N,

$$N = n - 1.$$

3. Calculate the radius of turn, r (not required if $N = 0$.),

$$r = \frac{V^2}{32.2N}.$$

4.* Select a point on the X_I - Z_I plane (side view) intercept-time envelope. Its coordinates are (X_I, Y_I, Z_I), with $Y_I = 0$.

5. Determine the slant range, R, from the center of burst to the selected intercept point.

$$R = \left(X_I^2 + Y_I^2 + Z_I^2\right)^{1/2}.$$

6. Calculate the equivalent range for a 1 kt burst in a sea level atmosphere by the scaling procedures described in paragraph 2-14, Chapter 2,

$$R_1 = R\left(\frac{P}{P_o W}\right)^{1/3} = R\left(\frac{P}{14.7W}\right)^{1/3}.$$

7. Enter Figure 13-22 with R_1, and read the time of arrival, t_1, for a 1 kt burst in a sea level atmosphere.† Calculate the time of arrival of the blast wave at a range R from a yield W at altitude h by the scaling procedures given in paragraph 2-14,

$$t_a = t_1\left(\frac{WP_o}{P}\right)^{1/3}\left(\frac{T_o}{T}\right)^{1/2}.$$

A satisfactory expression for the time of arrival within the accuracy of the methodology presented herein is

$$t_a = t_1\left(\frac{WP_o}{P}\right)^{1/3}\left(\frac{c_o}{c}\right)$$

$$= t_1\left(\frac{14.7W}{P}\right)^{1/3}\left(\frac{1{,}116}{c}\right).$$

8. Calculate the turn angle, Φ, in degrees (not required if $N = 0$),

$$\Phi = 57.3\,\frac{Vt_a}{r}.$$

9. Calculate the coordinates of the point in the burst frame (X_B, Y_B, Z_B).

a. If $N = 0$,

$$X_B = X_I + Vt_a,$$

$$Y_B = Y_I,$$

$$Z_B = Z_I.$$

b. If $N \neq 0$,

$$X_B = X_I \cos\Phi + (r - Z_I)\sin\Phi,$$

$$Y_B = Y_I,$$

$$Z_B = Z_I \sin\Phi - (r - Z_I)\cos\Phi + r.$$

10. Repeat steps 5 through 9 for other points on the intercept-time envelope, until the burst-time envelope has been defined satisfactorily.

11. Determine the intercept-time envelope for a "slice" parallel to the X_I - Z_I plane, with $Y_I \neq 0$. Repeat steps 5 through 10 for points on this envelope.

12. Repeat step 11 for as many "slices" as necessary to define the burst-time volume adequately. Note that only positive values of Y_I need be used since the envelopes are symmetric about the X_I - Z_I or X_B - Z_B plane.

[redacted] At this point, the problem is essentially solved, since the burst-time volume effectively has been defined. The burst-time envelope in any desired plane may be determined from the burst-time volume. The calculation of the burst-

*[redacted] In certain special cases, simpler procedures may be used, although the procedures given above are general and will work in all cases. A description of the special cases is given at the end of the Stepwise Calculation Procedure.

†[redacted] Note that Figure 13-22 is identical to Figure 2-5, Chapter 2. It is reproduced here for convenience.

time envelopes in three planes, The X_B - Z_B plane (side view), the Y_B - Z_B plane (front view), and the X_B - Y_B plane (top view) is described for illustration.

13. The side-view burst-time envelope is the intersection of the X_B - Z_B plane with the burst-time volume. This is just the transformed side-view intercept-time envelope (Y_I = 0), which was the first burst-time envelope defined in the steps given above.

14. The front-view burst-time envelope is the intersection of the Y_B - Z_B plane with the burst-time volume. For each of the burst-time volume "slices," determine the values of Z_B corresponding to X_B = 0, and plot these using the value of Y_B for the slice being considered.

15. The top-view burst-time envelope is the intersection of the X_B - Y_B plane with the burst-time volume. For each of the burst-time volume "slices," determine the values of X_B corresponding to Z_B = 0, and plot these using the value of Y_B for the slice being considered.

16. *Special Cases.* In certain cases, simpler procedures may be used. The methodology of Problem 13-5 results in a spherical intercept-time volume for overpressure effects on in-flight aircraft. The sphere is centered at the origin of the intercept frame (X_I, Y_I, Z_I). Hence, R, R_1, r, and Φ (steps 5-8) are the same for *all* points on the intercept-time volume, and the sphere transforms into a sphere of the same radius in the burst frame. The coordinates of the center of the sphere are

a. If $N = 0$,

$$X_B = Vt_a,$$

$$Y_B = 0,$$

$$Z_B = 0.$$

b. If $N \neq 0$,

$$X_B = r \sin \Phi,$$

$$Y_B = 0,$$

$$Z_B = r(1 - \cos \Phi).$$

Another special case occurs for the gust effects on in-flight aircraft (see Problems 13-3 and 13-4). The complete intercept-time volumes are made up of four spheres. The intersection of any plane with a sphere is a circle. Consider the intersection of a plane parallel to the X_I - Z_I plane and defined by constant Y_I with the sphere at the side of the aircraft. The intersection is a circle on the Y_I axis. All points on this circle are equidistant from the origin; hence, the circle transforms into a circle of the same radius in the burst frame. The coordinates of the center of the circle are

a. If $N = 0$,

$$X_B = Vt_a,$$

$$Y_B = Y_I,$$

$$Z_B = 0.$$

b. If $N \neq 0$,

$$X_B = r \sin \Phi,$$

$$Y_B = Y_I,$$

$$Z_B = r(1 - \cos \Phi).$$

For the case of $N = 0$ only, the intersection of a plane parallel to the X_I - Y_I plane and defined by constant Z_I with the sphere above or below the aircraft transforms into a circle of the same radius in the burst frame. The coordinates of the center of the circle are

$$X_B = Vt_a$$

[redacted]

$$Y_B = 0$$

$$Z_B = Z_I.$$

In all of the above transformations, it should be emphasized that t_a corresponds to a point on the intercept-time envelope being considered, *not* to the center of the circle.

[redacted]

DNA (G-1)

PAGES 13-73 THRU 13-74 DELETED

[redacted]

[redacted]

[redacted] *Reliability:* The aircraft is assumed to be represented by a point mass traveling at a constant velocity and performing a constant symmetric maneuver. As a result of this assumption, the flight path of the aircraft is circular (or straight for the special case of no maneuver). The maximum error is estimated to be a factor of 1.1.

[redacted] *Related Material:* See paragraphs 13-1, 13-2, 13-6, 13-7, and 13-11. See also Problems 13-3 and 13-4, and Table 13-1.

[redacted]

[redacted]

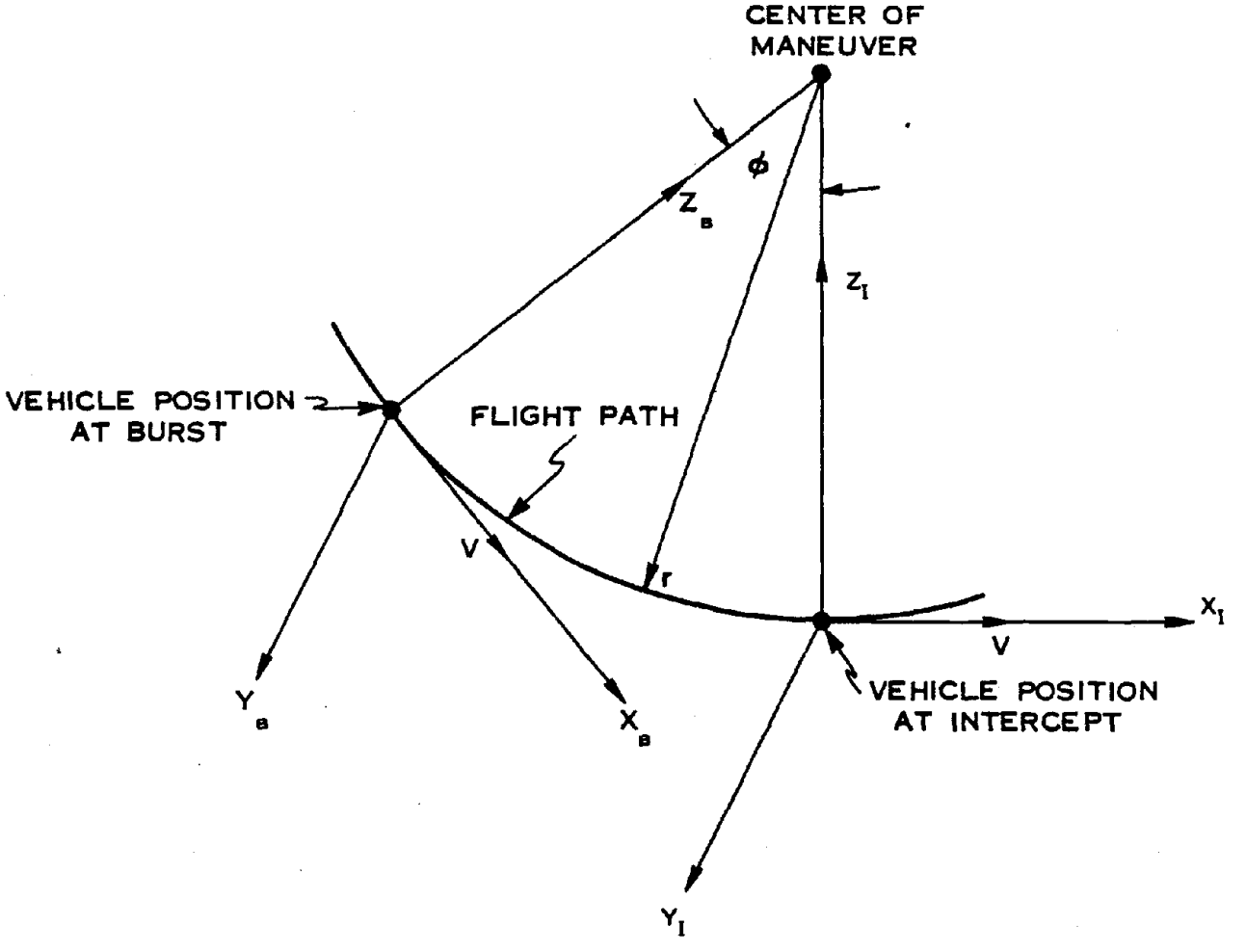

Figure 13-21. [redacted] Geometry of Burst and Intercept Reference Frames [redacted]

[redacted]

[redacted]

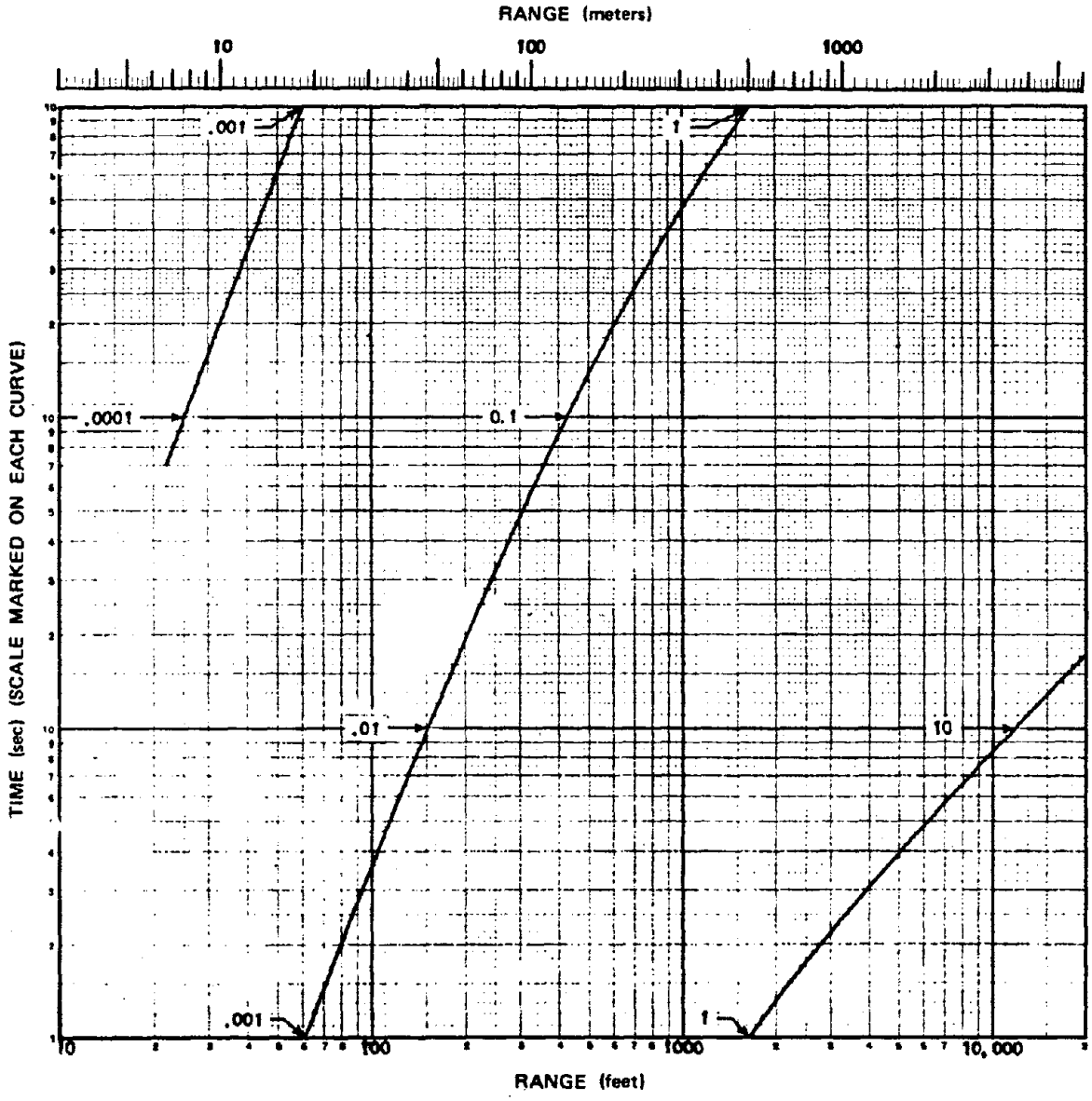

Figure 13-22. [redacted] Time of Arrival of the Shock Front from a 1 kt Free Air Burst in a Standard Sea Level Atmosphere [redacted]

[redacted]

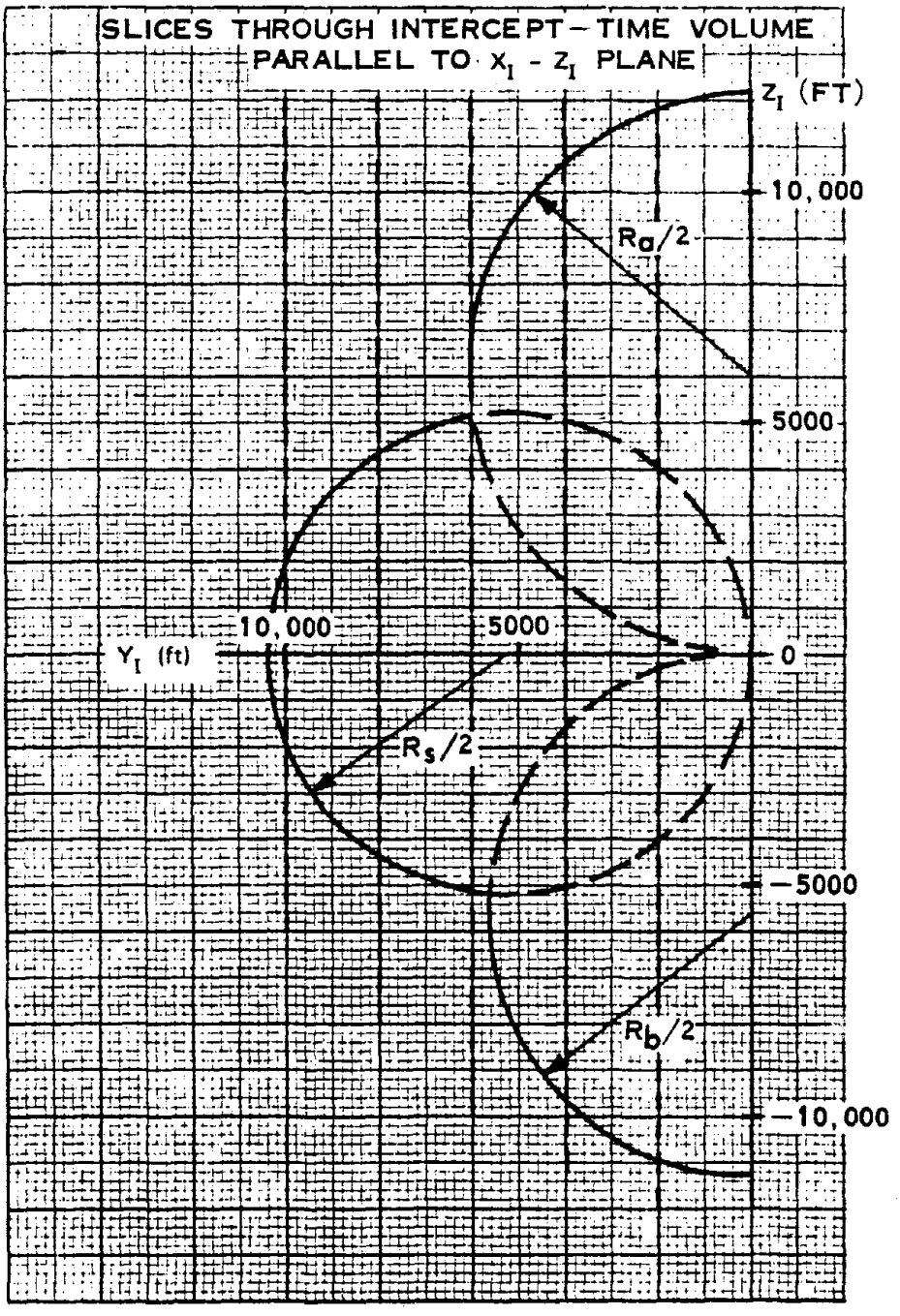

Figure 13-23. [redacted] Intercept-Time Envelope (Front View) [redacted]

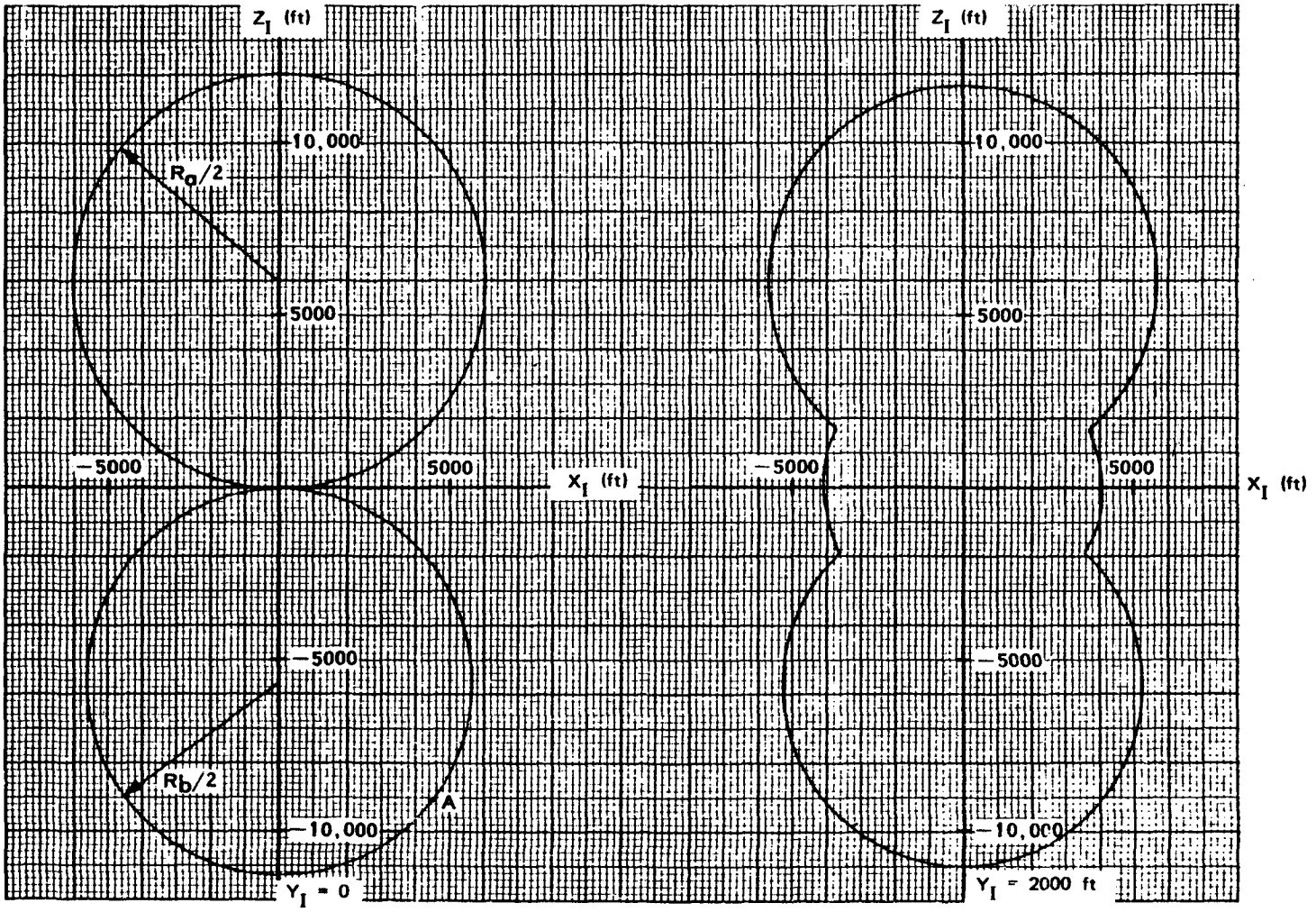

Figure 13-24a. [redacted] Intercept-Time Envelope (Side View) [redacted]

Figure 13-24b. [redacted] Slice Through Intercept-Time Volume at Y_I = 2,000 Feet [redacted]

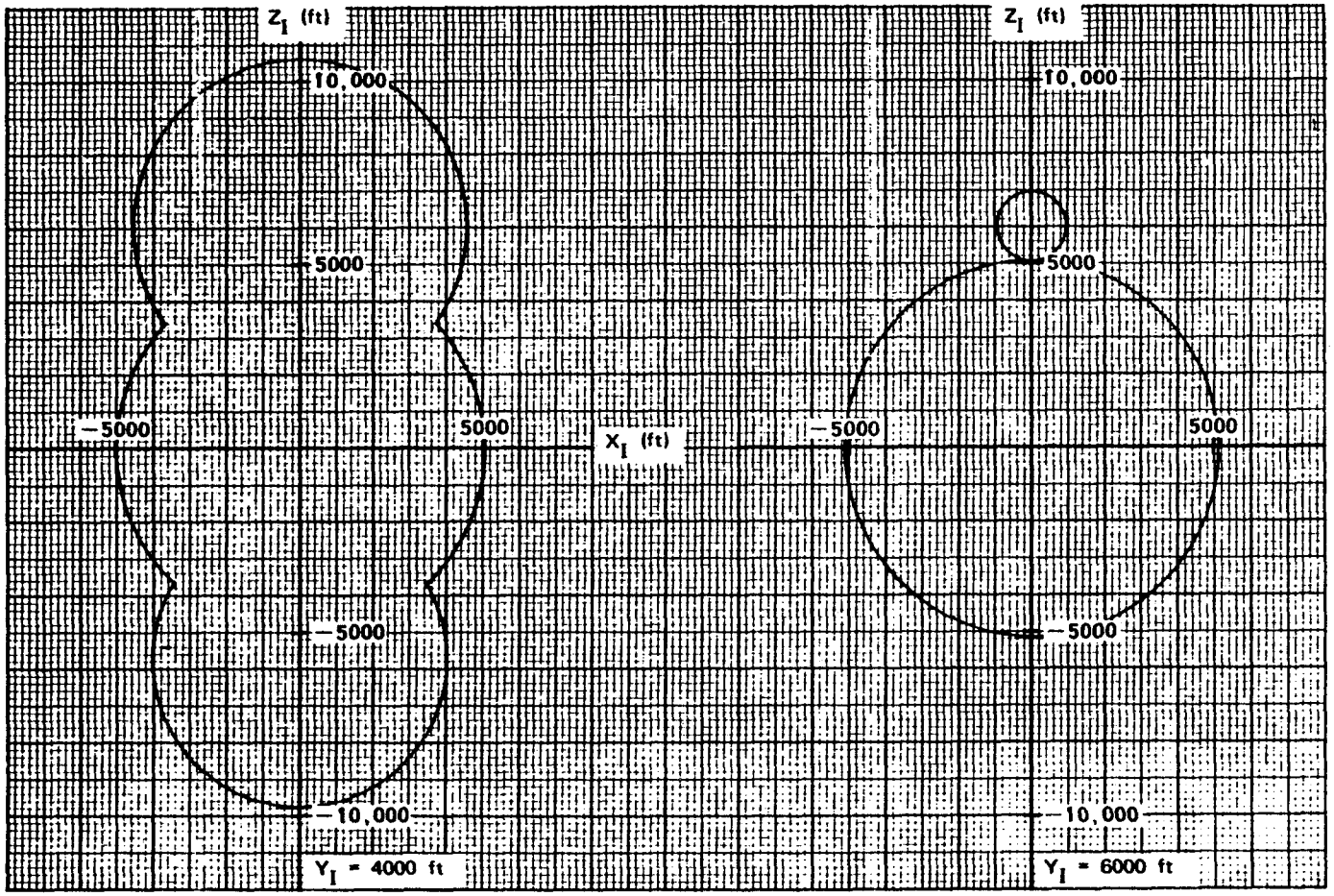

Figure 13-24c. [redacted] Slice Through Intercept-Time Volume at Y_I = 4,000 Feet [redacted]

Figure 13-24d. [redacted] Slice Through Intercept-Time Volume at Y_I = 6,000 Feet [redacted]

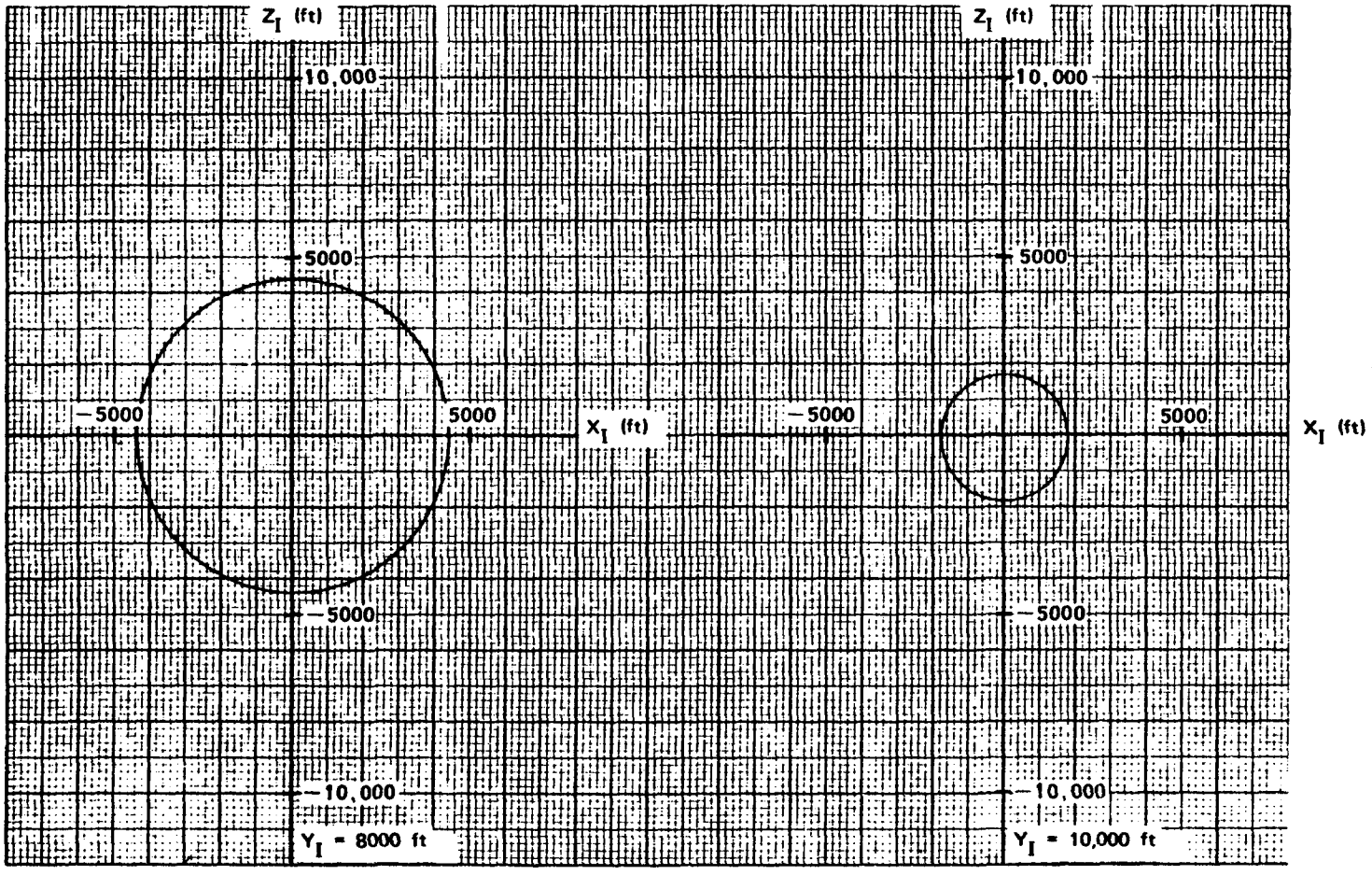

Figure 13-24e. Slice Through Intercept-Time Volume at Y_I = 8,000 Feet

Figure 13-24f. Slice Through Intercept-Time Volume at Y_I = 10,000 Feet

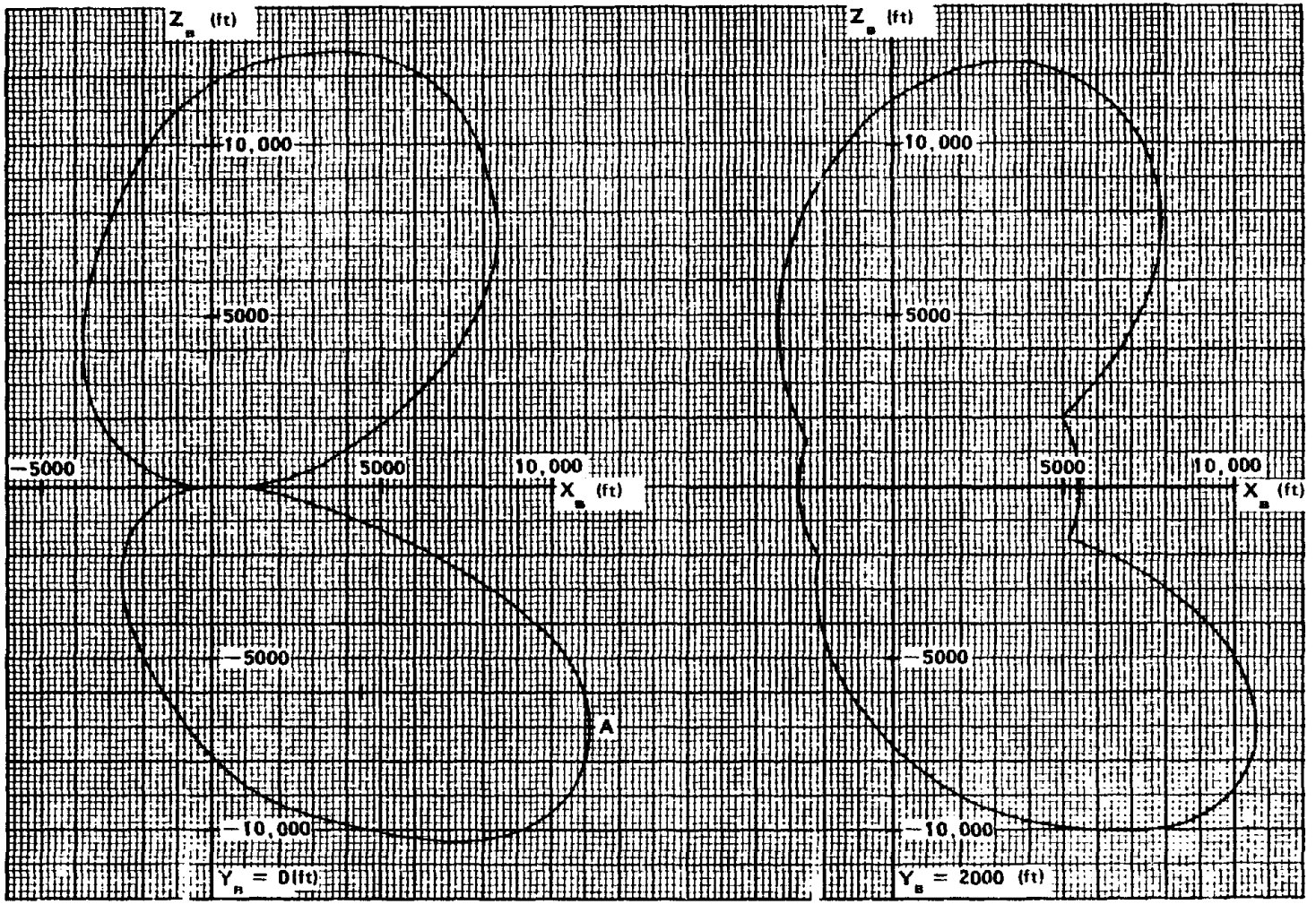

Figure 13-25a. [redacted] Burst-Time Envelope (Side View) [redacted]

Figure 13-25b. [redacted] Slice Through Burst-Time Volume at Y_B = 2,000 Feet [redacted]

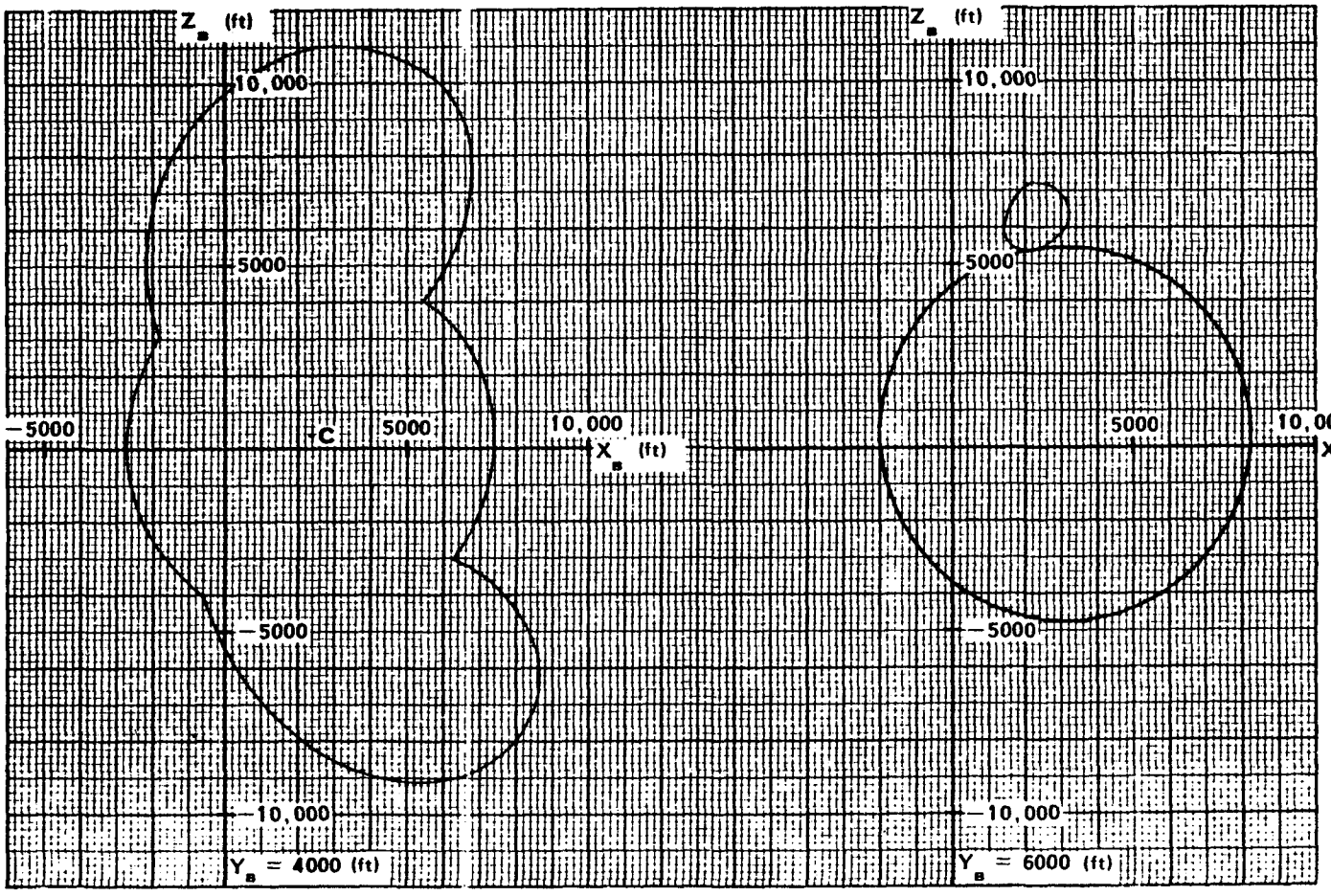

Figure 13-25c. [redacted] Slice Through Burst-Time Volume at Y_B = 4,000 Feet [redacted]

Figure 13-25d. [redacted] Slice Through Burst-Time Volume at Y_B = 6,000 Feet [redacted]

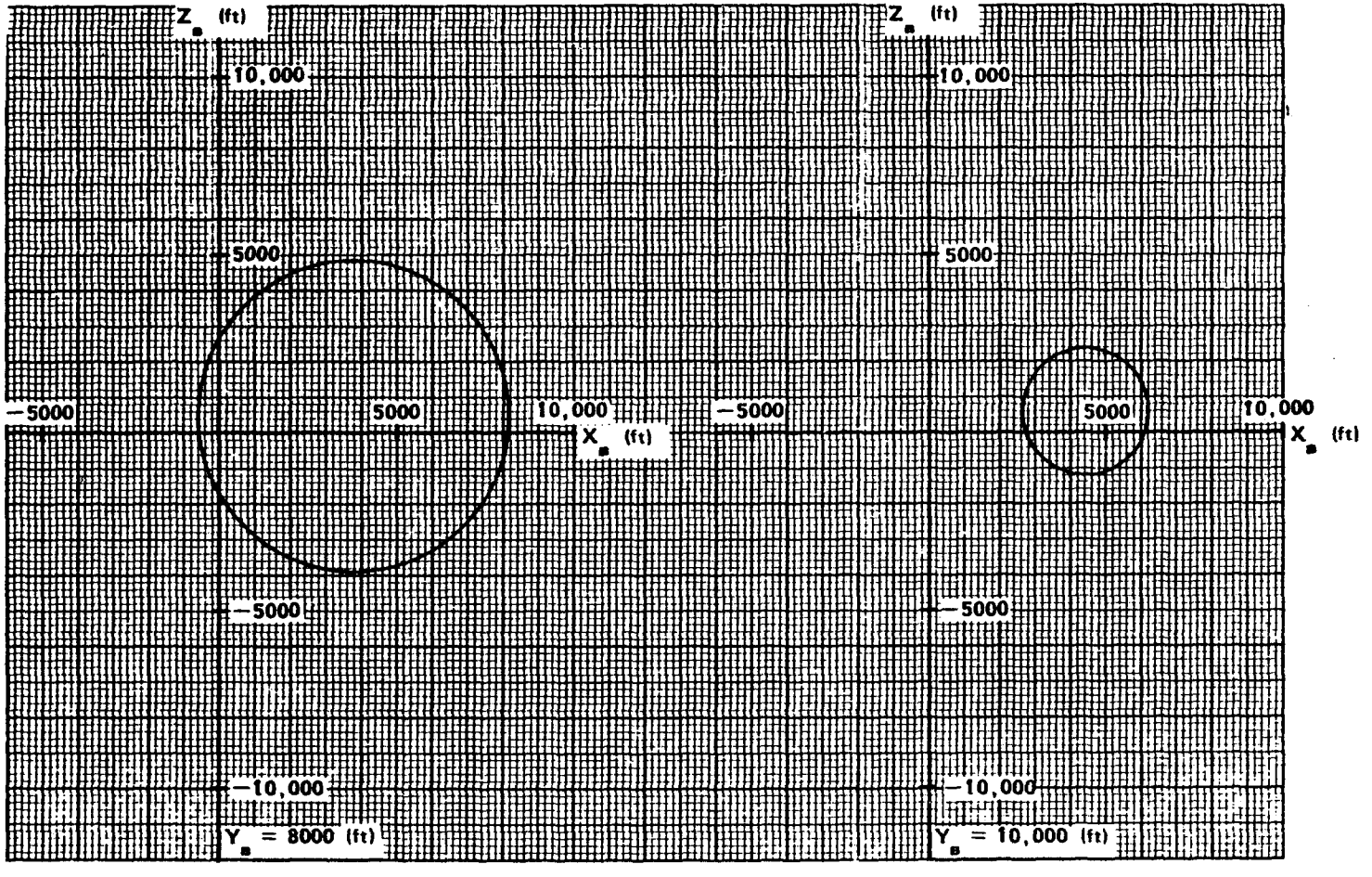

Figure 13-25e. [redacted] Slice Through Burst-Time Volume at Y_B = 8,000 Feet [redacted]

Figure 13-25f. [redacted] Slice Through Burst-Time Volume at Y_B = 10,000 Feet [redacted]

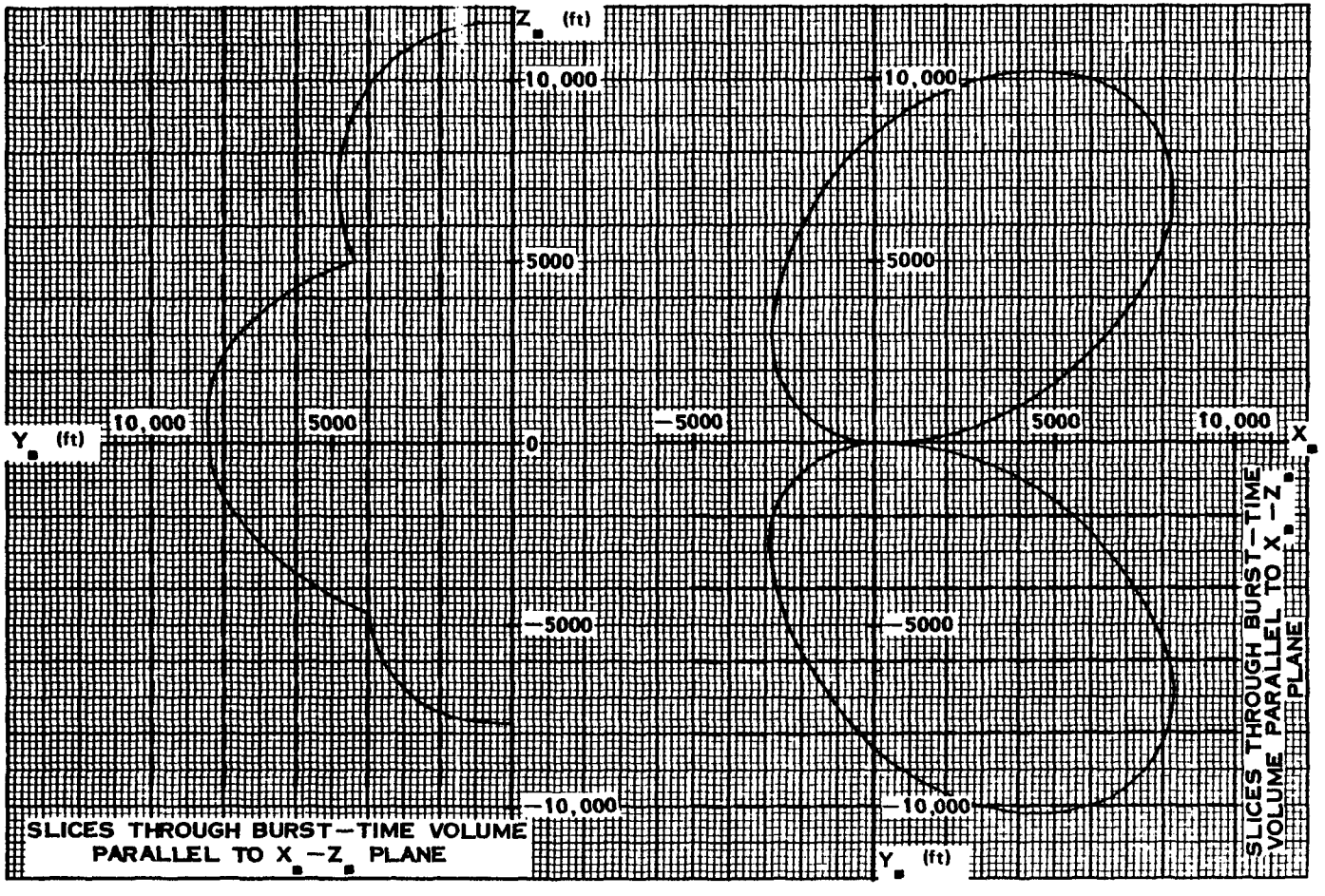

Figure 13-26a. [redacted] Burst-Time Envelope (Front View) [redacted]

Figure 13-26b. [redacted] Burst-Time Envelope (Top View) [redacted]

[redacted]

BIBLIOGRAPHY

Atkinson, G. W., and H. G. Laursen, *Nomographs for Determining the Relationships Between Pressure, Range, Altitude, and Yield in the Shock Front Resulting from a Nuclear Detonation* [redacted] NAVWEPS Report 8295, Naval Weapons Evaluation Facility, Albuquerque, New Mexico, 31 January 1965 [redacted]

Ayvazian, M., E. S. Criscione, and N. P. Hobbs, *Comparison Between Predicted and Measured Structural Responses of a Supersonic Delta Wing to Blast Loads,* AFFDL-TR-65-212, Kaman AviDyne, Burlington, Massachusetts, March 1966 [redacted]

Criscione, E., and J. Putukian, *Preliminary Estimates of the Effect of Blast-Thermal Interaction on the Vulnerability of High-Speed Aircraft in the Vicinity of a Nuclear Detonation* [redacted] ASD-TR-61-135, AviDyne Research Inc., Burlington, Massachusetts, January 1962 [redacted]

Davis, H. T., W. C. Kaufman, *An Experimental Determination of the Maximum Safe Thermal Radiation Loads for a Fighter-Bomber Cockpit,* ASRMDS-TM-63-4, Flight Dynamics Laboratory, Wright-Patterson, Ohio, January 1963 [redacted]

De Hart, R. C., N. L. Basdekas, *Response of Aircraft Fuselages and Missile Bodies to Blast Loading,* ASD TDR-62-458, Southwest Research Institute, San Antonio, Texas, January 1963 [redacted]

Donovan, A. F., and H. R. Lawrence, eds., *Aerodynamic Components of Aircraft at High Speeds, Volume VII of High Speed Aerodynamics and Jet Propulsion,* Princeton University Press [redacted]

Friedman, M. D., and J. R. Ruetenik, *An Analysis of Measured Blast Loads on Swept Wings at High Subsonic Speeds,* AFFDL-TR-65-170, MIT/ASRL TR-102-1, Massachusetts Institute of Technology, Cambridge, Massachusetts, March 1966 [redacted]

Handbook for Analysis of Nuclear Weapon Effects on Aircraft [redacted] DASA 2048, KA-TR-50A, Kaman AviDyne, Burlington, Massachusetts, April 1970 [redacted]

Hobbs, N. P., and K. R. Wetmore, *Lethality Criteria for Aircraft Exposed to Nuclear Blasts* [redacted] AFFDL-TR-66-221, Kaman AviDyne, Burlington, Massachusetts, April 1967 [redacted]

Hobbs, N. P., G. J. Frassinelli, and E. S. Criscione, *Effects of Variations in Aircraft Parameters on Blast Lethality Envelopes* [redacted] RTD-TDR-63-4087, AviDyne Research Inc., Burlington, Massachusetts, February 1964 [redacted]

Nuclear Weapons Blast Phenomena, Volume I, Source and Development of Blast Waves in Air [redacted] DASA 1200-I, DASIAC, Santa Barbara, California, 1 March 1971 [redacted]

Nuclear Weapons Blast Phenomena, Volume II, Blast Wave Interaction [redacted] DASA 1200-II, DASIAC, Santa Barbara, California, 1 December 1970 [redacted]

[redacted]

[redacted]

Nuclear Weapons Blast Phenomena, Volume III, Air and Subsurface Burst Explosions [redacted] DASA 1200-III, DASIAC, Santa Barbara, California, 1 March 1970 [redacted]

Pugh, E. J., and G. B. Bennett, *Vulnerability of Aeronautical Systems to Nuclear Effects, Volume I – Methods of Structural Analysis* [redacted] RTD-TDR-64-1, January 1965 [redacted]

Schlei, E. J., and D. H. Whitford, *The Vulnerability of Parked Army Aircraft to Nuclear Detonations* [redacted] WADC-TR-56-354, University of Dayton, Dayton, Ohio, June 1956 [redacted]

Sears, W. R., ed., *General Theory of High Speed Aerodynamics, Volume VI of High Speed Aerodynamics and Jet Propulsion,* Princeton University Press [redacted]

Witmer, E. A., J. F. Duvivier, and M. Ayvazian, *The Effects of Atomic Explosions on the Main Rotor of Helicopters in Flight* [redacted] WADC-TR-58-301, MIT/ASRL, November 1958 [redacted]

Whitaker, W. A., and R. A. Deliberis, Jr., *Aircraft Thermal Vulnerability to Large High-Altitude Detonations* [redacted], AFWL-TR-67-85, Air Force Weapons Laboratory, Kirtland Air Force Base, New Mexico, August 1967 [redacted]

PAGE 13-88 INTENTIONALLY LEFT BLANK

[redacted]